Marine Environmental Responses to Typhoon and Kuroshio Current in the Northwest Pacific Ocean

（北西太平洋における台風と黒潮に対する海洋環境応答）

JEON, Jonghyeok

（全　種赫）

Doctor of Environmental Studies

Graduate School of Environmental Studies, Nagoya University

（名古屋大学大学院環境学研究科 博士（環境学））

2022

Marine Environmental Responses to Typhoon and Kuroshio Current in the Northwest Pacific Ocean

By

JEON, Jonghyeok

DISSERTATION

Submitted in Fulfillment with the Requirements
For the Degree of Doctor of Environmental Studies

Graduate School of Environmental Studies, Nagoya University

Approved by the Dissertation Committee:

Prof. KATO, Hirokazu

Prof. TANIKAWA, Hiroki

Prof. TOMITA, Takashi

Approved by the Faculty Council:

December, 2022

SUMMARY

The Kuroshio, a warm current, flows in the Northwest Pacific Ocean (NPO), especially in the south of the Japanese archipelago, and the Kuroshio has the characteristic of continuing its large meander for an extended length of time. Changes in the trajectory of Kuroshio current affect not only ocean physics, such as sea level anomaly and current velocity, but also fishing grounds, marine ecosystems, and climate. Another distinct event in the NPO, which has the highest frequency of tropical cyclone activities worldwide. The region experiences an annual average of 16.5 events, of which 6.3 (38 %) are super typhoons. Even with a single strong typhoon, the ocean environment changes due to the turbulence and circulation of seawater caused by the cyclonic storm effects of the typhoon. However, in the process of estimating the actual situation, it is difficult to interpret the interaction between the strong typhoon, having wide-ranging storm and position change every moment, and the upper ocean. Through the recently available dataset of Copernicus Marine Environment Monitoring Service (CMEMS), this study comprehensively quantitative analysis is conducted using a wide variety of daily data to clarify the combined effects of the Kuroshio meander and strong typhoon in the NPO. The main objective is to reveal the physical and biological variables induced by typhoon in interaction with Kuroshio current, considering the categorization of spatial and temporal distinct effect and the responses using daily multi-observation and model data.

The findings of a systematic approach may lead to a greater insight into the physical and biological oceanography of the NPO;

Chapter 1 reviews the upper ocean variables response under the marine environment to typhoons in the NPO. The literature study was also conducted over the last ten years including remote sensing, in situ observations, and modelling. Based on this research background, the purpose of this research was set.

Chapter 2 describes the impacts of the Kuroshio meander on the economy (e.g. fisheries), coastal ecosystems, coastal disasters (storm surges and high waves), and the impact on Japan's abnormal climate. Data analysis, considering sea level anomaly (SLA), geostrophic velocity (GV), sea surface temperature (SST), and phytoplankton bloom (PB; estimated by the chlorophyll-a index) was compared with the 2016 and 2021 cases, respectively. The influence of large meandering was evaluated quantitatively and accompanied by high temperature, high salinity, large current velocity, and a massive cyclonic eddy. It will be used as a background condition for this study.

Chapter 3 focuses on the strong typhoon HAGIBIS (2019, Typhoon No.19), which passed through the large meander of the Kuroshio. The spatial effect of Kuroshio current, cyclonic eddy, and anticyclonic eddies are mainly analyzed based on the CMEMS platform. First, for applying global data (CMEMS and satellite data) to a regional area, those data are verified by the storm wind zone (estimated by the Japan Meteorological Agency), Kuroshio mainstream (provided by Japan Coast Guard), and SST/SSS (obtained by in situ data by Argo floats). Second, six-hourly CMEMS data for wind speed and stress is used to classify the typhoon effects according to spatial-temporally changes, which could not be expressed with conventional mean weekly, five-day, and three-day data. Third, in strong cyclonic eddy area on the north side of the large meander during HAGIBIS, the SST decreased by 0.5-1.5 ℃ in combination of the strong Ekman pumping. Regarding sea surface salinity (SSS), Chen et al. (2019) showed that Typhoon KAI TAK (2012, Typhoon No. 13) increased salinity on the right-hand side of the typhoon track and decreased on the left side along the coastline of China. However, in this study, some SSS decreased due to heavy rainfall (drop down 0.2 psu) on the left-hand side of the track, while other SSS on the right side slightly increased by the upwelling of high-salinity from deep water to the sea surface. It is due to the fast-moving speed of HAGIBIS did not compensate for the negative anomaly induced by heavy rainfall. Regarding mixed layer depth (MLD) in the cyclonic eddy area, some of the MLD was shallowed (rise 5-10 m) due to the combined effect (Ekman + eddy upwelling), and the relationship analysis revealed cyclonic eddy and Ekman pumping against MLD was linear. However, the other MLD was deepened by approximately 15 m on both right and left semicircles of HAGIBIS, it is due to Kuroshio current and anticyclonic eddies made the other MLD deepen in combination with the concentrated strong wind stress power. In addition, the high Kuroshio current velocity deepen MLD (drop 5 m) due to the feature of Kuroshio. We spatially and quantitatively show the phenomena that occur in the SST, SSS, and MLD due to the specific eddies effects 1) upwelling and downwelling associated with the cyclonic and anticyclonic area in combination with the distinct physical wind forcing 2) both Ekman upwelling and wind stress power area, simultaneously.

Chapter 4 provides the effect of typhoon HAGBIS on not only the depth-vertical variability of the Kuroshio current velocity (KCV; m/s) and but also the subsurface favorable environmental condition for nutrient growth with in situ data by Argo float. Regarding the KCV, on October 11, where the center of HAGIBIS approached the mainstream of the Kuroshio

meander, it not only generated the wind blowing northward with anticlockwise forcing on the right-hand side of typhoon trajectory, but also intensified the Kuroshio current velocities. On October 12, when HAGIBIS made landfall on the Japanese archipelago, it was shown that the wind blowing southward on the left side of HAGIBIS, then the wind strengthened the southward-flowing Kuroshio current. Previous studies based on satellite data have shown that such phenomena occur at the sea surface, but this study based on vertical spatial and daily CMEMS, has shown that the effects of the typhoon can occur even 60 m below the sea surface. On the other hand, the effect was newly clarified that it was not reached by 100 m depth.
Regarding favorable environmental conditions leading to phytoplankton bloom (PB), the Argo float data analysis when a day after HAGIBIS hit revealed that not only the nutrient's favorable depth moved from 60 m to below sea surface, but also cooling temperature, lower salinity, higher oxygen, and higher nitrate were occurred than before HAGIBIS. According to comprehensive quantitative analysis, especially related to PB, 1) Before HAGIBIS, the Chl-a appeared on sea surface due to the cyclonic eddy upwelling and the high subsurface Chl-a (HSC; 0.5 mg/m^3) layer existed area from 100 m to 80 m depth near Kuroshio channel. However, 2) During HAGIBIS when typhoon affected each distinct regions, the surface Chl-a increased by 0.5 mg/m^3 because of HSC rose to 45 m induced by the combined upwelling phenomenon with cyclonic eddy and the typhoon. Even the intensified Kuroshio current area, led to the surface Chl-a increase by 0.45 mg/m^3. It could be seen that the typhoon made the HSC redistribute up to 55 m, then the HSC easily supplied the sea surface regardless of the high current velocity area. 3) One day after HAGIBIS, the surface high PB occurred on 0.56 mg/m^3 as a result of not only the built-up subsurface Chl-a maximum layer (SCML; greater 0.7 mg/m^3 up to around 60 m depth) along strong Kuroshio current and cyclonic eddy area, but also the redistribution of large-scale HSC layer in a lift-up condition of favorable nutrient growth. Compared to previous studies that concluded with only conceptual diagrams, this study newly found the redistribution of nutrient-rich layers and the spatially distinct impact zones through depth-integrated quantitative analysis and daily hybrid in situ and model data.

Finally, Chapter 5 summarizes the study's findings as a conclusion, along with their limitations and recommendations for further research.

This research is a pioneering study that conducted assembled data analysis and associated mechanism estimation to advance understanding of physical and biological processes in the Northwest pacific environment and spatio-temporal dynamic outgrowth

affected by typhoons.

LIST OF ACRONYMS & ABBREVIATIONS

3DPWP	3 Dimensional Price Weller Pinkel model
AVISO	Arching, Validation, and Interpretation of Satellite Oceanographic
BGC-Argo	Biogeochemical Argo
Chl-a	Chlorophyll a
CMEMS	Copernicus Marine Environment Monitoring Service
COAWST	Coupled Ocean–Atmosphere-Wave-Sediment Transport
DO	Dissolved Oxygen
EPV	Ekman Pumping Velocity
GESDISC	Goddard Earth Sciences Data and Information Services Center
GNSS-R	Global Navigation Satellite Systems Reflectometry
GV	Geostrophic Current Velocity
HAGIBIS	Typhoon HAGIBIS
HF	High Frequency
HSC	High Subsurface Chlorophyll
JCC	Japan Coast Guard
JMA	Japan Meteorological Agency
JTWC	Joint Typhoon Warning Center
KCM	Kuroshio Current Meander
KCV	Kuroshio Current Velocity
MAFF	Ministry of Agriculture, Forestry, and Fisheries
MLD	Mixed Layer Depth
MOST	Ministry of Science and Technology

NPO	Northwest Pacific Ocean
NPT	Near Real Time
PB	Phytoplankton Bloom
PPT	Precipitation
PR	Precipitation Radar
P_w	Wind Stress Power
ROMS	Regional Oceanic Modelling System
SAR	Synthetic Aperture Radar
SCML	Subsurface Chlorophyll Maximum Layer
SLA	Sea Level Anomaly
SS	Sea Salinity (defined the surface and subsurface water)
SSS	Sea Surface Salinity
SST	Sea Surface Temperature
ST	Sea Temperature (defined the surface and subsurface water)
SWAN	Simulating Waves Nearshore
SWZ	Storm Wind Zone
TC	Tropical Cyclone
TMPA	TRMM Multi-satellite Precipitation Analysis
TRMM	Tropical Rainfall Measuring Mission
TS	Translation Speed

TABLE OF CONTENTS

SUMMARY 3

LIST OF ACRONYMS & ABBREVIATIONS 7

TABLE OF CONTENTS 9

LIST OF TABLES 12

LIST OF FIGURES 13

CHAPTER 1. INTRODUCTION 18

1.1. Research Background 18

1.2. Observational Technologies and Modelling 23

1.3. Research Gaps 24

1.4. Research Objectives and Originalities 27

1.5. Structure of Dissertation 28

CHAPTER 2. OCEANIC BACKGROUND IN THE NORTHWEST PACIFIC OCEAN 31

2.1. Kuroshio Current 31

2.1.1. Environmental background 31
2.1.2. A modern large Kuroshio current meander 31

2.2. Effect of Large Kuroshio Current Meander 32

2.2.1. Effect on economic aspects 32
2.2.2. Effect on marine ecological aspects 34
2.2.3. Effect on climatic aspects 34

2.3. Materials 35

2.3.1. Data access 35

2.4. Kuroshio Current in 2016 and 2021 37

2.4.1. Sea level anomaly and geostrophic velocity 37
2.4.2. Sea surface temperature 37
2.4.3. Sea surface phytoplankton bloom 38

2.5. Summary 39

CHAPTER 3. SURFACE OCEAN RESPONSES TO HAGIBIS 40

3.1. Introduction 40

3.2. Target Event and Region 41

3.2.1. Super typhoon HAGIBIS 41
3.2.2. Study area 42

3.3. Multi-source Surface Observational and Model Data 42

3.3.1. Wind product and estimated typhoon effects 42
3.3.2. Sea surface ocean variables 44
3.3.3. Methodology 45

3.4. Wind Effects Induced by HAGIBIS 46

3.4.1. Validation of CMEMS model data by comparison with JMA 46
3.4.2. Wind stress power and Ekman pumping velocity 47
3.4.3. Missing value: three-day mean wind stress power 49

3.5. Response of Surface Kuroshio Current 50

3.5.1. Validation of the KCM & tracking cyclonic and anticyclonic eddies 50
3.5.2. Missing value: three-day mean sea surface salinity 51

3.6. Response of Surface Ocean Variables 52

3.6.1. Validation of SST and SSS via In-Situ data 52
3.6.2. Cause analysis via spatial distribution of SST and SSS 53
3.6.3. Cause analysis via daily MLD and precipitation 54
3.6.4. Relationship analysis based on linear regression 55

3.7. Summary 57

CHAPTER 4. SUBSURFACE OCEAN RESPONSES TO HAGIBIS 59

4.1. Introduction 59

4.2. Multi-source Subsurface Observational and Model Data 60

4.2.1. Vertical profile of subsurface ocean variables 61
4.2.2. Methodology 61

4.3. Response of Subsurface Kuroshio Current 62

4.3.1. Variability of the KCM according to 0, 60, and 100 m depth 63

4.4. Response of Surface Ocean Variables 64

4.4.1. Cause analysis via spatial distribution of SST, SSS, and Chl-a 64
4.4.2. Cause analysis via daily MLD and precipitation 68

4.5. Response of Subsurface Ocean Variables 69

4.5.1. Favorable environmental conditions in phytoplankton bloom 69
4.5.2. Relationship analysis based on linear regression 72
4.5.3. Comprehensive Quantitative Analysis 73

4.6. Summary 78

CHAPTER 5. CONCLUSIONS 79

5.1. Main Findings 79

5.2. Implications 81

5.3. Limitations and Further Research 83

REFERENCES 85

LIST OF PUBLICATIONS 101

ACKNOWLEDGEMENT 102

LIST OF TABLES

Table 1.1 Research gaps with previous studies and this study..... 26

Table 3.1 Validation of oceanic CMEMS values compared with In-situ data..... 52

Table 4.1 General information regarding to three Argo floats..... 61

LIST OF FIGURES

Figure 1.1 Sketch diagram of the surface and subsurface ocean process under a tropical cyclone. 23

Figure 1.2 Sketch diagram in comparison with previous studies and several research gaps for challenges in this study. 26

Figure 1.3 Sketch diagram of the dissertation structure. 30

Figure 2.1 Typical Kuroshio paths overlaid on bathymetry from ETOPO2 (colors; deep blue 0 m to white over 2000 m). Black dotted line defines a non-large meander and red dotted line is a large Kuroshio meander. 32

Figure 2.2 Affected areas in fishery and logistic industries. (a) geographical locations; 1. Wakayama Prefecture, 2. Mie Prefecture, 3. Shizuoka Prefecture, 4. Chiba Prefecture, and 5. The route of commercial Ships, (b) Annual catch "Sakura Shimp" in Shizuoka Prefecture, (c) Annual Catch "Shirasu" in Shizuoka Prefecture. 34

Source: b, c graphs were obtained by Shizuoka Prefectural Research Institute of Fishery. .. 34

Figure 2.3 Affected areas in marine ecosystem. (a) geographical locations; 1. South coastal area in Wakayama Prefecture, 2. Southwest coastal line in Wakayama Prefecture, (b) Amamo prior to 2017 and thereafter in 2020, and (c) Hijiki prior to 2017 and thereafter in 2021. 34

Figure 2.4 Affected areas in climate change. (a) geographical locations; 1. Shizuoka Prefecture, and 2. Kanto region, (b) The tide level in Yaizu and Shimizu port, and (c) Damage situation in Shimizu Port- Falling Fence. 35

Figure 2.5 Change of Kuroshio current pathway; (a) October 10, 2016 and (b) October 10, 2021. Kuroshio mainstream (red arrows; above 1 m/s) provided by the AVISO dataset indicating cyclonic (counterclockwise; -value, blue shades) and anticyclonic (clockwise; +value, red shades). 37

Figure 2.6 Change in sea surface temperature; (a) October 10, 2016 and (b) October 10, 2021. 38

Figure 2.7 Change in phytoplankton bloom represented by the concentration of

chlorophyll a; (a) October 10, 2016 and (b) October 10, 2021..... 39

Figure 3.1 Six-hourly HAGIBIS best track on October 09-13, 2019 obtained by JMA and daily Kuroshio current meander (KCM; red dotted line) provided by JCC. (a) at the wide area; including the typhoon central location with intensity (dots in red to yellow), the radius of a storm wind zone (SWZ; black circles), date (month/day), and central pressure (hPa)/maximum sustained wind speed (m/s), and (b) at a boundary of the study area; including same components as (a) and adding time (UTC) and translational speed (TS; km/h), respectively 42

Figure 3.2 Flowchart showing how individual estimated the physical process at the KCM environment of the Northwest Pacific Ocean in response to typhoon HAGIBIS. 46

Figure 3.3 Validation of each six-hourly storm wind zone of HAGIBIS; (a) October 11, 18UTC, (b) October 12, 00UTC, (c) 06UTC, and (d) 12UTC, respectively. Black circles indicate JMA (black circles) and white contour is CMEMS data with the typhoon central location according to time. 47

Figure 3.4 Spatial distribution of wind stress power (Pw; W/m2); (a) October 11, 06UTC, (b) 12UTC (c) 18UTC, (d) October 12, 00UTC (e) 06UTC, and (f) 12UTC with wind speed vectors (black arrows) provided by CMEMS, storm wind zones (black circles), and the typhoon track with the intensity (black line; red dots) obtained by JMA, respectively. 48

Figure 3.5 Spatial distribution of Ekman pumping velocity (EPV; × 10-5 m/s**)**; (a) October 11, 06UTC, (b) 12UTC (c) 18UTC, (d) October 12, 00UTC (e) 06UTC, and (f) 12UTC with wind stress vectors (black arrows) provided by CMEMS, storm wind zones (black circles), and the typhoon track with the intensity (black line; red dots) obtained by JMA, respectively..... 49

Figure 3.6 Three-day mean spatial distribution of wind stress power (Pw; W/m2) **with wind speed vectors (black arrows) in comparison between (a) All Metop ASCAT and (b) CMEMS data**. 50

Figure 3.7 Validation of the daily Kuroshio mainstream between AVISO (red arrows) and JCC (black dotted line) data and tracking cyclonic and anticyclonic eddy in terms

of SLA; (a) October 10, (b) October 11, (c) October 12, and (d) October 13 with the typhoon track and intensity, respectively. 51

Figure 3.8 Three-day mean spatial distribution of sea surface salinity (SSS; psu) in comparison between (a) SMAP and (b) CMEMS data. 52

Figure 3.9 Daily surface temperature (SST) and salinity (SSS); (a, c) October 10 and (b, d) October 12, respectively. Black dotted line, black line, and red dotted denote the Kuroshio meander, the storm wind zone, and the typhoon central location according to date. Physical Argo floats (SST and SSS) are shown in points A and B, while a biogeochemical Argo float including SST and SSS as well as dissolved oxygen, nitrate, and chlorophyll a is shown in points C1. 53

Figure 3.10 Daily mixed layer depth (MLD) and daily cumulative precipitation (mm); (a, c) October 10 and (b, d) October 12. Black dotted line, black line, and red dotted denote the Kuroshio meander, storm wind zone, and the location of the center typhoon corresponding date. 55

Figure 3.11 Relationship analysis of distinct SLA, MLD, and wind effects in the sea surface; (a) SLA (cyclonic eddy, Kuroshio, and anticyclonic eddies), (b) MLD before and during HAGIBIS, and (c) wind effects during HAGIBIS based on zonal transect in the Northwest Pacific Ocean (latitude 31.5°N; longitude 135°–140°E) and (d, e) their relationship using linear regression. 57

Figure 4.1 Flowchart depicting the individually-estimated physical and biological processes at the KCM environment of the Northwest Pacific Ocean in response to typhoon HAGIBIS. 62

Figure 4.2 Kuroshio current velocity (m/s) on the boundary of longitude 135–140°E and latitude 30–34°N based on depth and date; 0 m (a1, b1, c1, and d1), 60 m (a2, b2, c2, and d2), and 100 m (a3, b3, c3, d3) on October 10, 11, 12, and 13 respectively. The figures are focused on the strong cyclonic eddy area with the typhoon's track and intensity (black line and red dots). 64

Figure 4.3 Daily sea surface temperature (SST); (a) October 10, (b) October 11, (c) October 12, and (d) October 13. Black dotted line, black line, and red dotted denote the Kuroshio meander, the storm wind zone, and the typhoon central location according to date.

Physical Argo floats (ST and SS) are shown in points A and B. 65

Figure 4.4 Daily sea surface salinity (SSS); (a) October 10, (b) October 11, (c) October 12, and (d) October 13. Black dotted line, black line, and red dotted denote the Kuroshio meander, the storm wind zone, and the typhoon central location according to date. Physical Argo floats (ST and SS) are shown in points A and B. 66

Figure 4.5 Daily sea surface phytoplankton bloom indicated by chlorophyll a; (a) October 10, (b) October 11, (c) October 12, and (d) October 13. Black dotted line, black line, and red dotted denote the Kuroshio meander, the storm wind zone, and the typhoon central location according to date. Solid red lines indicate a boundary of high Chl-a is over 0.5 mg/m3. A biogeochemical Argo float (ST, SS, DO, nitrate, and Chl-a) is depicted in points C1, C2, and C3 based on the dates of October 9, 14, and 19, respectively. 67

Figure 4.6 Daily mixed layer depth (MLD) and daily cumulative precipitation (PPT; mm); (a1, b1) October 11, (a2, b2) October 12, and (a3, b3) October 13. Black dotted line, black line, and red dotted denote the Kuroshio meander, the storm wind zone, and the location of the center typhoon corresponding date. The blue and red contour lines indicate 30 m and 60 m thickness in terms of MLD, respectively. 69

Figure 4.7 Depth-integrated temperature (℃, solid) and salinity (psu, dotted) in the upper 100 m depth; Before (C1; October 9 in black), a day after (C2; October 14 in blue), and a week after (C3; October 19 in red) the passage of HAGIBIS observed by Code 2,902,754 BCG Argo float, respectively. 70

Figure 4.8 Depth-integrated dissolved oxygen (μmol/kg**, solid) and nitrate (**μmol/kg**, dotted) in the upper 100 m depth**; Before (C1; October 9 in black), a day after (C2; October 14 in blue), and a week after (C3; October 19 in red) the passage of HAGIBIS observed by Code 2,902,754 BCG Argo float, respectively. 72

Figure 4.9 Depth-integrated Chl-a (mg/m3**, solid) in the upper 100 m depth**; Before (C1; October 9 in black), a day after (C2; October 14 in blue), and a week after (C3; October 19 in red) the passage of HAGIBIS observed by Code 2,902,754 BCG Argo float, respectively 72

Figure 4.10 Scatterplots of oceanic variables to examine the relationship of (a) temperature, (b) salinity, (c) dissolved oxygen, and (d) nitrate compared to the Chl-a

concentration; Before (C1; October 09 in blue), a day after (C2; October 14 in red), and a week after (C3; October 19 in black) the passage of HAGIBIS, respectively. 73

Figure 4.11 Quantitative schematic diagram of ocean variability from 100 m depth to the sea surface before HAGIBIS. Zonal transect in the Northwest Pacific Ocean (latitude 31.5°N; longitude 135°–140°E) including cyclonic eddy area [blue isolines; (a–c) in the sea surface], the Kuroshio current depicted by integrated horizontal velocities on different depths with orange; 1.0 < V < 1.5 m/s, and yellow; over 1.0 m/s. The subsurface layers comprise the MLD (Violet), HSC (light green; 0.5 mg/m3). The two graphs indicate (b) surface sea temperature (℃) and (c) surface Chl-a (mg/m3) before HAGIBIS. 75

Figure 4.12 Quantitative schematic diagram of ocean variability from 100 m depth to the sea surface during HAGIBIS. Zonal transect in the Northwest Pacific Ocean (latitude 31.5°N; longitude 135°–140°E) including cyclonic eddy area [blue isolines; (a–c) in the sea surface], the Kuroshio current depicted by integrated horizontal velocities on different depths with red; over 1.5 m/s, orange; 1.0 < V < 1.5 m/s, and yellow; over 1.0 m/s, and typhoon HAGIBIS represented by the affected area where strong Pw (gray circles) and high EPV (red circle) in the sea surface. The subsurface layers comprise the MLD (Violet), HSC (light green; 0.5 mg/m3). The three graphs indicate (b) surface sea temperature (℃) and (c) surface Chl-a (mg/m3), and (d) Pw (W/m2) and EPV (× 10-6 m/s) during HAGIBIS. Two vertical dashed lines marked on both the main plot and the subplot indicate the region with the strongest typhoon effect along the typhoon's center (longitude 136.5°–138°E). 76

Figure 4.13 Quantitative schematic diagram of ocean variability from 100 m depth to the sea surface a day after HAGIBIS. Zonal transect in the Northwest Pacific Ocean (latitude 31.5°N; longitude 135°–140°E) including cyclonic eddy area [blue isolines; (a–c) in the sea surface], the Kuroshio current depicted by integrated horizontal velocities on different depths with orange; 1.0 < V < 1.5 m/s, and yellow; over 1.0 m/s. The subsurface layers comprise the MLD (Violet), HSC (light green; 0.5 mg/m3), and SCML (deep green; above 0.7 mg/m3). The two graphs indicate (b) surface sea temperature (℃) and (c) surface Chl-a (mg/m3) a day after. 77

CHAPTER 1. INTRODUCTION

1.1. Research Background

The ocean contains more than 70 percent of the planet's surface and supplies oxygen, food, and employment to millions of people. However, pollution, overfishing, and climate change are having a negative effect on the oceans' health. To ensure the long-term health of the ocean, its resources, and the surrounding ecosystem, it is necessary to address a wide range of topics in oceanography, including physics, biology, and geology. Remote sensing is becoming more significant in the study of global change, resource exploration, environmental monitoring and prediction, and other related topics. Monitoring and understanding the status of the ocean may assist in making informed decisions about how to maintain this critical resource, as well as contributing to the sustainable development of marine resources and ecological and biological preservation. Therefore, monitoring and visualizing the character of the ocean from the surface to the subsurface in responses to various events (cyclone, tsunami, sea level rise, etc.). Chapter 1 provided an overview of Tropical Cyclones (TCs), upper oceanic response to TCs in the Northwest Pacific Ocean (NPO), and the development of observational methods. Many studies have established that systematic and aggregate knowledge of the influence of the TCs affects multiple elements of the NPO, considering sea temperature (ST), salinity (SS), mixed layer depth (MLD), and phytoplankton bloom (PB; estimated by chlorophyll a). Some ocean responses to TCs are critical in the NPO due to the existence of the Kuroshio and specific geographical features.

- **Tropical cyclones (TCs)**

TCs, which can also be called hurricanes or typhoons depending on where they make landfall, are among the deadliest and most terrifying types of natural disasters. According to the Saffir-Simpson TC's scale, typhoons can be classified into five categories by the maximum sustained wind (1-min mean) according to Joint Typhoon Warning Center (JTWC): Category one: 33–42 m/s, Category two: 43–48 m/s, Category three: 49–58 m/s, Category four: 59–69 m/s , and Category five: $\geq$ 70 m/s. The NPO has experienced more frequency of TCs than any other cyclone-rich basin, and the intensity of storm are stronger than in other basins (Webster et al. 2005). Especially, the Philippine Sea, Taiwan, Japan, Korea, and mainland China have the largest concentration of storms in the world. The majority of a TC's life is spent traveling above the ocean. As a form of feedback, the ocean supplies the necessary amount of

energy for the intensification of storms by transferring heat from the sea to the air. In the opposite process, TCs induce kinetic power into surface waves, currents, and potential gravitational flux, hence contributing to ocean circulation on both regional and global scales. (L. L. Liu, Wang, and Huang 2008). TCs can alter regional water heat intake (Emanuel 2001) and influence global ocean heat transmission (Sriver and Huber 2007; Emanuel et al. 2004; Hu et al. 2009). Further, TCs have a significant role in both sustaining the ongoing El Niño and modulating the emergence and progression of the El Niño-Southern Oscillation (Fedorov, Brierley, and Emanuel 2010). Even still, the interaction between TC and the ocean have complicated due to a coupled system involving a wide variety of complex physical processes, such as heat transfers over the air-sea interface (Emanuel 2001, 2003; Shay, Goni, and Black 2000).

To provide understanding of the complex physical processes, there are some previous empirical and theoretical literatures of upper ocean responses to TCs such as ST, SS, and MLD as well as biological and marine environmental background responses.

- **Sea Temperature**

TCs make the upper marine mixed layer deeper and cool the water's surface (J. F. Price 1981; J. F. Price, Sanford, and Forristall 1994; Jacob et al. 2000; Sanford, Price, and Girton 2011; C. Jiang et al. 2020), which is referred to as the "heat pump" effect (X. Zhang et al. 2018; Han Zhang et al. 2016). In the north of the equator, sea cooling in surface is typically amplified by from 1 to 6 ℃ and is biased toward the TC track's right side (J. F. Price 1981; I. I. Lin et al. 2003; P. G. Black et al. 2007), occasionally dropping as low as 11 ℃, which was caused by the sensible and latent heat flux between the air and the sea's surface (Glenn et al. 2016). In the other hand, the warm anomaly in subsurface temperature due to wind-induced stirring can reach temperatures of up to 4 ℃, and is generally controlled by TC-induced upwelling at the ocean's surface(Han Zhang et al. 2019; Ning et al. 2019). Subsurface temperature lacks air contact, hence it typically recovers more slowly than surface water (Emanuel 2001; G. Wang et al. 2016). However, the sea surface temperature (SST) typically returns to its former value within a few days to a few weeks (J. F. Price, Weller, and Pinkel 1986; James F. Price, Morzel, and Niiler 2008; Emanuel 2001; Hart, Maue, and Watson 2007), for approximately seven days (Jansen, Ferrari, and Mooring 2010; Dare and Mcbride 2011). In general, the upper ocean temperature response to a TC is determined by the TC's strength, size, and moving speed (Emanuel et al. 2004; Chen et al. 2007; S. Lin et al. 2017). For example, lower categories (categories one-two)

are more effective in generating cooling than those of higher categories (categories three-five), which provide less anomaly (Lloyd and Vecchi 2011). In contrast, Lin et al. 2009 demonstrated that a high translational speed of TC can intensify over a shallow temperature of 26 ℃ due to less SST cooling. However, when the storm moves slowly, the exposed depth of the water is substantially deeper, hence a relatively thick 26 ° is required.

- **Sea Salinity**

In the north of the equator, TCs usually cause a right side bias with an increase in sea surface salinity (SSS) and a reduction in subsurface salinity of up to 1 psu (Domingues et al. 2015; Han Zhang et al. 2016). Sometimes, the positive anomaly of SSS might even reach from 1.5 to 3 psu concentration (Chaudhuri et al. 2019). In contrast, rainfall accompanied with TCs generally decrease in the density of a plus SSS anomaly (Girishkumar et al. 2014; S. Liu et al. 2020) and cause a minus SSS anomaly to the left bias of the TCs trajectory in the north of the equator (Desbiolles et al. 2017; Fu Liu et al. 2020). The fresh water input from precipitation promotes upper ocean stratification and decreases the TC-induced vertical mixing (Jullien et al. 2012; Vissa, Satyanarayana, and Prasad Kumar 2012; X. Liu and Wei 2015; S. Liu et al. 2020). According to an estimate by Girishkumar *et al.*, 2014, the salinity response in the upper ocean can last from 10 to 12 days.

- **Phytoplankton Bloom**

TCs are responsible for an increase in phytoplankton bloom (PB; indicated by chlorophyll a concentration) and primary production, which can be mainly due to the enhanced nutrient supply in the euphotic area generated by vertical stirring, entrainment, and other processes that occur during TCs (Morimoto et al. 2009; Zheng et al. 2010; Chiang, Wu, and Oey 2011; Hung et al. 2013). These processes also contribute to the local long-term PP (Foltz, Balaguru, and Leung 2015). In the north of the equator, an increase in chlorophyll a (Chl-a) often results in a right-side bias of TC trajectory (I. I. Lin et al. 2003; Yin et al. 2007; Shang et al. 2008; Zhao, Tang, and Wang 2008; Zheng et al. 2010; Shibano et al. 2011). The amplitude and extent of surface PBs are dependent on the properties of the TC. (Zheng et al. 2010; Shibano et al. 2011). For instance, slow-moving speed and weak TCs induce PBs with high Chl-a concentration, whereas fast-moving speed and powerful TCs trigger widespread blooms (Zhao, Tang, and Wang 2008). The Chl-a maximum occurs two-three days after nitrate maximum after a storm (S. Pan et al. 2017), and storm-induced PBs often can stay two-three weeks (Y. Chen and Tang 2012; Foltz, Balaguru, and Leung 2015; Y. Wang and Gao 2020).

- **Ocean Current**

The ocean current is the periodic and directed flow of saltwater that delivers nutrients, energy, heat, and harmful materials throughout the globe (Amani et al. 2022; Fu et al. 2019). Ocean currents influence the temperature, the ocean's ecological system, and the fishing yield. Ocean currents can be caused by several causes, including wind, the Coriolis effect, water density fluctuation, ocean tide, SST, and ocean surface changes.(Amani et al. 2022; Fu et al. 2019; Isern-Fontanet et al. 2017). In general, ocean currents are classified into four types: (i) geostrophic current, which is balanced under pressure gradient force by the Coriolis force; (ii) tidal current, which is produced by the gravitational force of the lunar, sun, and Planet; (iii) wind-driven Ekman transport current, which is generated by the steady ocean wind (trade wind and westerlies; and (iv) small-scale current, which is formed by the minor characteristics such as eddies and fronts (Dagestad and Röhrs 2019). Ocean currents are divided into two categories according to their degree of heat: warm and cold ocean currents. For example, the Gulf Stream and Kuroshio are warm currents which move heat from the tropics to the poles and have a substantial impact on the planetary climate (Amani et al. 2022; Ribbe and Brieva 2016). The Oyashio cold currents maintain significantly upwelling seas by transporting cold water toward the equator (Ribbe and Brieva 2016).

Ocean currents are further divided into two types based on their deepness: surface and subsurface. The surface flows are horizontal water flows that occur at both regional and global scales (Amani et al. 2022; Dagestad and Röhrs 2019). Along the coastlines and offshore, there are often short-period (hourly/seasonal) surface currents caused by ocean tides, waves, and local-scale winds (Amani et al. 2022; Constantin 2021). Currents drive local floods, marine contamination, sediment transfer, and ship navigation (Amani et al. 2022; Constantin 2021). The global surface currents (Gulf stream and Kuroshio) are generally governed by the primary global winds (westerlies and trade wind), the Coriolis force and the flow restriction given by continental diversion (Dohan and Maximenko 2010). These long-distance currents flow in the same direction as the wind at around three to four percentage of wind speed (Amani et al. 2022; Constantin 2021). However, the Coriolis force deflects the current from the equator in the correct direction in the north of the equator, resulting in the formation of clockwise circular gyre patterns (Dagestad and Röhrs 2019; Constantin 2021). In contrast, deep ocean currents (below 400 m depth) are vertical streams influenced by thermohaline circulation triggered by changes in water density and dependent on temperature. With upwelling and downwelling

directions of the sea surface, deep ocean currents form (Rahmstorf 2003).

- **Oceanic Background**

The background ocean state influences the temperature response of the upper ocean during a storm condition. For example, in the center of a cyclonic (anticyclonic) eddy, cold upwelling (warm downwelling) occurs, which increases (decreases) the rate at which the surface cooling (Fenfen Liu and Tang 2018; R. Wu and Li 2018; Ning et al. 2019). The background ocean condition (massive eddies) induces the response of the sea salinity during a TC. For instance, the upwelling (downwelling) that occurs as a result of cyclonic (anticyclonic) eddies causes the salinity concentration of the upper ocean to increase (reduce) (Jaimes and Shay 2009; Fenfen Liu and Tang 2018). In terms of biology, the extent and magnitude of surface PBs are dependent on ocean environment condition (I. I. Lin et al. 2003; Zhao, Tang, and Wang 2008; Mei et al. 2015; Liao et al. 2017). Existing cold core eddies contribute significantly to the increase in Chl-a concentration during TCs. (Mei et al. 2015; Xu et al. 2017; Han Zhang et al. 2020a).

Figure 1.1 summarized the previous research on an upper ocean response to a storm, which is a key topic due to their role in climate change, environmental variability, and air-sea heat flux exchange. The upper ocean response is determined by wind-induced stirring, advection, upwelling, and air and sea fluxes (such as fresh water supply and heat flux). There are two main effects induced by tropical cyclone to the ocean such as wind-induced energy flux and Ekman pumping. Vertical mixing explains strong wind power transfers its energy from the sea surface to deep water by stirring water, while the Ekman pumping is significant in the sea subsurface moving and lifting water density such as temperature, salinity, and nutrient. In that process, TC typically raises high surface waves, cooling (warming) temperature, and increases (reduce) in salinity on the surface (subsurface), in addition to triggering plankton blooms at a particular depth. Further, in the north of the equator, wind mixing and upwelling are much stronger on the right side; hence, the upper ocean responses are generally biased to the right-hand side of the TC trajectory. In addition, the characteristics of the upper ocean reaction are primarily determined by the TC factors (such as TC strength, moving speed, and size) and oceanic environment conditions (such as ocean stratified thickness, long-term current and eddies).

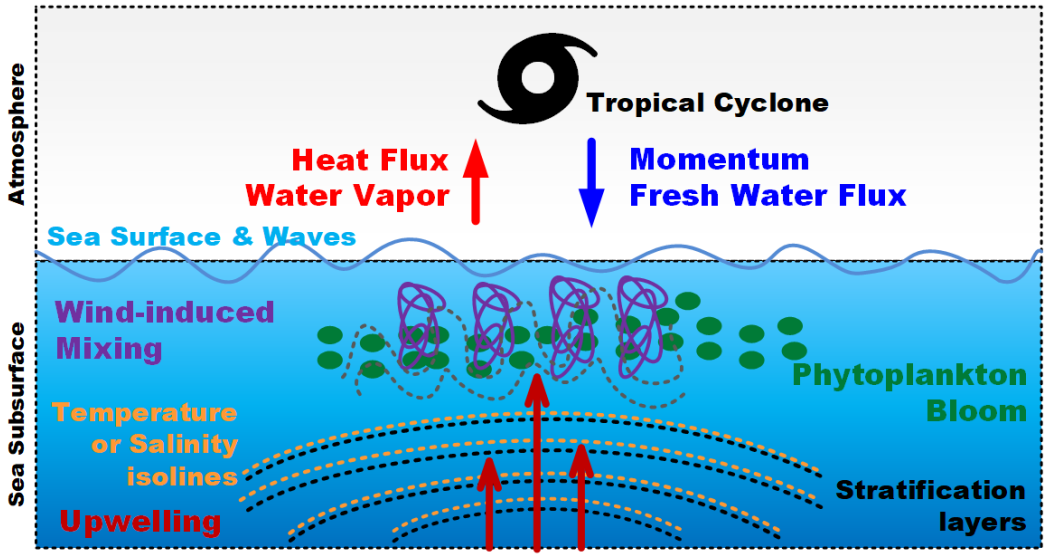

Figure 1.1 Sketch diagram of the surface and subsurface ocean process under a tropical cyclone.

1.2. Observational Technologies and Modelling

The development of observational technologies and modelling over last few decades has led to a better understanding of the ocean responses to TCs. As a result of their advancements, oceanographers and meteorologists are now able to do in-depth research on the water beneath TCs. In details, traditional observation methods including moorings and buoys (J. F. Zhang, and Yu 2016; Y. Zhang, Deng, and Zhang 2019; Y. J. Yang et al. 2019), drifters deployed from air and oceanic floats (E. A. D'Asaro et al. 2007; Pun et al. 2011; E. D'Asaro et al. 2011), Argo floats (Park, Kwon, and Price 2011; Q. Wu and Chen 2012; Z. Liu et al. 2014; S. Lin et al. 2017b; Xing et al. 2020) and satellite images (X. Li et al. 2018; Yue et al. 2018; Ning et al. 2019; Han Zhang et al. 2019), as well as modern advancement technology such as gliders (Glenn et al. 2016; Hsu and Ho 2019), are now applied to the upper ocean response to TCs monitoring. Especially, biogeochemical Argo floats have been used to observe how the undersea response to TCs in terms of thermodynamic and biogeochemical marine factors (Chai et al. 2020; Qiu et al. 2021; Ning and Xu 2021). In the early days of numerical model simulations, the ocean model was used to simulate the ocean current response. This was followed by the development of various numerical models, including the three dimensional Price Weller Pinkel model (3DPWP) (J. F. Price, Sanford, and Forristall 1994; Sanford et al. 2007; Han Zhang et al. 2020b), the regional ocean modelling system (ROMS) (Yue et al. 2018) is used to simulate the three-dimensional responses in terms of temperature, salinity, and current.

In recent years, atmosphere-ocean-wave models, including the Coupled Ocean Atmosphere Wave Sediment Transport (COAWST) system model (Prakash and Pant 2017; R. Wu et al. 2018) has been progressively implemented in order to predict the ocean's response to TCs. However, there are certain shortcomings in oceanic technology and data extraction such as missing values because of cloud cover (Groom et al. 2019), biased values due to individual satellite data methods (M. Li et al. 2017), and temporal gaps such as weekly, five-day, and three-day mean datasets (Banzon et al. 2016).

One of the opportunities to fill in the gap left by the shortcomings, the Copernicus Marine Environment Monitoring Service (CMEMS) is currently providing periodic and systematic reference standard data on the biogeochemical ocean and sea state for both the global ocean and the European local seas.

The CMEMS works consist of (Le Traon et al. 2019)

- Providing short and long-term global oceanic data via a combination of multi-observational platforms and atmospheric/oceanic model data
- Tracking and reporting on previous and recent maritime environmental circumstances (physics and biogeochemistry), climate change and other stresses;
- Examining and evaluating changes in the marine environment;

CMEMS product is founded on cutting-edge data processing, modelling, and data assimilation methodologies. The product's unpredictability is examined utilizing rigorous, widely acknowledged quality evaluation methods (Hernandez et al. 2015). CMEMS offers approximately 160 different observational and computational outputs including ocean physics (temperature, salinity, sea level anomaly, currents, and waves), and biogeochemistry (oxygen, pH, Chl-a, and nutrients). Modeling products offer a international scale resolution of 1/12° and regional applications with resolutions ranging from 1/24° to 1/72°.

1.3. Research Gaps

According to previous studies, as TCs travel the ocean, their powerful cyclonic winds influence the upper ocean from the surface to depths of 100-200 m. However, evaluating the exchange between TCs' effects and ocean variables is particularly difficult. Despite advances in our knowledge of the upper ocean's reaction to a TC has grown over the past few decades, there are still areas that require additional research. Figure 1.2 indicate there are many previous studies about the characteristics of different TCs (1) intensity (strong/weak), (2) translation

speed (fast/slow), and (3) size (large/small storm wind zone) and their effects on the upper ocean variables, respectively. Mainly, TCs induce wind stress power, Ekman pumping and cyclonic eddy intensity. Those physical processes generate vertical mixing and upwelling, and the combined upwelling with pre-existing eddy. As results of them, the sea surface temperature is decreased, salinity is increased and mixed layer depth raise up, whereas the subsurface temperature is increased, salinity is decreased, as well as the amount of nutrient concentration increase and the nutrient-rich layer moved up to the surface. Further, there are several findings of the combined effects of TCs and the surface Kuroshio current meander (KCM) to the upper ocean responses.

Especially, some previous studies largely related to my dissertation approach are compared in order to seek out what is the remaining issues in this field (Table 1.1). S. Lin et al. 2017b tried to conduct various tropical cyclones to classify different typhoon characteristic (size, moving speed, intensity) and their effects and SST and SSS responses in surface and subsurface using five-day Argo floats. Y. Liu, Tang, and Evgeny 2019 showed that various surface and subsurface variables response to single typhoon LINFA and ocean current effects using eight-day multiple satellite and CTD. However, they left behind as one of the remaining study as daily ocean response. Han Zhang et al. 2019 improved the results of Y. Liu, Tang, and Evgeny 2019 by estimating physical ocean variables especially, focusing on the dynamics of massive eddy area using a multiple satellites, buoy and mooring. Although they identified the relationship between physical variables and oceanic eddy feature, however, Han Zhang et al. 2019 concluded their relationship as a conceptual schematic diagram and introduced the necessary of further research of quantitative impact analysis. Most similar with my study as Y. Liu et al. 2020, conducted individual-estimated weekly physical-biogeochemical ocean response to Typhoon Linfa and 2015 Kuroshio current using multi-satellite, in situ and HYCOM model data to reveal the phytoplankton bloom processes in the surface and subsurface. Y. Liu et al. 2020 concluded their results to conceptual diagram indicating their findings and estimation. T. Wang et al. 2022 conducted that daily surface and subsurface phytoplankton blooms during sequential typhoons using multiple satellites, Argo floats, and CMEME in Arabian sea. However, T. Wang et al. 2022 did not address the daily quantitative analysis between physical and phytoplankton dynamics because low-pitch sample data fail to identify daily or weekly variations.

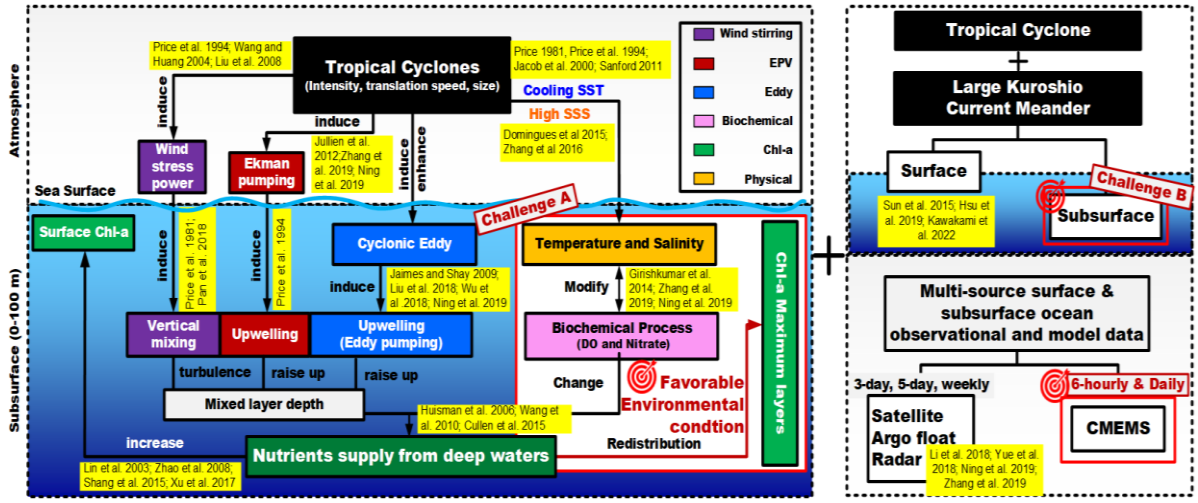

Figure 1.2 Sketch diagram in comparison with previous studies and several research gaps for challenges in this study.

Table 1.1 Research gaps with previous studies and this study

Factors / Authors	Surface variables					Subsurface variables			Physical forcing	Materials
	SST	SSS	Eddy	Chl-a	Rainfall	Physical	Biochemical	SCML		
Lin et al. 2017b	●	●				●			Various tropical cyclones	Argo floats (5 days)
Liu et al. 2019	●	●	●	●	●	●	●		Typhoon Linfa and ocean current	Multiple satellites & CTD (8 days)
Zhang et al. 2019	●	●	●		●	●			Successive typhoons (Sarika and Haima) and ocean current	Multiple satellites, Buoy & Mooring (daily)
Liu et al. 2020	●	●	●	●	●	●	●	●	Typhoon Linfa and 2015 Kuroshio current	Multi satellites, Argo float & HYCOM model data (Weekly)
Wang et al. 2022	●		●	●		●	●	●	Sequential typhoons (Kyarr and Maha)	Multiple satellites, Argo floats & CMEMS data (daily)
Jeon and Tomita, 2022	●	●	●	●	●	●	●	●	Typhoon HAGIBIS and 2019 Kuroshio current	Multiple satellites, radar, Argo floats & CMEMS data (daily)

* Relevant studies were retrieved for research gaps.

Research gaps were explored in a comprehensive literature review regarding the individual-estimated or collaborative way of the sea surface and subsurface response to storm conditions, especially in the NPO in which Kuroshio current existed as oceanic background.

Previous studies have been well demonstrated using weekly, five-day, and three-day source in order to deal with internal factors and external factors in the NPO. However, there are still several research gaps can be found in this field;

1) The investigation of favorable environmental condition for nutrient growth, where, when and how the ocean internal factors help the high nutrient layer movement is still unknown. Therefore, this study analyzes not only sea surface oceanic variables affected by external factors (TCs), but also internal oceanic factors (favorable environmental conditions for nutrient growth estimating temperature, salinity, DO, and nitrate)

2) Two physical forcing to the ocean such as TCs and the Kuroshio current meander studies are well known in the surface. However, the subsurface variability is still unknown. Further research is, therefore, to evaluate the subsurface Kuroshio current variability through not only induced internal ocean processes (eddy dynamic, current velocity) but also atmospheric forcing interaction (TCs).

As mentioned above, since the challenge issues mainly bring about the at least daily movement of the TCs and its effects in comparison with relatively long-term (weekly, three days) uncertainties for observing ocean responses, it is necessary to evaluate the combined effect considering TCs and Kuroshio current meander filling in the lack of temporal and spatial distribution. The challenges should at least be able to answer a main question as follows;

- How clearly is it revealed that typhoons cause changes in upper ocean physical and biological variables, particularly, in interaction with Kuroshio current, which specifies the NPO using daily multi-source data? If so, could we categorize spatially distinct effects and responses? Could a comprehensive quantitative analysis replace the role of a theoretical synthesis explanation?

Here, a comprehensive quantitative analysis is described in this study as a visualized quantitative package analysis, classifying as functional integral information that may be arranged categorically based on the features and properties of variables or phenomena.

1.4. Research Objectives and Originalities

To answer the preceding research question, the main purpose of this study is to clarify the sea surface and subsurface response to the extreme events that are the combined effects of Kuroshio current meander and a strong typhoon during short-term period in the NPO using multi-source observational and model data. It is anticipated to contribute to the environmental

studies from the following four perspectives listed below:

- **Study area**: Evaluate the superimposed event between the strong typhoon and the large Kuroshio current meander in 2019 to verify their different effects on the ocean via sea temperature, sea salinity, and chlorophyll with several cause analyses.
- **Framework development**: Apply a distinct spatio-temporal methodology to daily term events by analyzing the comprehensive quantitative impact based on each individual-estimated cause and effect.
- **Database application**: Apply for a universal database to the open ocean close to the south of Japan and contribute to guidelines for cost-effective local ocean monitoring methods for further research. For this progress, the applied regional database is verified such as wind products, ocean currents, and marine variables in both the sea surface and subsurface.

Therefore, this Remote Sensing of Environment research offers the findings of studies in theories, sciences, and technology that have contributed to the advancement of remote sensing science including planetary, oceanic, and atmospheric sensing. This study focuses on physical, biological, and quantitative approaches to oceanography, marine, and atmospheric science at local scales and covers a wide range of applications and methods. The originality of this study is summarized as follows:

- **Study area**: A specific case of abnormal oceanic background (a large Kuroshio meander inducing cyclonic and anticyclonic eddy area) and strong typhoon HAGIBIS.
- **Comprehensive quantitative impact analysis**: A combined atmospheric/oceanic quantitative analysis to classify the distinct physical driving force area and ocean response dynamics, simultaneously.
- **Multi-source database for daily analysis**: A variety of sources from measurements (Satellite image, Argo floats, etc.) and assembled data (CMEMS platform).

1.5. Structure of Dissertation

Figure 1.3 shows this dissertation proceeds with five chapters, including this introduction as literature reviews. In the following parts, Chapter 2 is, based on reviews of the

regional-level oceanic background for Chapters 3 and 4, about the effect on relations between a non-large Kuroshio meander in 2016 and a large Kuroshio meander case in 2021. It also investigates several viewpoints, such as economic, marine biological, and climatic, in a border of local south Japan, in an attempt to understand where the Kuroshio current's effects are concentrated by using remote satellite images and model data.

Chapter 3 is, based on first published paper (Jeon and Tomita 2022-1), focusing on spatial sea surface ocean responses to typhoon HAGIBIS using multi-source observational and model data; 1) Six-hourly effects of Typhoon HAGIBIS in 2019, 2) validation and tracking of Kuroshio current and cyclonic and anticyclonic eddies 3) Daily surface ocean responses focusing on SST and SSS, 4) Cause analysis exploring daily MLD and precipitation. This chapter offers a description of oceanic physical response and mechanism taking an example of the strong typhoon related to wind stress power and upwelling system under a large Kuroshio current meander.

Tuning to the sea subsurface, based on second published paper (Jeon and Tomita 2022-2), Chapter 4 highlights the internal and external cause analysis via the changes in ST, SS, and biological factors from sea surface and 100 m depth, especially considering the vertical variability of Kuroshio current velocity at specific depths and favorable condition for nutrient growth before, during, and after the typhoon using an up-to-date multi-source assemble dataset

Finally, Chapter 5 provides a concluding discussion of this dissertation, including an overview of the main findings, limitations, and some recommendations regarding further studies.

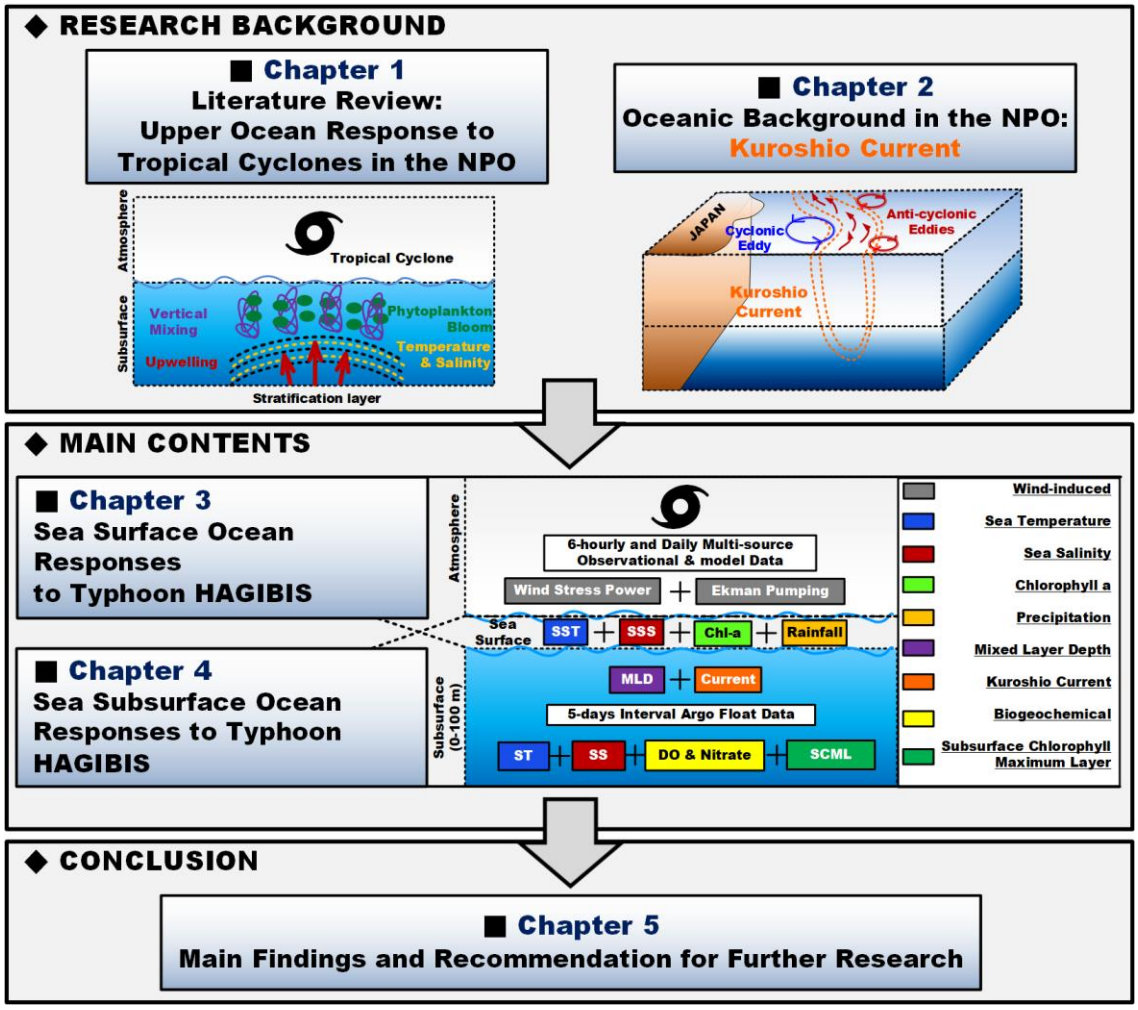

Figure 1.3 Sketch diagram of the dissertation structure.

CHAPTER 2. OCEANIC BACKGROUND IN THE NORTHWEST PACIFIC OCEAN

2.1. Kuroshio Current

2.1.1. Environmental background

The Kuroshio is a western-boundary current that flows northeast along the East China Sea (ECS) continental slope and the south coast of Japan, transporting high temperature, high salinity, and large kinetic energy water from the tropics. The Kuroshio region has a deeper mixed layer and thermocline than other neighboring ocean region (X. Liu and Wei 2015). The Kuroshio is characterized by small and large meanders in a meridional direction (Sekine 1990; Kawabe 1995), which have substantial effects on the spatial distribution of regional environmental conditions. It is believed that ocean density variations play a significant role in triggering small meandering off Kyushu island in southwestern Japan (Feng, Mitsudera, and Yoshikawa 2000; Ebuchi and Hanawa 2003; Usui et al. 2008, 2013). As a result of the variations, small meanders may form off the southwest coast of Shikoku island and large meanders may develop off the Kii Peninsula on interannual intervals (Kawabe 1985; Sekine 1990). Kawabe 1985 divided common transit routes into three types: the conventional large-meander route, the nearshore non-large meander route, and the offshore non-large meander route. In subsequent research, Kawabe 1995. examined the correlation between Kuroshio's route variations, velocity changes, and volume transport changes, all of which contributed to the development of the oceanic background's characteristics in different meander cases. The surface variability of the Kuroshio has been widely studied on a broad range of spatial and temporal scales, making use of observational data and various modeling approaches (Feng, Mitsudera, and Yoshikawa 2000; Ebuchi and Hanawa 2003).

2.1.2. A modern large Kuroshio current meander

Since August 2017, the Japan Meteorological Agency (JMA) and the Japan Coast Guard (JCC) announced that the large meandering of the Kuroshio near south coast of Japan continued for 4 years and 11 months as of July 2022, and it was actually the longest ever (Sugimoto, Qiu, and Schneider 2021). It has been usually said that the large KCM has been affecting a more significant shift in fishing businesses, marine ecosystems, shipping routes, and local weather

abnormal patterns nearshore and offshore of south Japan. However, it is yet unclear whether the changes are due to the large KCM or other potential impacts, such as climate change, or long-term oceanic circulation in the NPO. Therefore, the proposed oceanic background information is to better understand the two cases of non-large KCM and the large KCM based on several aspects utilizing a couple of multiple datasets and spatial distributions in 2016 and 2019. The coordinated oceanic background area is longitude 134°–143°E and latitude 30°–37.5°N, with a boundary including the KCM as shown in Figure 2.1. Two Kuroshio current paths derived by the Japan Coast Guard (JCC; *https://www1.kaiho.mlit.go.jp/KANKYO/KAIYO/qboc/ accessed on 01 April 2022*). It describes the bathymetry and a non-large (black dotted line) and a large (red dotted line) Kuroshio meander flow off the South Japan.

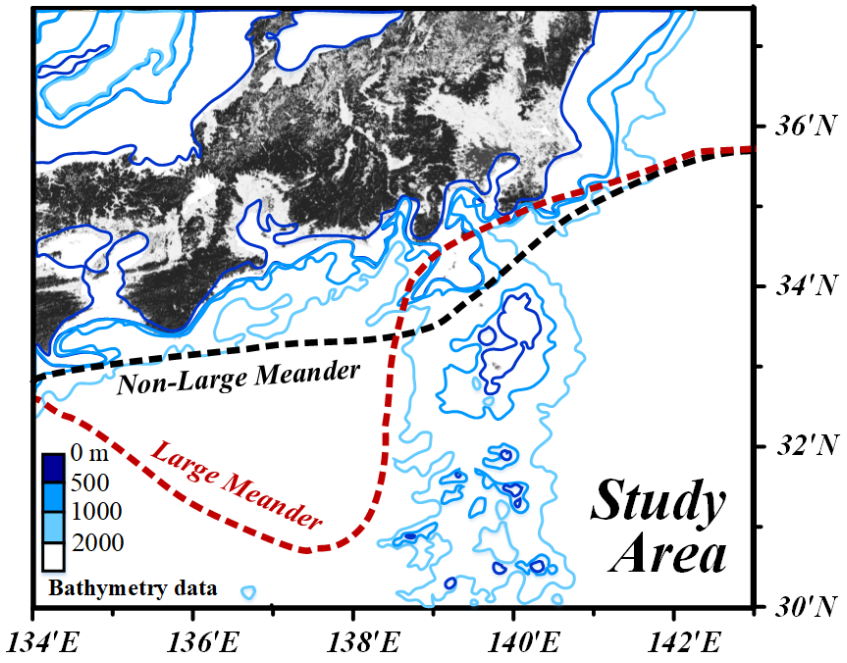

Figure 2.1 Typical Kuroshio paths overlaid on bathymetry from ETOPO2 (colors; deep blue 0 m to white over 2000 m). Black dotted line defines a non-large meander and red dotted line is a large Kuroshio meander.

2.2. Effect of Large Kuroshio Current Meander

2.2.1. Effect on economic aspects

There are a few key impacts of an unusual Kuroshio current meandering. In terms of economic aspect, the abnormal trajectory has caused hazardous environment to the south of Japan and often unpredictable environment for the local fishing grounds and marine ecosystem

(Morioka, Varlamov, and Miyazawa 2019). Firstly, there are affected areas in fishery and logistics industry in Figure 2.2. (1) At offshore of Wakayama prefecture, the stock of Bonito (Katsuo) has been depleted since 2016 according to NHK News on June 15, 2022. (2) At Owase and Shima city in Mie Prefecture, the stock of Yellowtail has become unfished since 2016 and the catch of Abalone has sharply declined by one third compared to 2017 and 2021 as reported by NHK News June 09, 2022. (3) In accordance with the Ministry of Agriculture, Forestry, and Fisheries (MAFF) statistics, in Figure 2.2b indicates since 2010, the annual catch of Sakura shrimp in Shizuoka prefecture has been greater than 900 tons, but it declined significantly to 320 tons in 2018. Since then, it has never been higher than 300 tonnes. (Shizuoka Prefectural Research Institute of Fishery; *https://fish-exp.pref.shizuoka.jp/02fishery/2-5.html accessed on July 20, 2022*). Further, in the Shizuoka prefecture, the catch of Shirasu has often exceeded 10,000 tons in 2010, but it dropped sharply to approximately 5100 tons in 2017. Since then, it has never been more than 7,000 tons; in 2018 with 5827 tons, in 2019 with 4980 tons, and in 2020 around 6100 tons. (Shizuoka Prefectural Research Institute of Fishery; *https://fish-exp.pref.shizuoka.jp/02fishery/2-5.html accessed on July 20, 2022*). (4) The economic route for ships to navigate would be changed due to the lager Kuroshio meander, and fuel efficiency would be deteriorated through a further distance to coast as stated by NHK News June 09, 2022. Meanwhile, (5) In Chiba prefecture's southwest, the catch of Bonito has recently increased greatly. For the past five years, there has been a noticeable shift in the location of Bonito fishing ground. Many environmental indicators also suggested that the anomalous Kuroshio flow is already having severe economic damage in the South of Japan (Ho et al. 2021).

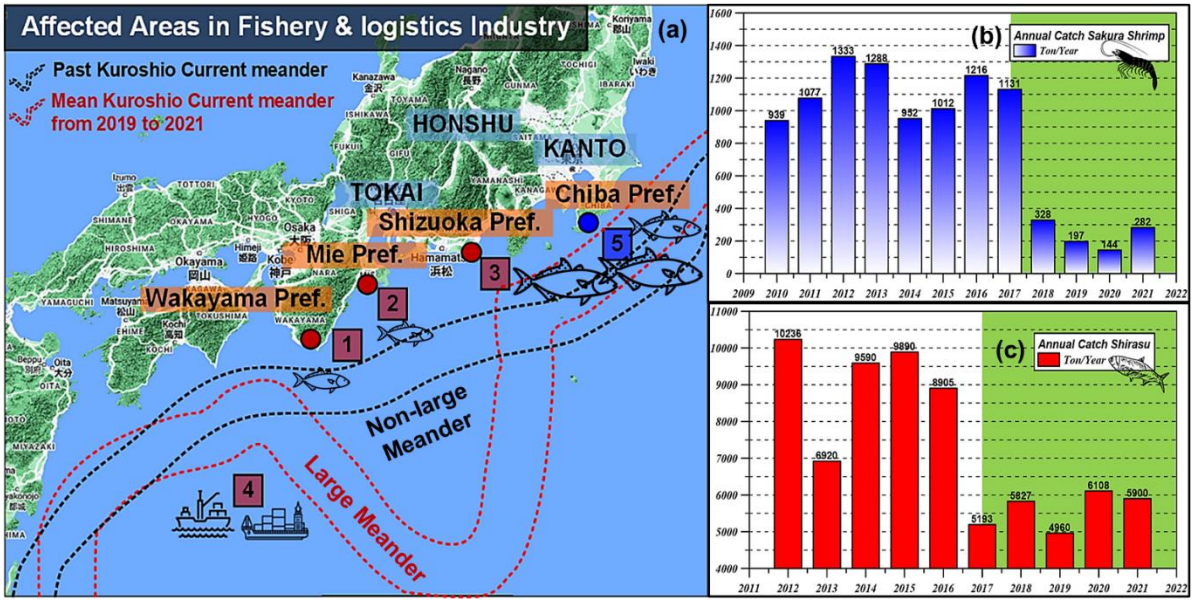

Figure 2.2 Affected areas in fishery and logistic industries. (a) geographical locations; 1. Wakayama Prefecture, 2. Mie Prefecture, 3. Shizuoka Prefecture, 4. Chiba Prefecture, and 5. The route of commercial Ships, (b) Annual catch "Sakura Shimp" in Shizuoka Prefecture, (c) Annual Catch "Shirasu" in Shizuoka Prefecture.
Source: b, c graphs were obtained by Shizuoka Prefectural Research Institute of Fishery.

2.2.2. Effect on marine ecological aspects

In terms of the marine ecosystem (Figure 2.3), the seaweeds, which are called Amano and Hijiki, provide important ecosystem functions, have disappeared rapidly in 2020 and 2021 in Wakayama's coastal sea, respectively. The result of the disappearance could become oligotrophic conditions disrupting the primary food chain and severely damaging coastal areas. Some researchers said that the cause is the increase in sea temperature around Wakayama's sea due to either the large KCM or climate change (KanTere 8 News July 22, 2021).

Figure 2.3 Affected areas in marine ecosystem. (a) geographical locations; 1. South coastal area in Wakayama Prefecture, 2. Southwest coastal line in Wakayama Prefecture, (b) Amamo prior to 2017 and thereafter in 2020, and (c) Hijiki prior to 2017 and thereafter in 2021.
Source: Photos obtained by KanTere 8 News July 22, 2021.

2.2.3. Effect on climatic aspects

Regarding climate change aspect, there are two issues. Firstly, the sea level rises from Tokai to the Kanto coast where the close approach of the warm Kuroshio path, may cause extraordinary damage in combination with storm surge induced by typhoons and low-pressure systems (Figure 2.4). As a result of it, in the Tokai region, the tide level will be 10 cm to 20 cm higher than usual due to the influence of large warm Kuroshio meandering

(Sakajo, Ohishi, and Uda 2022). Furthermore, in October of 2019, the strong typhoon HAGIBIS came through the area where the large Kuroshio meander occurred, and the tide level at Shimizu Port reached as the highest record of roughly 170 cm (Figure 2.4a; Number 1 and 2.4b). A post-field survey (Jeon et al, 2020) revealed that the anomaly contributed to the inundation damage in Shimizu port's wharf facilities (Figure 2.4c). Secondly, the abnormal trajectory led to locally varying effects such as a warm sea temperature and high humidity in the air around the Kanto region (Figure 2.4a; Number 2). Sugimoto, Qiu, and Schneider 2021 showed that the influence of the large Kuroshio meander affects the region becoming hotter and hotter in summer, while Nakamura, Nishina, and Minobe 2012 estimated that the Kanto district becomes easier to snow in winter. Therefore, the south of Japan has experienced an unexpected environment due to the irregular path of the Kuroshio, which has localized climatic consequences.

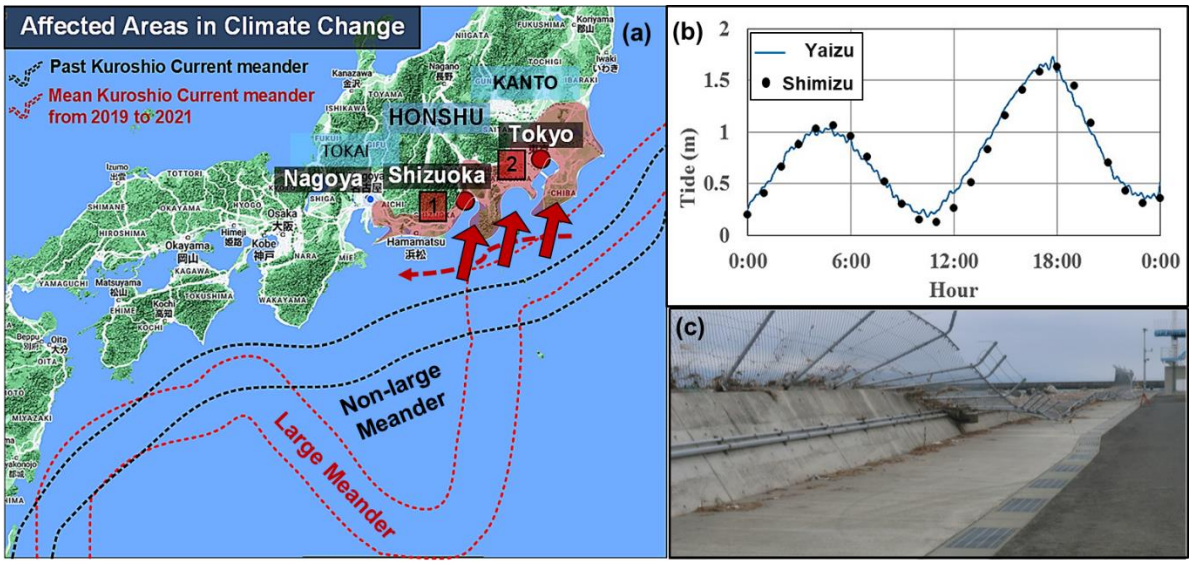

Figure 2.4 Affected areas in climate change. (a) geographical locations; 1. Shizuoka Prefecture, and 2. Kanto region, (b) The tide level in Yaizu and Shimizu port, and (c) Damage situation in Shimizu Port- Falling Fence.

2.3. Materials

2.3.1. Data access

The Kuroshio current meander in 2016 and in 2021 was analyzed using data assemble based on the remote satellite image, in-situ observational, and model data. Monitoring the impact of the each Kuroshio current and identifying the various responses of the upper ocean variables were both feasible with the use of the combined observational and model data. Some surface oceanic data are separated into three parts: (1) Model data; sea surface temperature

(SST) and Phytoplankton bloom (PB) presented by Chlorophyll a (2) Satellite data; sea level anomaly (SLA) with geostrophic current velocity (GV) representing the KCM.

- **Sea Surface Temperature**

  Since December 30, 2015, the CMEMS has been providing a global physical analysis and coupled forecasting product with the quality identifier *GLOBAL_ANALYSISFORECAST_PHY_CPL_001_015*. This product is made up of 3D global average temperature and 2D daily global average fields of sea surface height, bottom temperature. The daily predictions are generated with a combined atmosphere-ocean system, which results in a mean interpolated to a regular 1/4-degree latitude-longitude grid and 43 vertical levels retrieved by sea water potential temperature.

- **Phytoplankton Bloom**

  GLOBAAL_ANALYSIS_FORECAST_BIO_001_028 is the name of a high-quality product for analyzing and predicting global biogeochemistry. This product is provided on a normal 0.25° 0.25° grid with 50 vertical levels over the world's oceans. It contains daily fields of primary production, chlorophyll, pH, and surface partial pressure of carbon dioxide in addition to nitrates, phosphates, silicates, iron, dissolved oxygen, and dissolved iron. Specifically, in the worldwide ocean, the modelled chlorophyll fields displayed significant correlations with satellite data and BGC-Argo measurements (correlation coefficient 0.81, RMSD 0.59; *https://marine.copernicus.eu/ accessed on 04 March 2021*).

- **Sea Level Anomaly and Geostrophic Velocity**

  Since April 2019, the AVISO (Arching, Validation, and Interpretation of Satellite Oceanographic) has made public the SLA data, also known as the near-real-time-global-altimetry dataset (version NRT 3.0 exp), which can be used to detect the Kuroshio current and mesoscale oceanic eddies. In the north of the equator, a cyclonic (anticyclonic) eddy can be identified by the contours of maximum −1.00 (+1.00) m above the mean surface level (MSL) with divergence (convergence) motion and anti-clockwise (clockwise) rotation. A cyclonic (anticyclonic) eddy is identified with the contours of maximum −1.00 (+1.00) m above the mean surface level, divergence (convergence), and anti-clockwise (clockwise) based on the

north of the equator. The meridian (V) and zonal (U) components of GV (m/s) are used to infer magnitude and direction at the ocean's surface flow. (*http://www.aviso.altimetry.fr/en/home.html accessed on 08 June 2022*)

2.4. Kuroshio Current in 2016 and 2021

2.4.1. Sea level anomaly and geostrophic velocity

Figure 2.5 indicates the distribution of sea surface elevation of KCM is produced by SLA and GV on October 10, 2016 and 2021, respectively. The path of Kuroshio extension influences the ocean heat, and the geostrophic current, moving at a speed of about 1 m/s (indicated by the red arrows), and the cyclonic (anticlockwise; -value, blue shades) and anticyclonic (clockwise; +value, red shades) eddies. The non-large meander moves from the west to the east due to the geostrophic force pushing toward the east in 2016 (Figure 2.5a). In recent years, the large meander is farther from Wakayama prefecture than 2016. Forces pulling it eastward weaken, and its flow changes westward with the motion of a massive cyclonic eddy, keeping the large meandering going for a long time (Figure 2.5b). However, to well understand the process behind the emergence and development of the KCM, it needs to require further analysis.

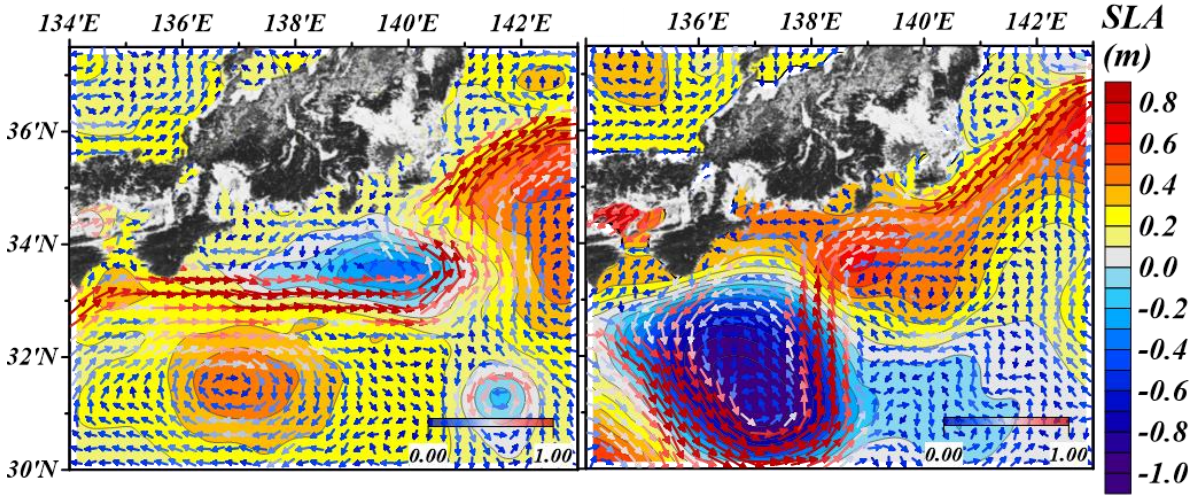

(a) October 10, 2016 (b) October 10, 2021

Figure 2.5 Change of Kuroshio current pathway; (a) October 10, 2016 and (b) October 10, 2021. Kuroshio mainstream (red arrows; above 1 m/s) provided by the AVISO dataset indicating cyclonic (counterclockwise; -value, blue shades) and anticyclonic (clockwise; +value, red shades).

2.4.2. Sea surface temperature

On October 10, 2016, the small meander moves through the powerful eastward force,

then the sea temperature appears a large difference in the boundaries in the southern coastal area at Wakayama prefecture (Figure 2.6a). When the KCM approaches Kanto coast in 2021 maintains a far distance from Wakayama prefecture and the sea temperature anomalies is small (Figure 2.6b). On the other hand, in Shizuoka prefecture the KCM directly affects the offshore then the SST increase. The changes in the anomaly of SST could explain that the ecological habitat and fishing area may have shifted in Wakayama and Shizuoka Prefecture.

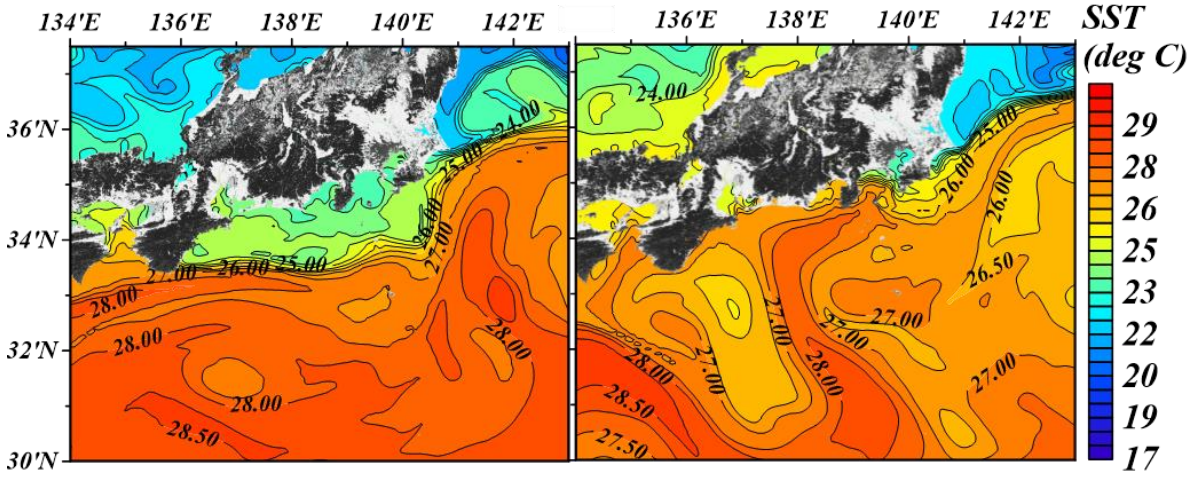

(a) October 10, 2016 (b) October 10, 2021

Figure 2.6 Change in sea surface temperature; (a) October 10, 2016 and (b) October 10, 2021.

2.4.3. Sea surface phytoplankton bloom

In terms of Chl-a concentration in the sea surface, on October 10, 2016 the NPO is influenced by the oligotrophy zones such as poor nutrients (Figure 2.7a). However, in October 10, 2021, the oligotrophic surface ocean condition changed above 0.30 mg/m^3 to the sea surface. It was due to the mesoscale cyclonic eddy induced by the large meander, and particularly in the area near the coast of Chiba prefecture (Figure 2.7b). Further, unlike the non-larger meander, the large meander closely approached the coastal line of south of Japan and proceeded northward, the large-scale phytoplankton bloom occurred in the area where the temperature difference of more than 4 degrees (change orange to sky blue sharply in Figure 2.6b) occurred due to direct ocean convection. The coast area is also affected by the confluence of the warm Kuroshio current and the cool Oyashio cold current inducing a nutrient-rich environment. This spatial distribution of Chl-a could provide evidence for why the fishing grounds changed more eastward than in 2016.

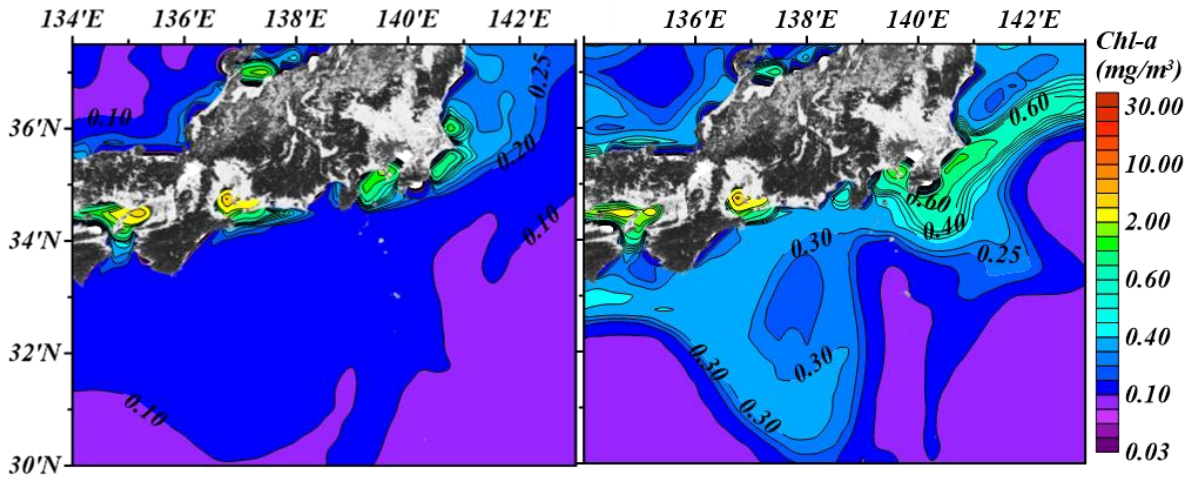

(a) October 10, 2016 (b) October 10, 2021

Figure 2.7 Change in phytoplankton bloom represented by the concentration of chlorophyll a; (a) October 10, 2016 and (b) October 10, 2021.

2.5. Summary

Since August 2017, the reoccurrence of the large Kuroshio meander off the south of Japan was observed from satellite altimeter (AVISO) measurements and CMEMS model data to identify the potential impacts along the Kuroshio path. Chapter 2 has some key findings as below,

- The non-large KCM and large KCM cases were introduced for Research Background.
- A large KCM affected the economic, marine ecological, and climatic aspects on the coast and offshore of the south of Japan.
- A comparison of two different years (2016 and 2021) revealed that the Kuroshio forced high temperature, salinity, and velocity water to the sea close to Japan, and their features affected ocean variables within a boundary of Kuroshio mainstream.
- In 2021, the motion of massive cyclonic eddy induced by the large KCM, generating ocean vertical convection, small SST anomaly and high Chl-a concentration in the sea surface.
- In 2021, the confluence area confirmed by the large anomaly SST in 2021, it contributed the high concentration nutrient area.
- These spatial distributions are a key predicting and protecting marine resources such as a shift of fishing ground and ecosystem. The identified relationship would be beneficial for establishing oceanic background to further studies.

CHAPTER 3. SURFACE OCEAN RESPONSES TO HAGIBIS

3.1. Introduction

When compared to other regions, the NPO has the greatest frequency of tropical cyclones. Typically, 16.5 storms occur in the area each year, with 6.3 (or 38%) being classified as super typhoons (Chan 2005), defined as a storm with maximum sustained winds of 150 mph (241 km/h), a low central pressure of 910 hPa, and accompanied by high precipitation and storm surges. The ocean response to super typhoons has been a frequently discussed topic, given its significance for climate change, environmental unpredictability, and the conservation of ocean resources. Numerous scientific studies have found that high winds, via the vertical surface entrainment process, cause modifications in ocean variables including temperature and salinity directly beneath storms. Vertical stirring and upwelling processes are triggered by the energy transmitted from the atmosphere to the ocean. (J. F. Price, Sanford, and Forristall 1994; W. Wang and Huang 2004; Liu, Wang, and Huang 2008). Vertical mixing is mostly responsible for the change in surface ocean variables in the open ocean, whereas the Ekman upwelling plays a significant role in the underwater (J. F. Price 1981; Jullien et al. 2012). At the sea surface in the north of the equator, decreases in sea surface temperature (SST) (Lin et al. 2003), high concentrations of sea surface salinity (SSS) (Zhang et al. 2016), and deepening of mixed layer depth (MLD) (Yue et al. 2018) are generally more observable on the right-hand part of the trajectory of typhoons. Especially, SSS typically increases through vertical mixing and upwelling, whereas typhoon-induced heavy rainfall decreases SSS on the left-hand part of typhoons' path (Han Zhang et al. 2020c). In addition, in the initial shallow MLD condition, typhoon-induced vertical entrainment from warm and low-salinity surface water to cold and high-salinity water is easier than in the deeper MLD (J. F. Price 1981; Vincent et al. 2012). In the underwater layer, the initial deep MLD induces higher temperature and salinity anomalies than the shallow MLD.

Various observational approaches and technological advances are enhancing our insights of the upper ocean's reactions to typhoons and marine conditions. The physical oceanic factors involved in the interaction between typhoons and regional seas have been studied using observation platforms like buoys and moorings since the 1940s (Steinberg et al. 2001), satellite

remote sensing since the 1980s (Groom et al. 2019), and Argo floats since the 2000s (Chai et al. 2020). However, there are limitations to ocean technology, such as data gaps such as weekly, five-day, and three-day mean datasets and missing values owing to cloud covering (Banzon et al. 2016; Groom et al. 2019). Six-hourly wind speed and daily ocean variables in surface data are currently available from the CMEMS platform owing to a blend of multi-observational platforms and oceanic and atmospheric models. (Le Traon et al. 2019). However, there is still a lack of operational regional-scale application and verification from global data.

The unprecedented Kuroshio current meander (KCM), which flows from low latitudes to offshore southern Japan and affects SST, SSS, water density, MLD and mesoscale eddies, is another feature of the NPO as shown in Chapter 2. In particular, the MLD and thermocline are frequently deeper in the Kuroshio area than in the surrounding ocean water (X. Liu and Wei 2015), which confines the typhoon-generated SST decrease. Wu et al. 2008 used satellite remote sensing data and model simulation to find that Typhoon NARI (2001) caused no substantial SST decrease in the Kuroshio stem, where the thermocline depth is 80-100 m, whereas NARI generated considerable decrease in SST in the shelf zone north of the Kuroshio, where the thermocline depth is 20-30 m. especially, in the cyclonic eddy region. However, depending on typhoon's moving speed, further research are required to understand typhoon's effects in combination with the KCM at six-hourly or daily level.

To better understand the relationship between various upper marine physical variables and distinct environmental characteristics, Chapter 3 investigated the cause analysis of physical processes via changes in SST, SSS, and MLD at the surface of the ocean in response to the impact of 2019 super typhoon HAGIBIS under the large KCM condition.

3.2. Target Event and Region

3.2.1. Super typhoon HAGIBIS

Figure 3.1 displays the best HAGIBIS track provided by the Japan Meteorological Agency (*https://www.data.jma.go.jp/fcd/yoho/typhoon/index.html accessed on 25 March 2022*). Typhoon factors are derived based on the following data shown in Figure 3.1a: typhoon central location, date, estimated central pressure (hPa)/maximum sustained wind speed (m/s), and the estimated radius of the storm wind zone (SWZ), where a wind speed of 25 m/s or more. HAGIBIS was the strongest tropical cyclone in 2019, and was classified as a category five storm with a maximum sustained winds of 160 mph (260 km/h) in the open ocean.

3.2.2. Study area

As can be seen in Figure 3.1b, the study region is bounded by the central of the HAGIBIS track and the KCM, which are located at longitude 134°-143°E and latitude 30°-37.5°N, respectively. During the period of this typhoon, the environment off the coast of the South Japan archipelago was characterized by a daily big KCM derived by the Japan Coast Guard (JCC, red dotted line; *https://www1.kaiho.mlit.go.jp/KANKYO/KAIYO/qboc/ accessed on 01 April 2022*). The maximum sustained wind speed was reduced from 45 to 35 m/s, central pressure was weakened from 945 to 965 hPa passing through south of Japan, and another important typhoon factor was the translation speed (TS; km/h), which increased when HAGIBIS approached the Japanese archipelago (from 16.7 to 58.2 km/h) with a wide SWZ (radius of storm wind; from 324 to 296 km). In terms of time, HAGIBIS had a continuous impact on the study area for 30 hours.

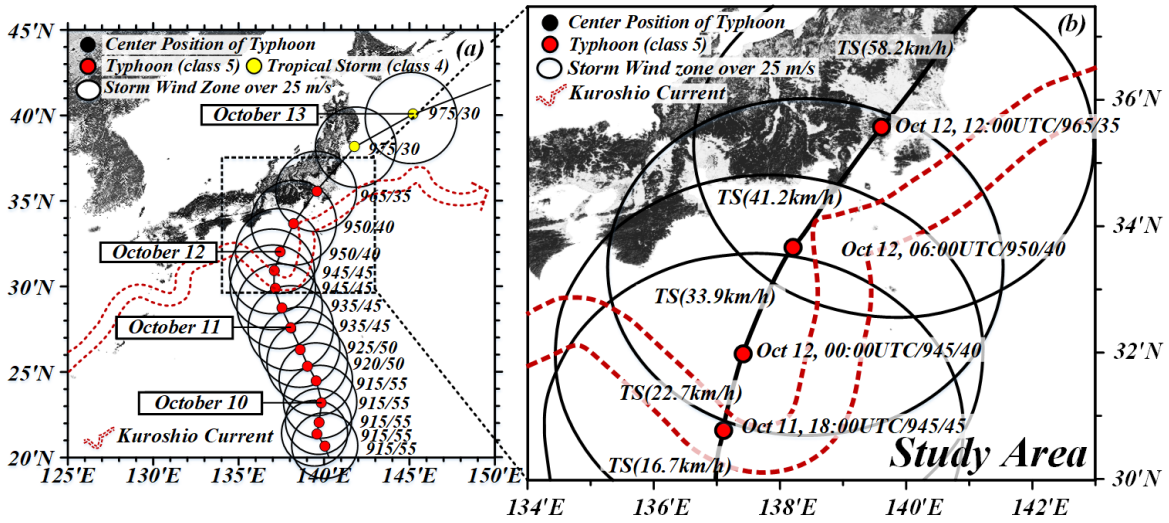

Figure 3.1 Six-hourly HAGIBIS best track on October 09-13, 2019 obtained by JMA and daily Kuroshio current meander (KCM; red dotted line) provided by JCC. (a) at the wide area; including the typhoon central location with intensity (dots in red to yellow), the radius of a storm wind zone (SWZ; black circles), date (month/day), and central pressure (hPa)/maximum sustained wind speed (m/s), and (b) at a boundary of the study area; including same components as (a) and adding time (UTC) and translational speed (TS; km/h), respectively

3.3. Multi-source Surface Observational and Model Data

3.3.1. Wind product and estimated typhoon effects

To evaluate the effect of HAGIBIS on the open ocean, the wind stress power (P_w), which causes the breaking of stratified layers forced by vertical wind stirring in an upper ocean, and

an Ekman pumping velocity (EPV; $\times 10^{-5}$ m/s), which can drive the upwelling of temperature, salinity, and water density from a underwater layer to an upper ocean layer were calculated as the following;

- **Wind speed and wind stress**

  Wind near the ocean's surface is a crucial parameter for several applications, considering monitor of marine disasters, climate change output, water mass structure, and statistical weather forecasting (Chelton et al. 2004; Rodríguez et al. 2019; Bôas et al. 2019). Considering the limitations of conventional ocean surface wind estimate techniques (ships and buoys; (Fang et al. 2017)), remote sensing observations have developed as low-cost approaches (Bourassa et al. 2019). The link between ocean surface wind and sea surface harshness, which reflects the emissive and reflective qualities of the sea surface, is the main indicator of remotely measured ocean surface wind (Bôas et al. 2019). According to previous review study (Amani et al. 2022) (2022, ocean part1), five remote sensing technologies have been used often to estimate wind speed; microwave radiometer, GNSS-R (Global Navigation satellite systems reflectometry), SAR, scatterometer, and HF radar. Among them, the global blended mean CMEMS wind product consisted of six hourly averaged fields for sea surface wind speeds and wind stress, including zonal/meridional wind components as well as wind stress curl. First, the scatterometers on-board ASCAT-a and -b were used to derive the NRT L4 product for sea surface wind variables. Second, the SSMIS radiometer on the F16, F17, F18, and F19 satellites acquired remote wind speeds. Third, a WindSat radiometer on the Coriolis spacecraft measured wind velocities and directions. The blended dataset was executed at 00UTC, 06UTC, 12UTC, and 18UTC, with a longitude and latitude resolution of 0.25° over global ocean (*https://marine.copernicus.eu/ accessed on 08 June 2022*).

- **Equations**

  The P_w in the upper ocean layer is a result of the wind-generated kinetic energy flux ($\mathrm{W/m^2}$) used by Pan et al. 2018;

$$P_w = \tau_0 U_{10} = \rho_{air} C_D U_{10}^3 \quad (1)$$

where τ_0 is the wind stress at the surface water ($\tau_0 = \rho_{air} C_D U_{10}^2$); U_{10} is the wind speed at 10 m height on the mean sea level provided by the CMEMS dataset; ρ_{air} is the density of air ($\approx 1.22\ \mathrm{kg/m^3}$ at 20 ℃); and C_D is the drag coefficient.
The EPV is calculated using the quantitative wind stress curl, defined in Price, Sanford, and Forristall 1994;

$$EPV = Curl(\frac{\tau_0}{f \times \rho_w}) \quad (2)$$

where f is the Coriolis parameter ($f = 2\Omega \sin \phi$); Ω is Earth's rotation vector (2π radians per sidereal day); ϕ is the latitude; ρ_w is the density of seawater (1025 $\mathrm{kg/m^3}$).

3.3.2. Sea surface ocean variables

Monitoring the effects of typhoons and identifying their effects on the upper ocean variables were used by the combined observational and model data. The surface oceanic and meteorological data are divided into three types: (1) Model data; SST, SSS, and MLD (2) Satellite data; SLA with GV represents the KCM. (3) Radar data; daily cumulative rainfall.

- **Sea Surface Temperature and Salinity, and Mixed Layer Depth**
  The quality of *GLOBAL_ANALYSISFORECAST_PHY_CPL_001_015*, which is the global physical analysis and coupled forecasting product provided by the CMEMS, is composed of daily 3D average temperature and salinity, zonal and meridional velocities, as well as daily 2D average fields of sea surface level, bottom temperature, and MLD since 30 December 2015. The daily forecasts are produced using a coupled atmosphere-ocean system, resulting in a mean interpolated to a regular 1/4-degree latitude-longitude grid and 43 vertical levels extracted by sea water potential temperature and seawater salinity. The depth of the mixed layer is generally calculated using a hydrographic method conducted by water property measurements with two parameters of temperature and water density shift from a reference value on the surface. For this study, the density threshold as Δθ=0.8 ℃ decrease was used as a reference temperature by Kara, Rochford, and Hurlburt 2000.
- **Sea Level Anomaly and Geostrophic Velocity**

To identify the KCM and mesoscale oceanic eddies, the SLA data, also known as the near-real-time-global-altimetry dataset (version NRT 3.0 exp), provided by AVISO (Arching, Validation, and Interpretation of Satellite Oceanographic) has been available since April 2019 to present. A cyclonic (anticyclonic) eddy is identified with the contours of maximum −1.00 (+1.00) m above the mean surface level, divergence (convergence), and anti-clockwise (clockwise) based on the north of the equator with GV (m/s), which is used by the meridian (V) and zonal components (U) under format for inferring the magnitude and direction at the ocean surface (*http://www.aviso.altimetry.fr/en/home.html accessed on 08 June 2022*).

- **Daily Cumulative Precipitation**

  The tropical rainfall measuring mission (TRMM) precipitation radar (PR) measured the average daily precipitation with gauge calibration as mm units. This dataset is derived from a TRMM multi-satellite precipitation analysis conducted by every three hours at a research-grade level. (TMPA; 3B42 L3 version 7). Data from the Goddard Earth Sciences Data and Information Services Center (GESDISC) is available, and it consists of a 0.25°×0.25° grid covering one daily particle quantity per every 24 h (*https://disc.gsfc.nasa.gov/datasets/TRMM_3B42_Daily_7/summary accessed on 02 May 2022*).

3.3.3. Methodology

Figure 3.2 depicts the study's illustrative step-by-step approach. The three subchapter were as follows:

- **Subchapter 3.4**

  The typhoon effects on the NPO were estimated in terms of P_w and EPV. Firstly, six-hourly wind speed data was validated by JMA data (3.4.1). The visualized spatial distribution shows the magnitude, direction, and impacted area of strong P_w and high EPV every six hours (3.4.2). Then, the comparison in three-day mean wind stress power between All Metop ASCAT and CMEMS data was conducted (3.4.3).

- **Subchapter 3.5**

  To interpret the physical KCM features such as meander and eddies, the AVISO's

KCM was expressed by SLA and GV and validated the KCM by JCC data (3.5.1). Further, the spatial distribution of SLA and GV detected tracking cyclonic and anticyclonic eddies. Then, the three-day mean SSS in comparison with SMAP and CMEMS data is conducted prior to the estimation of surface ocean responses (3.5.2).

- **Subchapter 3.6**

  The response of surface ocean variables was conducted considering SST, SSS, MLD, and daily cumulative rainfall. Further, the values were also conducted to validate the CMEMS model data by in-situ data (3.6.1). The changes in surface physical variables (SST and SSS) could be estimated by where, when, and to what extent the typhoon affects the study area (3.6.2). The following work as cause analysis via daily MLD and precipitation to evaluate other significant evidence (3.6.3).

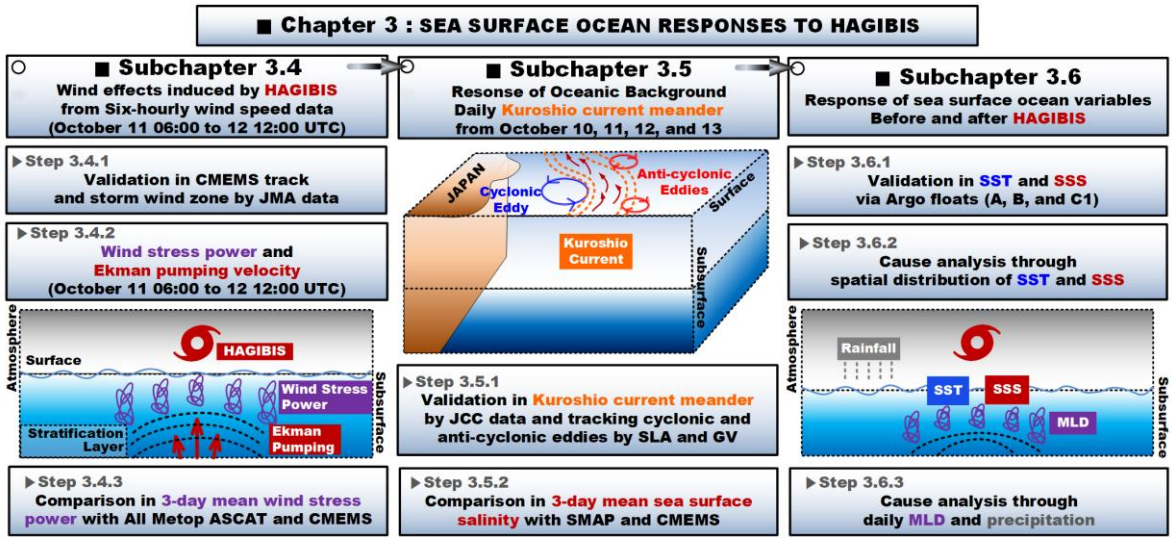

Figure 3.2 Flowchart showing how individual estimated the physical process at the KCM environment of the Northwest Pacific Ocean in response to typhoon HAGIBIS.

3.4. Wind Effects Induced by HAGIBIS

3.4.1. Validation of CMEMS model data by comparison with JMA

Based on the size of SWZs, global CMEMS data was compared to JMA data in Figure 3.3. The JMA provided a SWZ of above 25 m/s using a Himawari-eight geostationary satellite image (Bessho et al. 2016), while the global wind blended data obtained by the CMEMS dataset showed a white lines of 23 m/s. Comparing the two data revealed that the differences between

CMEMS and JMA were approximately 2 m/s. According to the estimated bias difference between in situ and blended wind data, it is in line with Bentamy et al. 2021. Further, Figures 3.3a, b, and d indicated the daily asymmetric typhoon's activities illustrating the different affected areas on the left and right semicircle. However, Figure 3.3c presents that the blended wind speed in CMEMS shows that the spatial distribution is underestimated in nearshore sites (< 50 km in shoreline) because geographical interpolation is conducted close to the shoreline (Abderrahim Bentamy et al. 2021).

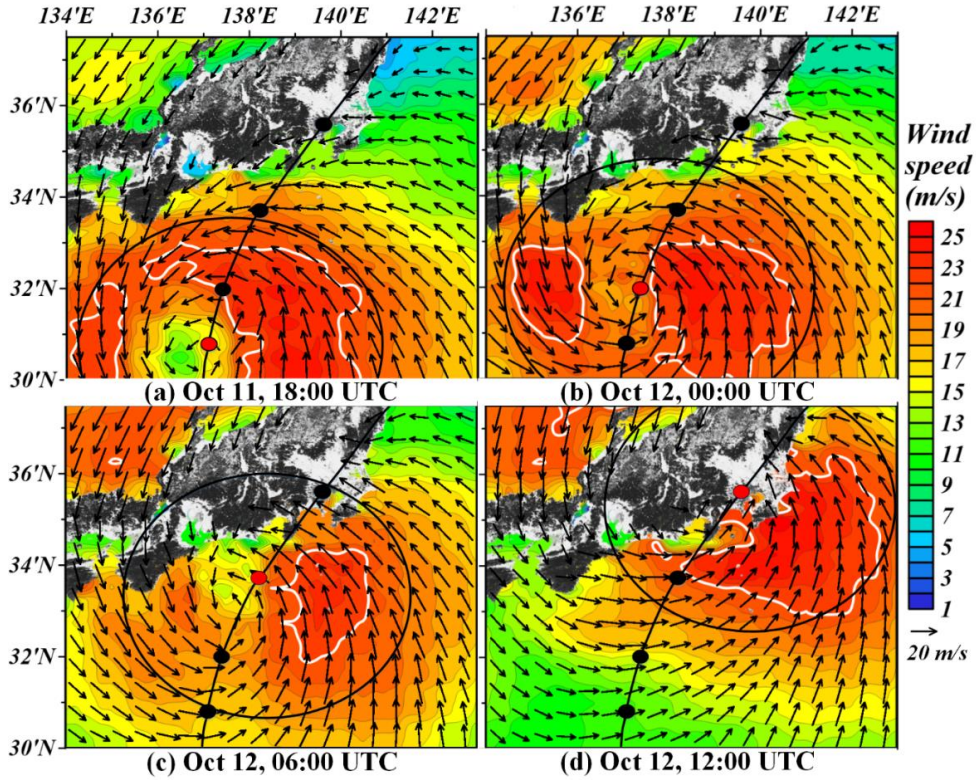

Figure 3.3 Validation of each six-hourly storm wind zone of HAGIBIS; (a) October 11, 18UTC, (b) October 12, 00UTC, (c) 06UTC, and (d) 12UTC, respectively. Black circles indicate JMA (black circles) and white contour is CMEMS data with the typhoon central location according to time.

3.4.2. Wind stress power and Ekman pumping velocity

To evaluate the impact of HAGIBIS on the NPO, Figure 3.4 depicts the spatial distribution of P_w corresponding to the HAGIBIS track. Figure 3.4 shows a more expanded time from October 11, 06 UTC to October 12, 12 UTC compared with Figure 3.3. The strong P_w appears in the study area on October 11, 06 UTC. It can be shown that the strong P_w affects the ocean along the typhoon track, except for the center of the HAGIBIS track (Figure 3.4b). Then, the P_w intensity is sharply reduced on the typhoon's left semicircle, whereas another P_w on the right semicircle continues to have a strong impact (Figure 3.4c and d). When HAGIBIS

entered the study area boundary, the translation speed was slower than when traveling long distances across the ocean (Figure 3.1a), and the movement going straight northward close to Japan became oblique with Japan. In this process, the P_w on the left semicircle decreases faster than on the right-hand part. When the typhoon made landfall on the Japanese archipelago, the value of P_w is weakened due to the nearshore bias (Figure 3.4e). When leaving from Japan, the P_w increased from the right-hand part of the typhoon (Figure 3.4f).

Meanwhile, the physical value of EPV is shown in Figure 3.5; upwelling in red and downwelling in blue contour, respectively. When the HAGIBIS's effect become visible, as shown in Figure 3.5a, the upwelling appears within the SWZ, while the downwelling occurred outside the SWZ. Moreover, the strong upwelling is distributed in the study area along the center location of the typhoon track (5×10^{-5} m/s at maximum value, invisible in Figure 3.5c). The upwelling energy is concentrated at the typhoon's center. When making landfall, as shown in Figures 3.5e and f, the HAGIBIS still have strong upwelling along the typhoon's path.

Note that the influence of the typhoon, the wind stress power was much stronger on the right and left semicircle than on the typhoon's center, whereas Ekman pumping velocity was much higher along the typhoon's center.

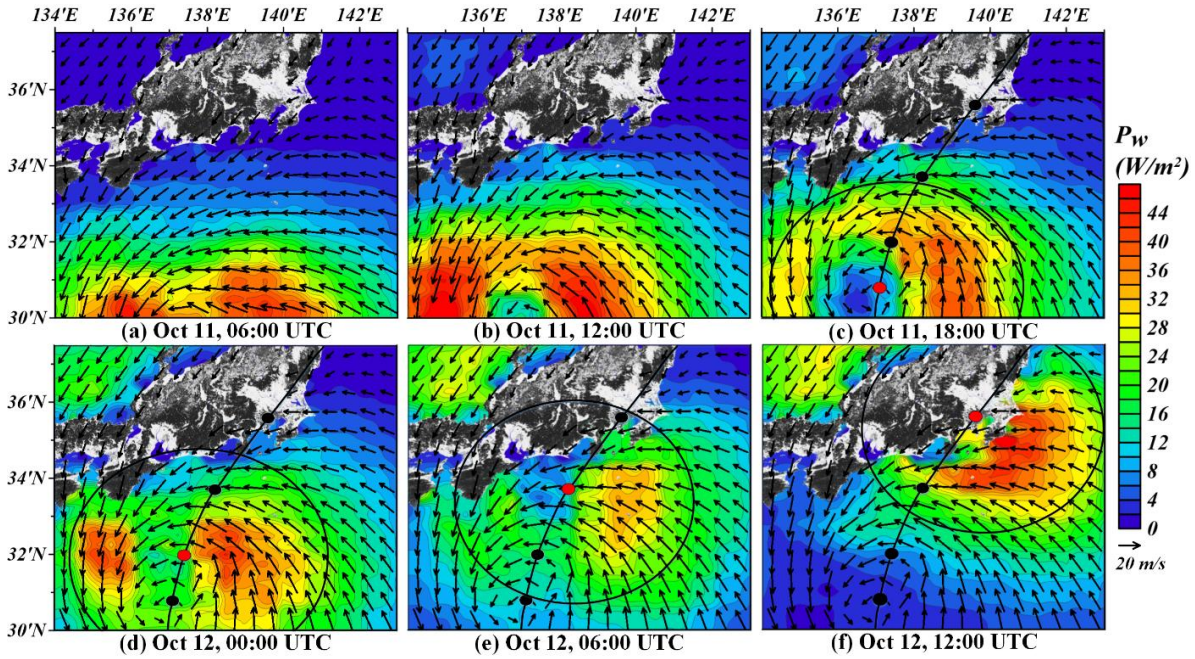

Figure 3.4 Spatial distribution of wind stress power (P_w; $\mathbf{W/m^2}$); (a) October 11, 06UTC, (b) 12UTC (c) 18UTC, (d) October 12, 00UTC (e) 06UTC, and (f) 12UTC with wind speed vectors (black arrows) provided by CMEMS, storm wind zones (black circles), and the typhoon track with the intensity (black line; red dots) obtained by JMA, respectively.

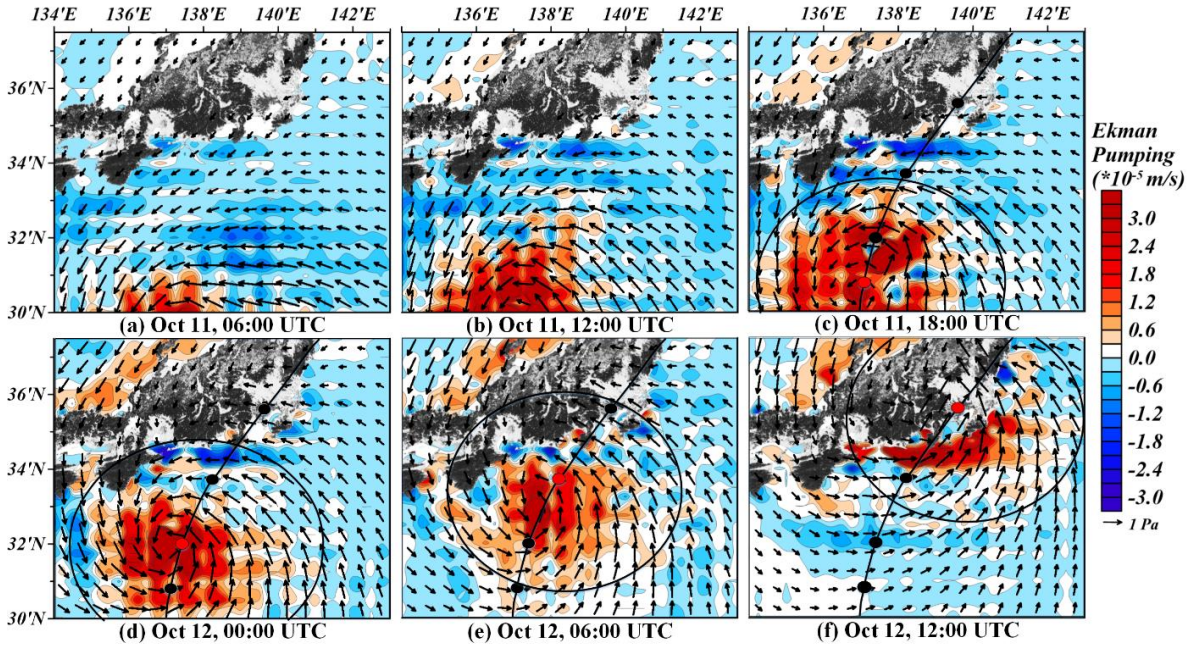

Figure 3.5 Spatial distribution of Ekman pumping velocity (EPV; $\times 10^{-5}\ m/s$); (a) October 11, 06UTC, (b) 12UTC (c) 18UTC, (d) October 12, 00UTC (e) 06UTC, and (f) 12UTC with wind stress vectors (black arrows) provided by CMEMS, storm wind zones (black circles), and the typhoon track with the intensity (black line; red dots) obtained by JMA, respectively.

3.4.3. Missing value: three-day mean wind stress power

When three-day mean P_w provided by six-hourly blended CMEMS wind data is compared to another data using three-day all Metop ASCAT satellite data (Bentamy et al. 2006) in Figure 3.6. The strong left biased P_w (over 20 $\mathrm{W/m^2}$; convergence values) in Figure 3.6a was caused by missing value due to widespread cloud cover in the right-hand side of the typhoon. On the other hand, the CMEMS data has certain benefits having values filled in and the visibility of wind stress power (over 16 $\mathrm{W/m^2}$; divergence values), which leads to occurrence of higher P_w on the right semicircle of the typhoon's trajectory than on the left-hand side as shown in Figure 3.6b. It is in consistent with previous study (Chereskin and Price 2019). The missing values in one of the shortcomings of ocean technology were filled up by combining satellite and CMEMS model data.

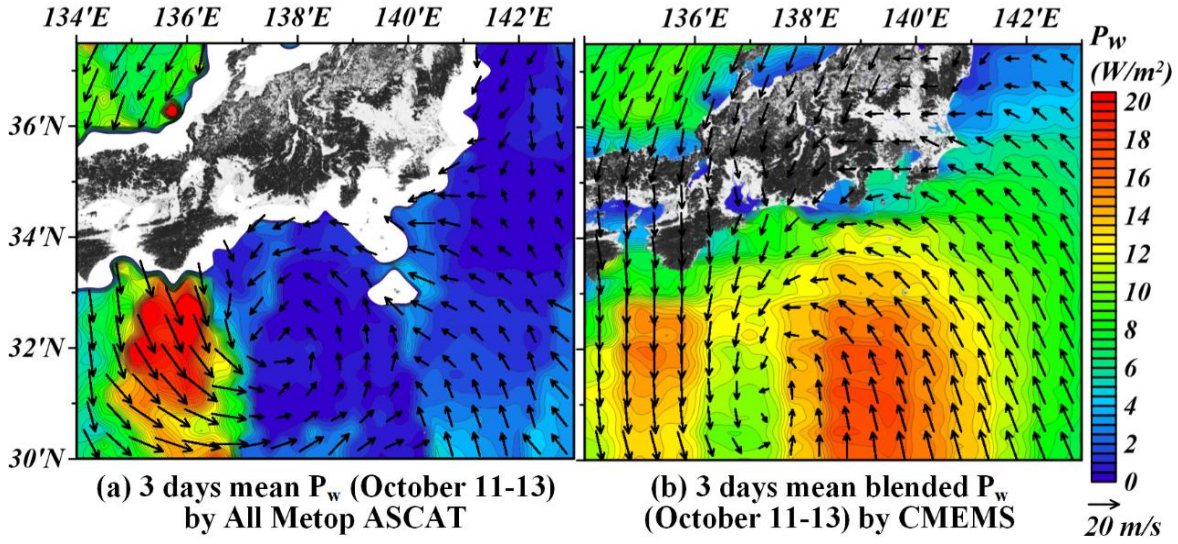

Figure 3.6 Three-day mean spatial distribution of wind stress power (P_w; $\mathbf{W/m^2}$) with wind speed vectors (black arrows) in comparison between (a) All Metop ASCAT and (b) CMEMS data.

3.5. Response of Surface Kuroshio Current

3.5.1. Validation of the KCM & tracking cyclonic and anticyclonic eddies

From existing environmental conditions ahead of HAGIBIS, this study focused on the KCM represented by the SLA and the GV. Figure 3.7 shows that the AVISO dataset's quantitative depiction of the Kuroshio mainstream (red arrows; greater than 1 m/s) agrees with the JCC's estimation for the period 10-13 October. Before the arrival of HAGIBIS (Figure 3.7a), pre-existing cyclonic (counterclockwise; -value, blue shades) and anticyclonic (clockwise; +value, red shades) eddies existed along the Kuroshio's passage, influencing the surface ocean heat transport and generating the cyclonic and anticyclonic eddies. The intensive cyclonic eddy region with a maximum depression of −1.11 m (longitude 137.8°E and latitude 31.45°N) was mainly located inside the KCM, whereas anticyclonic eddies were along and outside the KCM (longitude 139.3°E and latitude 33.7°N with + 0.50 m, and longitude 142.7°E and latitude 35.5°N with + 0.58 m). During the typhoon, the distribution is depicted in Figure 3.7c compared to before the typhoon (Figure 3.7a). The anomalies in the intensity and the extent of eddies were not changed. The mesoscale eddies were less affected by HAGIBIS than the KCM. Sun et al. 2014 suggested that 49 super typhoons moved across 192 cyclonic eddies in the NPO from 2000 to 2008, and the typhoons intensified only approximately 10% of these eddies. This study provides additional evidence of an ineffective effect on the strength of cyclonic eddies, despite the typhoon staying at the strong cyclonic eddy area for two days.

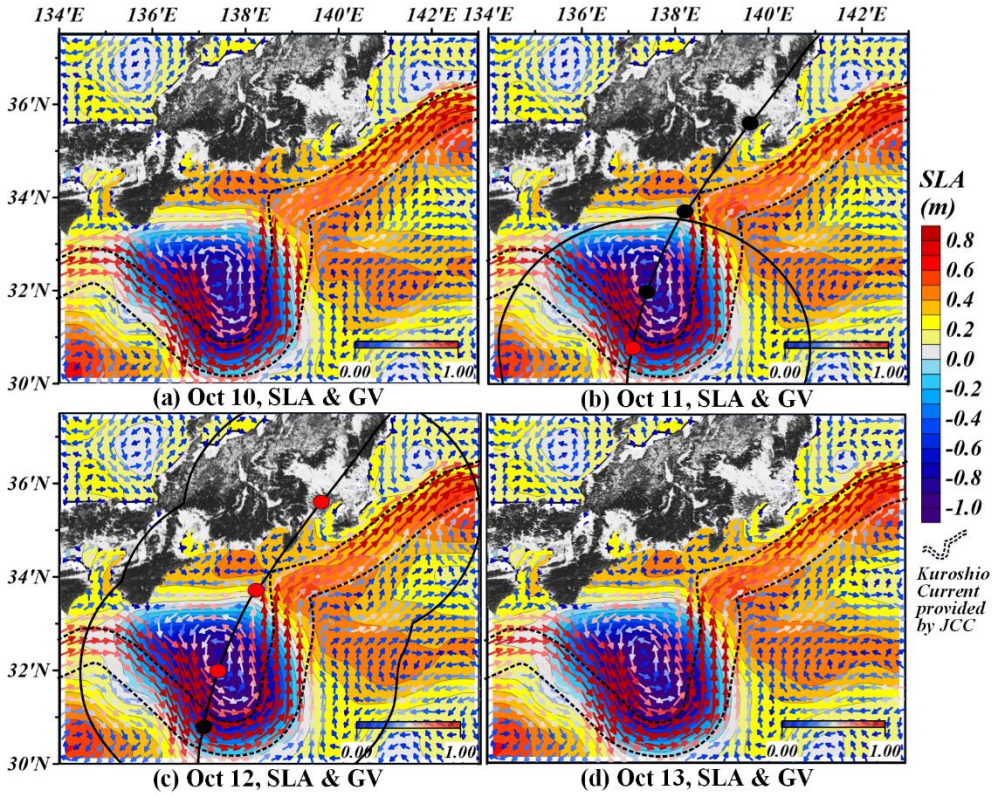

Figure 3.7 Validation of the daily Kuroshio mainstream between AVISO (red arrows) and JCC (black dotted line) data and tracking cyclonic and anticyclonic eddy in terms of SLA; (a) October 10, (b) October 11, (c) October 12, and (d) October 13 with the typhoon track and intensity, respectively.

3.5.2. Missing value: three-day mean sea surface salinity

Figure 3.8 describes a three-day averaged spatial distribution of sea surface salinity. In general, it is difficult to observe the value of sea salinity using individual satellite data, thereby a daily blended SSS L4 in CMEMS is estimated via collaboration with the numerical model (NEMO v3.4 and Met office unified model) and observational data (drifting buoys). Guinehut et al. 2012 have shown that the combined model and observational data provide consistent and complementary ocean values in some regional areas. Figure 3.8a presents a missing data as a result of a white-covered area observed by the Soil Moisture Active Passive (SMAP) satellite remote image, which was accessed on January 20, 2020, with the primary objective is to supply worldwide measurements of soil moisture and freeze/thaw status reading every three days (Du et al. 2018). The missing values was caused by severe weather conditions and cloud cover, whereas Figure 3.9b shows the three-day blended mean SSS, indicating that the value is visible and being filled. Therefore, the SSS provided by the CMEMS platform

demonstrated the viability of investigating the effects of typhoons on the ocean.

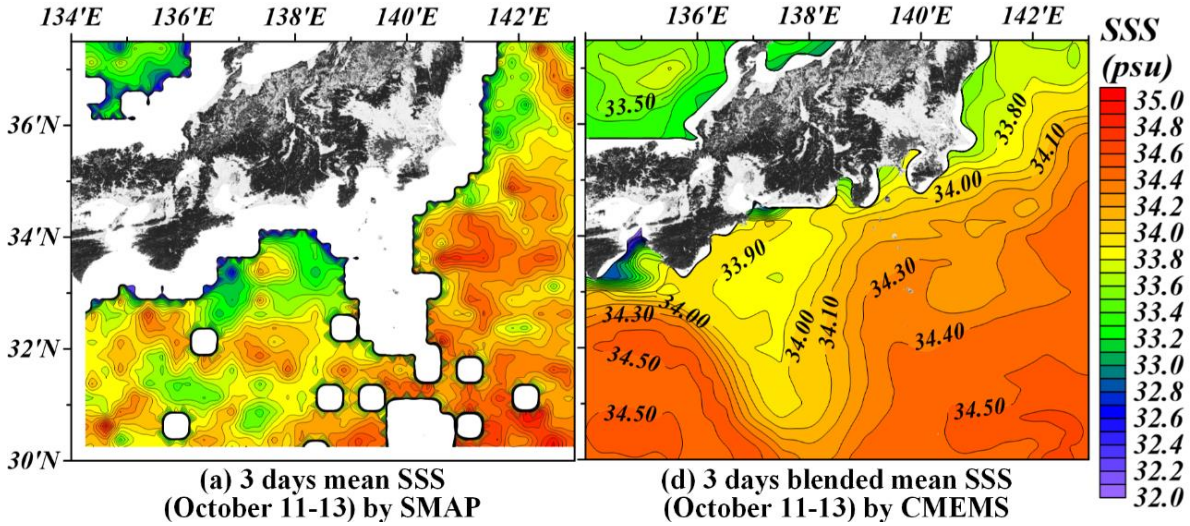

Figure 3.8 Three-day mean sea surface salinity (SSS; psu) distribution at the sea surface in comparison between (a) SMAP and (b) CMEMS data.

3.6. Response of Surface Ocean Variables

3.6.1. Validation of SST and SSS via In-Situ data

To estimate surface ocean variables in response to the typhoon, we validated the CMEMS model data such as SST and SSS compared with in situ data to apply to the study area. Table 3.1 indicates the Argo floats at A, B, and C1 including locations, dates, and values. The comparative result for SST has a difference ranging from −0.11 to −0.06 ℃, and for SSS, a distinction ranging from −0.01 to +0.06 psu. There is no significant difference in value between in situ and CMEMS data.

Table 3.1 Validation of oceanic CMEMS values compared with In-situ data

Factor	Argo floats	Latitude(°N)	Longitude(°E)	Date	In-situ Value	CMEMS Value
SST (℃)	A* 2903367	30.50	135.77	October 10	28.00	27.89 (-0.11)
	B* 2902754	33.58	138.61	October 9	26.47	26.41 (-0.06)
	C1* 2903376	33.72	137.40	October 9	26.17	26.06 (-0.11)
SSS (psu)	A 2903367	30.50	135.77	October 10	34.52	34.46 (-0.06)
	B 2902754	33.58	138.61	October 9	33.95	34.01 (+0.06)
	C1 2903376	33.72	137.40	October 9	34.02	34.01 (-0.01)

* The locations of Argo floats (A, B, and C1) are shown in Figure 3.9a and c.

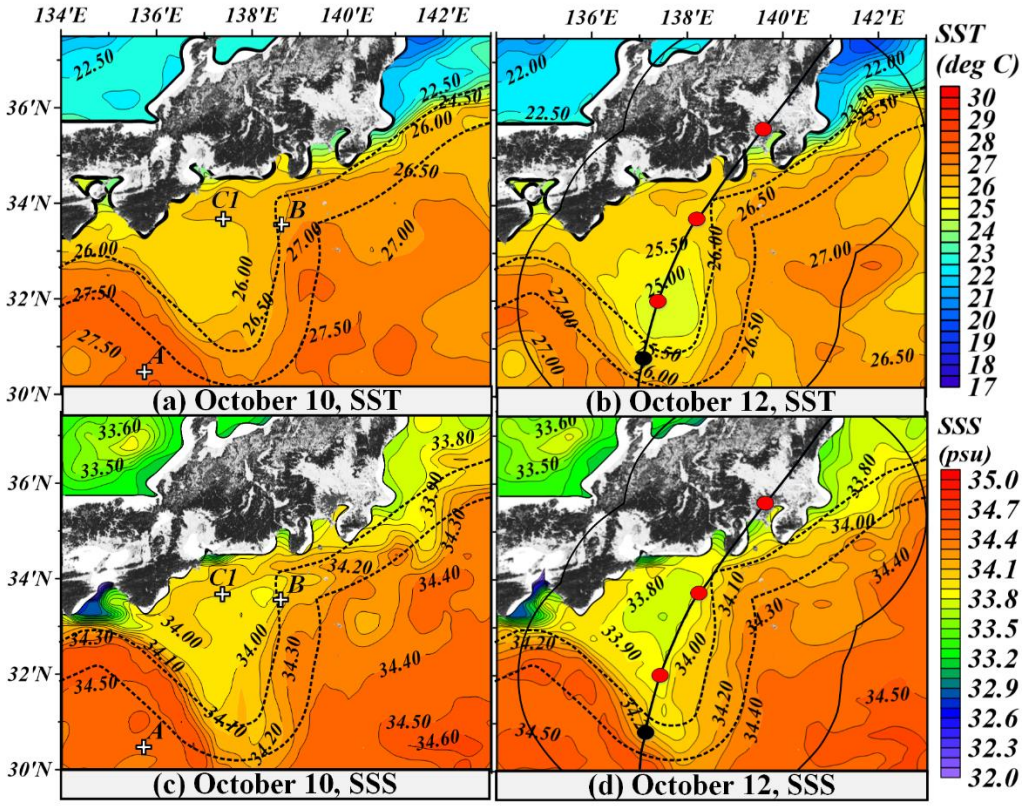

Figure 3.9 Daily surface temperature (SST) and salinity (SSS); (a, c) October 10 and (b, d) October 12, respectively. Black dotted line, black line, and red dotted denote the Kuroshio meander, the storm wind zone, and the typhoon central location according to date. Physical Argo floats (SST and SSS) are shown in points A and B, while a biogeochemical Argo float including SST and SSS as well as dissolved oxygen, nitrate, and chlorophyll a is shown in points C1.

3.6.2. Cause analysis via spatial distribution of SST and SSS

Figure 3.9 shows responses of daily SST and SSS according to the passage of HAGIBIS on October 10 and 12, 2019. The SST was measured at 26.5 ℃ along the strong cyclonic eddy area formed above Kuroshio's path before the arrival of HAGIBIS in Figure 3.9a. During HAGIBIS (Figure 3.9b), it shows a temperature drop down of about 0.5 to 1.5 ℃ inside SWZ in the strong cyclonic eddy area. It caused the cold temperature rising from the deep water to the sea surface due to the combined upwelling effect of the typhoon and the cyclonic eddy. The degree of the SST decrease (more than 2 ℃) is determined not only by the strength and moving speed of typhoons but also by the upper ocean's thermal structure (mixed layer depth and ocean stratificational layer). The thermal structure will be addressed in the next section (Section 3.6.3. Cause analysis via daily MLD and precipitation).

The spatial distribution of SSS in Figure 3.9c shows a low salinity concentration of at least 34.00 psu around the massive strong cyclonic eddy area before HAGIBIS. In general, SSS

normally increases during typhoons due to the upwelling and wind-induced vertical mixing. A previous study (J. Chen et al. 2019) demonstrated that high salinity appeared on the right-hand bias of the fast translation speed of typhoon KAI TAK's track due to upwelling of high salinity water of the bottom. However, HAGIBIS led to less increase the salinity of the surface water in the right-hand part of the typhoon's trajectory, while decrease it in the left side, as shown in Figure 3.9d. It could be due to HAGIBIS's high translation speed characteristics. According to Sun, Vecchi and Soden, 2021 that investigated the influence of typhoon intensity and translation speed on the surface response in the north of the equator. They explained that there were two mechanisms to change SSS induced by typhoons: freshwater intrusion from typhoon-related rainfall, and vertical mixing induced by high winds of typhoons. Based on these mechanisms, they indicated that slower-moving (below mean 9.61 km/h) typhoons concentrated negative SSS anomaly in a relatively small area near the typhoon's center, while faster-moving typhoons showed it in a much larger area with the maximum decrease weaker than that of the slow typhoons. Since this degradation of SSS is caused by the intrusion of freshwater from typhoon-related precipitation, fast-moving typhoons, which have a smaller amount of freshwater supply and stronger vertical mixing driven by higher winds, indicate a weaker negative SSS anomaly. Compared with Sun, Vecchi, and Soden, 2021, when HAGIBIS approached the Japanese archipelago where stronger winds blew, the fast-moving translation speed, which averaged 28.95 km/h, induced a negative SSS anomaly of 0.2 psu on the left semicircle of HAGIBIS's track due to heavy rainfall. However, a little anomaly of SSS occurred around a strong vertical mixing area compared with Sun, Vecchi, and Soden, 2021. It is due to the fast-moving speed of HAGIBIS could not compensate for the degradation of SSS generated by high precipitation, and results in a less drop of SSS on the right semicircle of the typhoon's path. Therefore, HAGIBIS which traveled fast northward and was accompanied by widespread heavy precipitation had a greater impact on the SSS response. To interpret the causes of the change in SSS, the following daily mixing layer depth and precipitation distribution will be addressed.

3.6.3. Cause analysis via daily MLD and precipitation

A relatively shallow MLD formed in a strong cyclonic eddy area, ranging from 30.0 to 36.0 m in thickness, was caused by pre-existing eddy upwelling as shown in Figure 3.10a. In general, anticyclones cause certain MLD to deepen while cyclones cause them to shallow. On October 12, the MLD in the cyclonic eddy area became shallow in an area along the track of typhoon's center, with a value of 25.0 m depth in Figure 3.10b. This lifted-up MLD generated

by the combined Ekman pumping and eddy upwelling could cause a decrease in SST, as shown in Figure 3.9b. In contrast, wind stress power deepens the MLD on the right and left sides of the typhoon parthway in the red contour area over 60 m to a maximum value of 83.6 m depth (Figure 3.10b). In areas of anticyclonic eddies that existed in the south of the KCM, the MLD and the thermocline were further deeper and thicker, respectively. It is due to additional forcing of typhoon-induced vertical mixing.

Figure 3.10c indicates the daily precipitation distribution observed by TRMM radar. Before the arrival of HAGIBIS in Japan, daily rainfall was under 60 mm. The typhoon on the left-bias sides was accompanied by daily heavy rainfall of over 200 mm. Due to the influence of precipitation, some oceanic variables changed. In particular, the SSS reduced within the rainfall zone during and after the typhoon's passage. Ekman pumping induced by HAGIBIS contributed to the increase in the SSS; however, heavy rainfall effectively reduced SSS. This finding is comparable with the results of Sun et al. 2014.

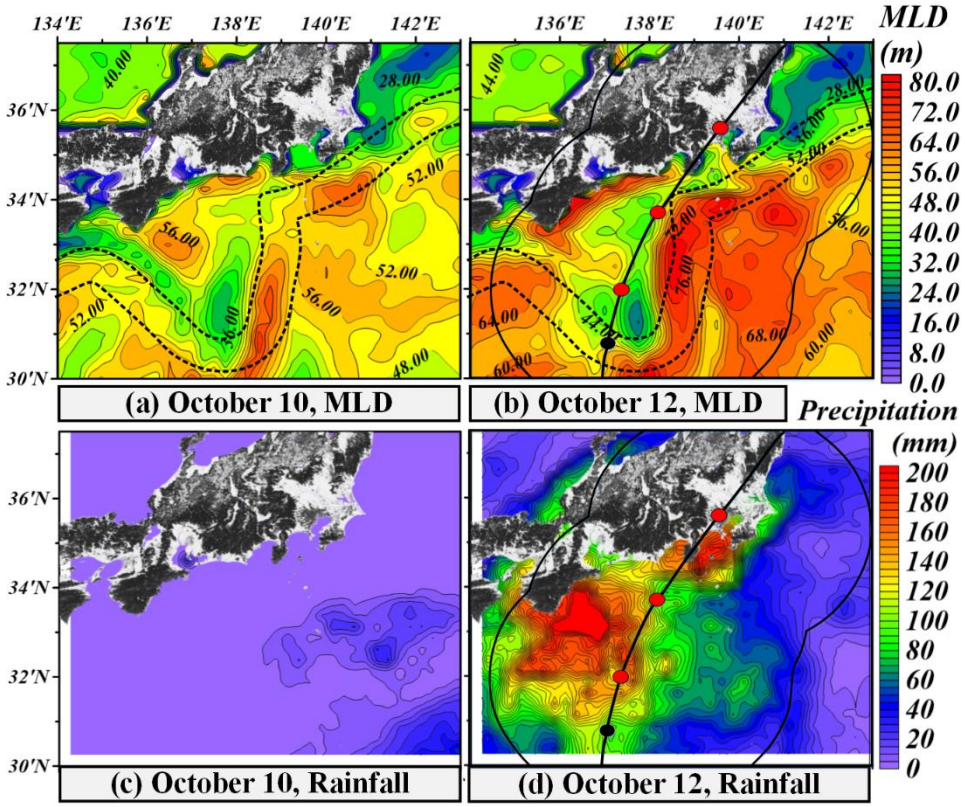

Figure 3.10 Daily mixed layer depth (MLD) and daily cumulative precipitation (mm); (a, c) October 10 and (b, d) October 12. Black dotted line, black line, and red dotted denote the Kuroshio meander, storm wind zone, and the location of the center typhoon corresponding date.

3.6.4. Relationship analysis based on linear regression

Figure 3.11 indicates a relationship analysis of distinct SLA, MLD, and wind effects in the sea surface. Before HAGIBIS, the prevailing oceanic background (longitude 136-138°E) was dominated by a massive cyclonic eddy (mean −0.5 m and maximum −1.1 m; 136.5-138.5°E), Kuroshio path (138.2-139°E), and anticyclonic eddy (135-136°E and 139-140°E) in Figure 3.11a. The pre-existing cyclonic eddy forced eddy upwelling, inducing the MLD was shallower than in other areas (approximately 30 m depth as shown in Figure 3.11b). The magnitude of the eddies' impact on the sea level height is linearly correlated with the extent of MLD (Gaube, J. McGillicuddy, and Moulin 2019). In contrast, the Kuroshio area had an MLD of 70 m, and the anticyclonic area had an average of 55 m. It is due to upwelling and downwelling dynamic of eddies. Anticyclonic eddies are usually associated to positive SSTA (Hausmann and Czaja, 2012), leading to enhanced ocean convection and therefore deeper MLD. The feature of Kuroshio current area agrees with the previous result of X. Liu and Wei 2015 about the deepening depth and the distribution of the Kuroshio current.

During HAGIBIS, the typhoon effects were distinct in each region (Figure 3.11c). HAGIBIS provided strong wind stress power on the left (maximum 35 W/m^2; 135°–136.2°E) and right (over 30 W/m^2; 138°–140°E) semicircles, while had relatively weak stirring power in the center of the typhoon (20 W/m^2) in Figure 3.11c. In contrast, the high EPV (136.2°–138°E) greatly influenced from a minimum of 0.5 to a maximum of $50 \times 10^{-6} m/s$ (Figure 3.11c) in the typhoon center. Along strong cyclonic eddy area, the combined of HAGIBIS's Ekman pumping reached to 25 m MLD, comparing to 30 m depth in the condition of only cyclonic eddy in Figure 3.11b. In contrast, anticyclonic eddies (downwelling) made the MLD deepen (anomaly 15 m deep) in combination with intensive wind stress power on the right and left sides of the typhoon. In summary, the shallow MLD largely affected by the combined effect on strong cyclonic eddy and intensive Ekman pumping while, the deep MLD affected by strong Kuroshio current area and anticyclonic eddy.

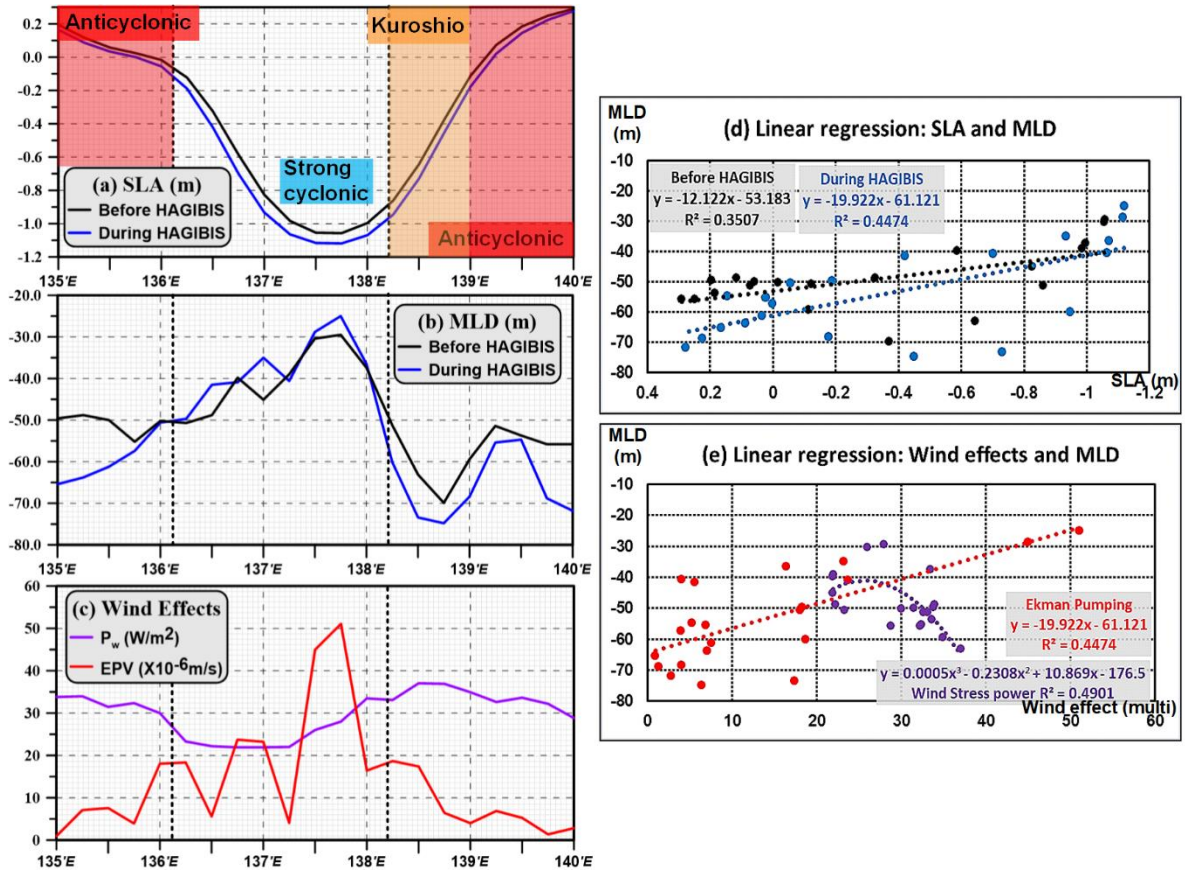

Figure 3.11 Relationship analysis of distinct SLA, MLD, and wind effects in the sea surface; (a) SLA (cyclonic eddy, Kuroshio, and anticyclonic eddies), (b) MLD before and during HAGIBIS, and (c) wind effects during HAGIBIS based on zonal transect in the Northwest Pacific Ocean (latitude 31.5°N; longitude 135°–140°E) and (d, e) their relationship using linear regression.

3.7. Summary

Chapter 3 shows the unequal ocean geographical distribution of SST and SSS based on the CMEMS satellite and model data in the NPO. The regional profiles of strong Kuroshio current meandering and intensive cyclonic eddy of cold water are presented incorporating with the distributions of the upwelling conditions while both heavy rainfall and strong wind stress power show different responses near the area. Especially, the impact of typhoon HAGIBIS was investigated using the CMEMS's six hourly wind and daily ocean datasets. Firstly, the wind speed in CMEMS was validated in comparison with JMA's estimated storm wind zones. Second, the KCM path was compared to JCC and AVISO. Finally, the SST and SSS were accepted using data from the Argo floats. The P_w and EPV calculated from wind speed data provided by CMEMS described typhoons' local characteristics within storm wind zones, despite a technical issue with biased values due to geographical interpolation in nearshore areas. The following is a summary of oceanic changes influenced by super typhoon HAGIBIS and the

Kuroshio current,

- Wind stress power, which was stronger on the left and right semicircles than the center of the typhoon, while Ekman Pumping velocity was powerful in the core of the typhoon.
- The SST was decreased by the strong Ekman upwelling along the core of HAGIBIS's track in combination with the strong cyclonic eddy generated by the large Kuroshio meander.
- Some of the SSS was reduced by a massive supply of freshwater due to heavy rainfall on the left-hand part of HAGIBIS's path, while the other SSS increased slightly despite strong Ekman upwelling along the center of HAGIBIS's track due to that fast translational speed.
- Some of the MLD was shallowed along the center of the HAGIBIS's track due to the combined effect (Eddy upwelling + Ekman upwelling), whereas other MLD was deepened by strong wind stress power on the right and left semicircles of HAGIBIS.

CHAPTER 4. SUBSURFACE OCEAN RESPONSES TO HAGIBIS

4.1. Introduction

Upper and deep oceanic responses to super typhoons have been a critical concern due to their significance in climate change, environmental variability, and conservation of marine resources (Han Zhang et al. 2021). Many studies have shown that strong typhoons induce changes in oceanic variables such as temperature, salinity, and nutrients beneath storms through the vertical entrainment process such as vertical mixing and Ekman upwelling (J. F. Price, Sanford, and Forristall 1994; W. Wang and Huang 2004; L. L. Liu, Wang, and Huang 2008). The role of super typhoons in the NPO has received increased attention in a variety of ocean physics subdisciplines.

At the sea subsurface in the north of the equator, warm sea temperature (ST) anomalies caused by the influence of the typhoon can reach approximately 4 ℃ (Han Zhang et al. 2019), and undersea salinity (SS) decreases within 1 psu (Girishkumar et al. 2014). In terms of nutrients, phytoplankton blooms (PB) estimated by a Chl-a concentration (I. I. Lin 2012) are generally more visible on the right bias side of typhoons' track. Further, some studies have revealed that the subsurface chlorophyll maximum layers (SCML) contribute substantially to the growth of upper oceanic phytoplankton biomass under appropriate conditions comprising light intensity, nutrient-flux, and primary production (Cullen 2015). The SCML's location, depth, and duration are modulated by vertical mixing, advection, and upwelling (Huisman et al. 2006; Z. Wang and Goodman 2010). The emergence of physical and biological changes in response to typhoons is well established; however, the cause of the underwater oceanic anomalies that depend on typhoon effects and ocean environmental conditions have remained unclear.

In terms of oceanic background in the underwater, wind stress from a typhoon induces upper ocean current response, which is often inclined to the right-hand side of the typhoon track in the north of the equator because of wind-current resonance (J. F. Price, Sanford, and Forristall 1994; J. Sun et al. 2015; Han Zhang et al. 2020a). The response of upper oceanic currents to typhoons can be classified as mixed layer current and thermocline current. The mixed layer current is directly driven by a typhoon, and the convergence and divergence of the

mixed layer current causes a hydrostatic pressure deviation, which causes the thermocline current (J. F. Price, Sanford, and Forristall 1994). A conversion layer exists between the mixed layer current and the thermocline current, with the current cycle changing clockwise (anticlockwise) as the deepness of the transition rises (declines) (J. F. Price, Weller, and Pinkel 1986; Sanford, Price, and Girton 2011; Han Zhang et al. 2016). As a result of their physical condition, typhoons import positive (counterclockwise) vorticity into the ocean, intensifying cyclonic eddies (Walker, Leben, and Balasubramanian 2005) and generating additional cyclonic eddies (Y. Chen and Tang 2012; L. Sun et al. 2014). After typhoon passage, the current response decays through dispersion from a few day to weeks (G. Chen et al. 2013). According to Wu et al. 2020, the current velocity to the right-bias side of the typhoon path fades quicker than the left-bias side in the north of the equator. However, it is uncertain how the strong typhoon influenced the large Kuroshio meander and how the current reacted beneath the sea surface.

Underwater responses to typhoons and marine conditions are becoming better understood due to various deep-observational methods and technological advancements. Specifically, the use of observation platforms such as biogeochemical Argo (BGC-Argo) floats since the 2000s (Chai et al. 2020) have been used to investigate the interaction between typhoons and regional seas regarding physical and biogeochemical marine factors. CMEMS operates a variety of multi-observational platforms and oceanic/atmospheric models to offer surface and subsurface data on ocean variables (Le Traon et al. 2019). In this study, changes in the subsurface variables are observed through two main data such as biogeochemical Argo float and CMEMS's model data.

To better understand the relationship of various upper marine physical and biological variables having distinct environmental characteristics in response to typhoon's effects, this Chapter 4 firstly investigated a variability of the large Kuroshio meander at specific depths for another physical driving force inducing and transferring the sea surface and subsurface ocean variables. Secondly, it determined supplementary biological mechanisms for favorable PB growth conditions and synthesized the response of undersea variables during the typhoon.

4.2. Multi-source Subsurface Observational and Model Data

The general information of super typhoon HAGIBIS and study area in the same as Chapter 3 in Figure 3.1. Further the typhoon related wind data and equation as well as the

various data of surface ocean variables such as temperature, salinity, mixed layer depth, sea level anomaly, geostrophic velocity and precipitation were dealt with previous chapter 3.

4.2.1. Vertical profile of subsurface ocean variables

An Argo observational system is a global and local scale array of temperature, salinity, and biogeochemical profiling floats are intended to be a significant component of the ocean observation system, capable of surveying the upper 2000 m. This study addressed three Argo floats, verifying physical and biological ocean surface model data, and estimating a favorable environment for the growth of a PB. The oceanic in situ data are obtained from platform numbers 2,903,367 and 2,093,376 provided by JMA's Argo and code 2,902,754 supported by the Ministry of Science and Technology (MOST)'s Argo of China. The data is extracted from the Copernicus Marine in situ TAC dataset (*http://www.marineinsitu.eu accessed on 31 May 2022*) and the real-time Argo database of the China (*http://www.argo.org.cn accessed on 23 June 2020*), respectively (Table 4.1).

Table 4.1 General information regarding to three Argo floats

Platform Code	Available Date	Parameters	Source
(A) Physical 2903367	28 May 2019 to 20 July 2020	Sea pressure, temperature, and practical salinity	*ftp://nrt.cmems-du.eu/Core/INSITU_GLO_NRT_OBSERVATIONS_013_030/glo_multiparameter_nrt/monthly/PF/201910/GL_PR_PF_2903376_201910.nc (accessed on 31 May 2022)*
(B) Physical 2903376	3 August 2019 to 1 October 2020	Sea pressure, temperature, and practical salinity	*ftp://nrt.cmems-du.eu/Core/INSITU_GLO_NRT_OBSERVATIONS_013_030/glo_multiparameter_nrt/monthly/PF/201910/GL_PR_PF_2903367_201910.nc (accessed on 31 May 2022)*
(C) BGC 2902754	30 August 2018 to 10 February 2021	Physical (pressure, temperature, salinity), biochemical (DO, nitrate, and Chl-a)	*http://www.ifremer.fr/co-argoFloats/float?ptfCode=2902754 (accessed on 23 June 2020)*

* The locations of Argo floats (A, B, and C) are depicted in Figure 3.9a and c.

4.2.2. Methodology

A follow-up framework with previous Chapter 3 is shown in Figure 4.1. It proceeds with the following four steps:

- **Subchapter 4.3**

  To interpret the vertical variability of the KCM, I reproduced the KCM expressed

by Kuroshio current velocity (KCV) based on 0, 60, and 100 m depths from October 10 to 13(4.3.1).

- **Subchapter 4.4**

  The response of sea surface ocean variables, considering SST, SSS, and Chl-a. The changes in surface variables (SST, SSS, Chl-a) can be estimated by where, when, and to what extent the typhoon affects the study area on October 10, 11, 12, and 13 (4.4.1). The following work was used through the MLD and daily precipitation to evaluate other significant evidence (4.4.2).

- **Subchapter 4.5**

  To interpret the sea surface PB one day after HAGIBIS, this Chapter 4 was expanded using vertical profiles showing the underwater variabilities according to a specific depth. These findings were conducted largely in two parts. Firstly, it was evaluated as a favorable environmental condition for PB growth via Argo float data (4.5.1). Secondly, the overall estimated spatial distribution was presented in a quantitative conceptual diagram using a comprehensive impact analysis to identify the biological growth process of the PB in the upper ocean (4.5.2).

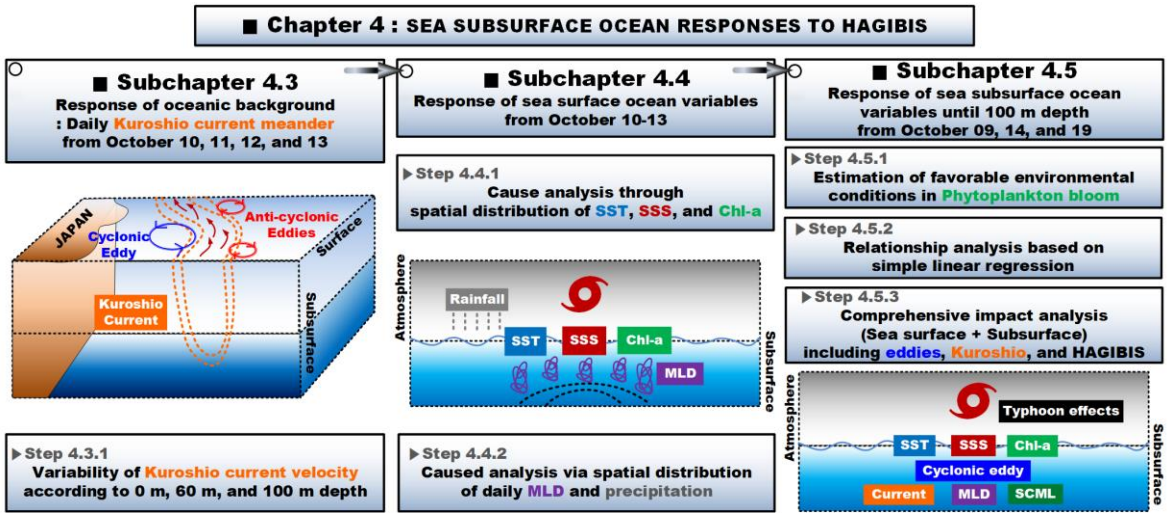

Figure 4.1 Flowchart depicting the individually-estimated physical and biogeochemical processes at the KCM environment of the Northwest Pacific Ocean in response to typhoon HAGIBIS.

4.3. Response of Subsurface Kuroshio Current

The daily SLA and the GV were used to confirm the Kuroshio mainstream and to

investigate the intensity and extent of eddies before and after HAGIBIS shown in Chapter 3. Specifically, whether or not to check the SLA change during the typhoon passage. The result was that the SLA were less affected by typhoon HAGIBIS than the Kuroshio Current Meander. It also provided additional evidence that the typhoon had less effect on the strength of cyclonic eddies despite spending about 30 hours in passing over the strong cyclonic eddy area. Although the SLA changed slightly during HAGIBIS, the Kuroshio current velocities (m/s) changed significantly as a result of the effects of HAGIBIS.

4.3.1. Variability of the KCM according to 0, 60, and 100 m depth

This study investigated the variability of KCM at 0, 60, and 100 m depths to estimate the influences of the typhoon on the KCM (Figure 4.2). We focused on an area where the strong Kuroshio current flows from longitude 135°–140E° and latitude 30°–34°N. Before the typhoon (Figure 4.2a1), the KCM flowed southeastward before turning northward at a speed of over 1 m/s, with a significant horizontal distribution, reaching a depth of 100 m (Figures 4.2a2 and a3). On October 11 of which the center of HAGIBIS approached the mainstream of the KCM around 12:00 UTC, the strong P_w on the right-hand side intensified Kuroshio's current velocity and extended the area (deeper red area; longitude 138°–139.5°E and latitude 30°–34°N). Specifically, the wind stress vector turned counterclockwise on the typhoon track's right side, intensifying current velocities in the same direction. This is caused when wind stress power greatly forces the right semicircle, and the movement's direction counterclockwise is similar to Kuroshio's path. In contrast, in the area that the direction of typhoon-related winds was opposite to that of Kuroshio current, the current velocity was weakened (Figure 4.2b1; on the left-hand part of the typhoon path). The effect of P_w became weaker as depth increased, and the spatial distribution of velocity of Kuroshio current at 100 m depth was no longer similar to that before the typhoon pathway. In addition, the high EPV on the center of the typhoon's track can induce the current velocity to increase from 100 m depth. On October 12 of which HAGIBIS made landfall before 10:00 UTC (Figure 4.2c1), HAGIBIS intensified a partially southward-flowing current of the Kuroshio on the left-hand side of the typhoon's trajectory. This is probably caused by that the typhoon's rotation on the navigable semicircle and the current's direction coincide. Meanwhile, at the center of HAGIBIS across the Kuroshio path, the current velocities were reduced because the P_w on the center of the typhoon was weaker than on the right and left semicircles of the typhoon. With an increased depth of 100 m, the KCM tended to be similar to before the typhoon. On October 13 when HAGIBIS passed through the study area, as shown in

a column of Figures 4.2d1, d2, and d3, the intensity of the current velocities returned to those before the typhoon while the expanded area (over 0.5 m/s; green area) was irrecoverable compared with that on October 10.

Overall, at 0 and 60 m depth, the high current velocity appeared in a larger area (above 1.0 m/s) induced by wind stirring in Figures 4.2b1 and c1 and then recovered at 100 m depth to that before the typhoon condition (Figures 4.2a3, b3, c3, and d3). The vertical feature of Kuroshio current velocities agrees with the previous result of X. Liu and Wei 2015 about the deepening depth and the distribution of the Kuroshio current.

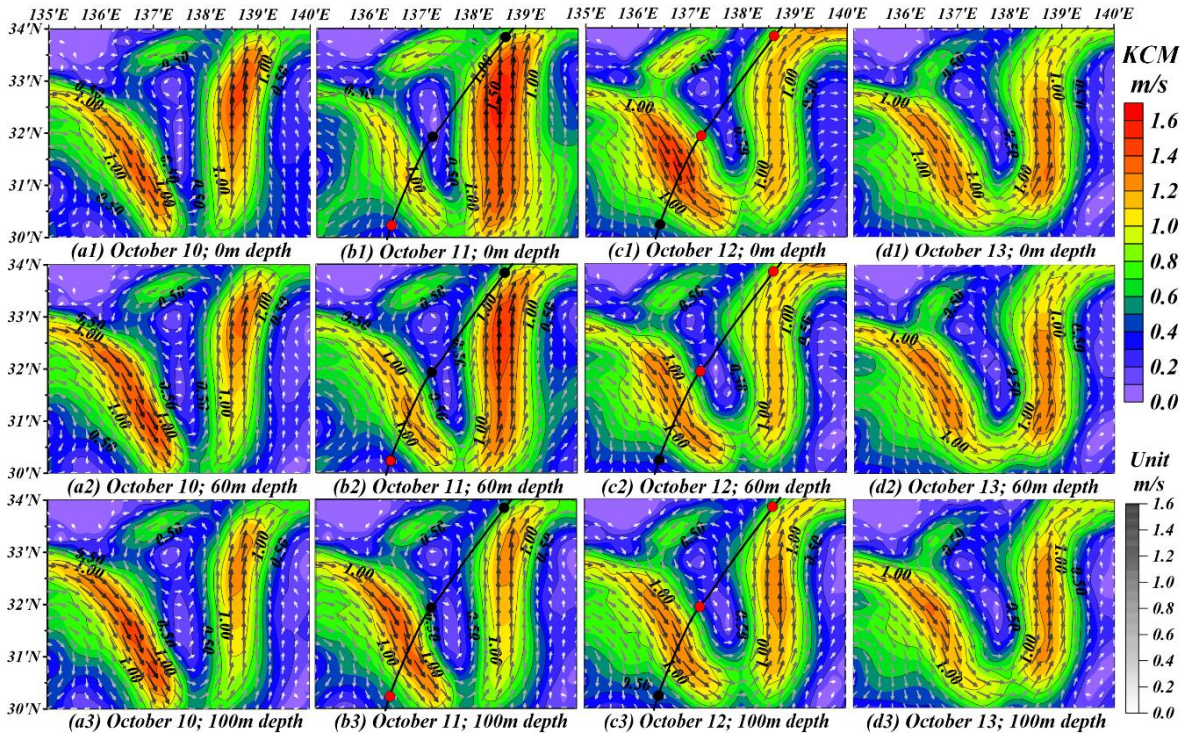

Figure 4.2 Kuroshio current velocity (m/s) on the boundary of longitude 135–140°E and latitude 30–34°N based on depth and date; 0 m (a1, b1, c1, and d1), 60 m (a2, b2, c2, and d2), and 100 m (a3, b3, c3, d3) on October 10, 11, 12, and 13 respectively. The figures are focused on the strong cyclonic eddy area with the typhoon's track and intensity (black line and red dots).

4.4. Response of Surface Ocean Variables

The previous Chapter 3 takes into account the surface physical changes in SST and SSS and analysis of their causes through the spatial distributions on October 10 (before) and October 12 (during) in Figure 3.9. When comparing and analyzing not only the physical but also the biological mechanisms as a result of the typhoon's influence, it is necessary to interpret the daily and more time-extended spatial distributions in order to fill the research gap that occurs.

4.4.1. Cause analysis via spatial distribution of SST, SSS, and Chl-a

Figures 4.3, 4.4, and 4.5 show the change in the SST, SSS, and Chl-a, respectively according to the passage of HAGIBIS on October 10, 11, 12, and 13, 2019. The observed SST was 26.5 ℃ in the strong cyclonic eddy area formed above Kuroshio's path before the arrival of HAGIBIS in Figure 4.3a. When HAGIBIS began affecting the study area, the SST changed from 26 to 25.5 ℃ at the strong cyclonic eddy (Figure 4.3b). During HAGIBIS, it showed a temperature drop of about 0.5 to 1.5 ℃ inside SWZ in the strong cyclonic eddy area. It could be caused by the cold temperature rising from the deep water to the sea surface due to the combined upwelling effect of the typhoon and the cyclonic eddy. The amount of the SST cooling (more than 2 ℃) is determined not only by the intensity and moving speed of typhoons, but also by the upper ocean's preexisting thermal structure. The thermal structure is addressed in the next section (Subsection 4.4.2. MLD and daily precipitation). One day after the typhoon, the decreasing SST remained at 25 ℃ in the strong cyclonic eddy zone (Figure 4.3d).

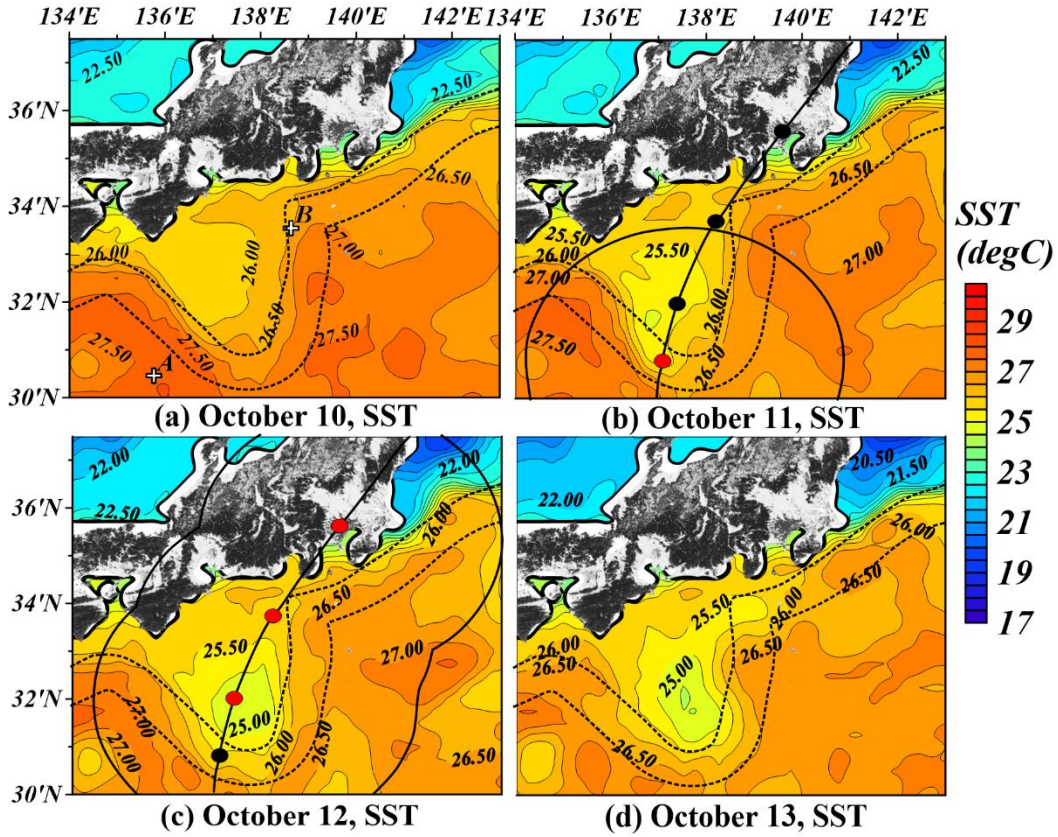

Figure 4.3 Daily sea surface temperature (SST); (a) October 10, (b) October 11, (c) October 12, and (d) October 13. Black dotted line, black line, and red dotted denote the Kuroshio meander, the storm wind zone, and the typhoon central location according to date. Physical Argo floats (ST and SS) are shown in points A and B.

The SSS distribution in Figure 4.4a shows a low salinity concentration of at least 34.00 psu around the massive strong cyclonic eddy area before the arrival of HAGIBIS. Oceanic

salinity normally increases after a typhoon due to the vertical entrainment from wind-induced vertical mixing; however, Figure 4.4b indicates a few changes in the SSS concentration, then a decrease of 0.2 as 33.80 psu on the left semicircle of the typhoon's center in the cyclonic eddy (Figure 4.3c). The SSS remains with 33.90 psu in the same area until 13 October. A previous study (J. Chen et al. 2019) demonstrated that high salinity appeared on the right-bias side of the typhoon pathway as a dangerous semicircle due to an asymmetrical effect. However, Chapter 4 confirmed that some SSS concentrations on the right side of the typhoon track increased by a few concentrations (from 34.20 to 34.30 psu) and to a small extent, while other SSS concentrations on the left-bias part of the typhoon passage significantly decreased. Compared to the effect of intense rainfall, the combined effect of strong Ekman and eddy upwelling may not greatly affect the increase in the SSS on the right and left sides of the typhoon's path. To interpret the causes of the change distribution of SSS, the following daily precipitation distribution will be analyzed in subsection 4.4.2.

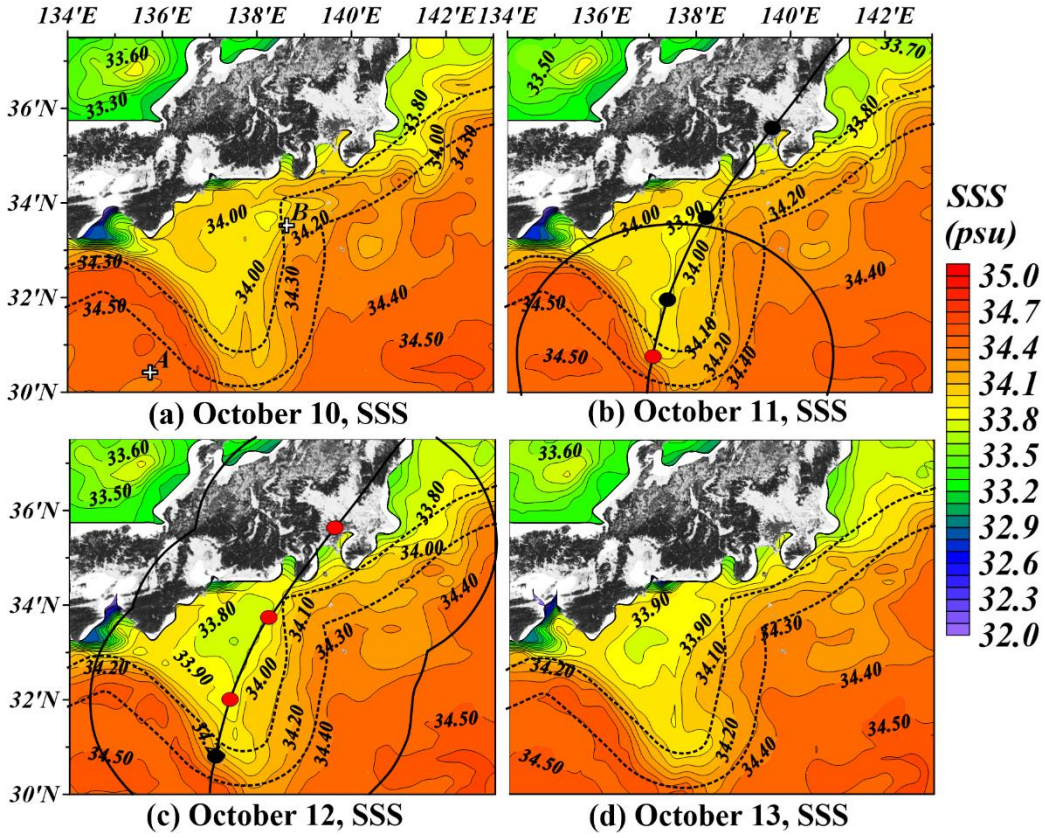

Figure 4.4 Daily sea surface salinity (SSS); (a) October 10, (b) October 11, (c) October 12, and (d) October 13. Black dotted line, black line, and red dotted denote the Kuroshio meander, the storm wind zone, and the typhoon central location according to date. Physical Argo floats (ST and SS) are shown in points A and B.

HAGIBIS had a wide SWZ encompassing the study area, strong wind stress power,

and high Ekman pumping velocity. These characteristics significantly affected biological processes in the ocean through direct or indirect effects on the phytoplankton bloom (PB). Before HAGIBIS, the PB existed along the KCM and in front of the offshore around the Kanto region, where the high Chl-a concentration remained at over 0.80 mg/m^3 within the red contour line (over 0.50 mg/m^3) due to the confluence area between the Oyashio cold and Kuroshio warm currents (location; longitude 140°–143°E and latitude 34°–36°N). This area gives rise to a natural fishing ground in Japan. In the cyclonic eddy area, the amount of Chl-a was from 0.25 to 0.30 mg/m^3 from 10 October to 11 in Figures 4.5a and b. The Chl-a then reached 0.40 and 0.45 mg/m^3 along the Kuroshio path in the cyclonic eddy area (Figure 4.5c). On 13 October, a massive growth of the PB (Chl-a reached 0.60 mg/m^3) occurred along the upper KCM and the center of the typhoon's path. That is, HAGIBIS and accompanying heavy rainfall directly affected the decreasing SST and the low SSS concentration on 12 October, while the large Chl-a anomalies occurred one day after the typhoon passed. These causes should be interpreted in conjunction with typhoon-related external and ocean internal factors simultaneously. This will be taken into account in the underwater.

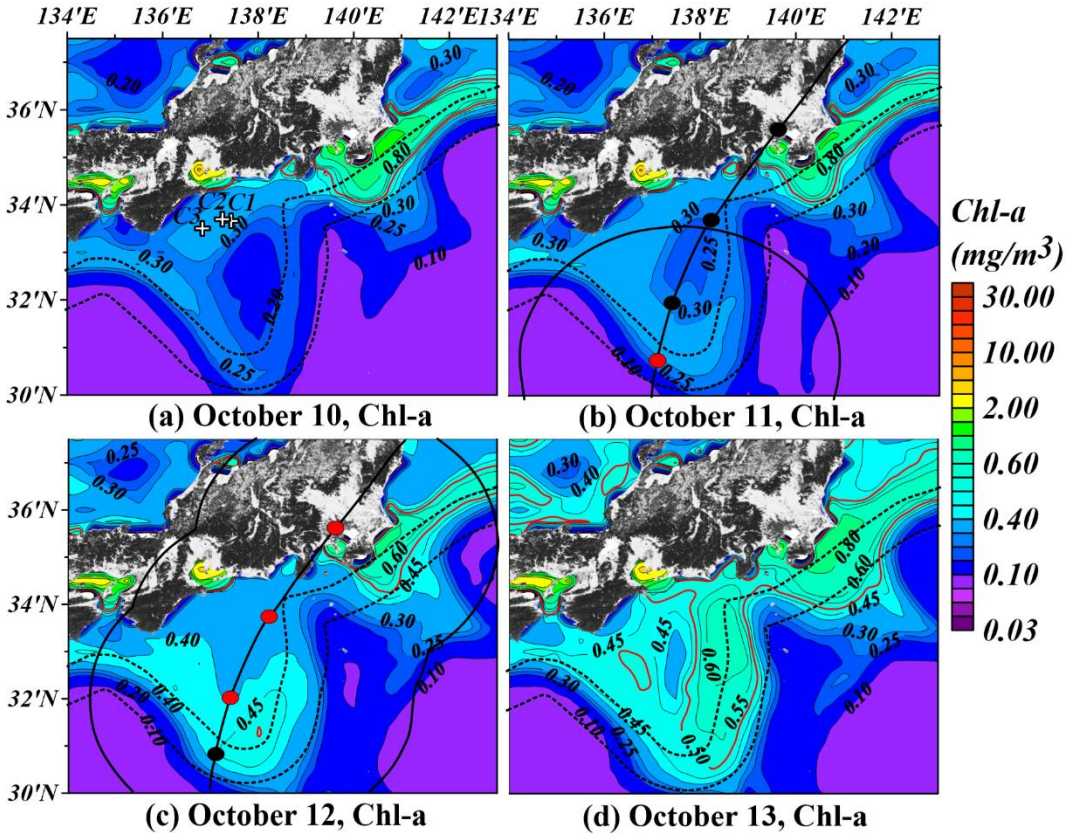

Figure 4.5 Daily sea surface phytoplankton bloom indicated by chlorophyll a; (a) October 10, (b) October 11, (c) October 12, and (d) October 13. Black dotted line, black line, and red dotted denote the Kuroshio meander, the storm wind zone, and the typhoon central location according to

date. Solid red lines indicate a boundary of high Chl-a is over 0.5 mg/m^3. A biogeochemical Argo float (ST, SS, DO, nitrate, and Chl-a) is depicted in points C1, C2, and C3 based on the dates of October 9, 14, and 19, respectively.

4.4.2. Cause analysis via daily MLD and precipitation

A relatively shallow MLD formed in a strong cyclonic eddy area, ranging from 30.0 to 35.0 m in thickness, was caused by pre-existing eddy upwelling as shown in Figure 4.6a1. Maúre *et al.*, 2017 confirmed that modification of the mixed layer by mesoscale eddies led to deeper (shallower) MLDs in pre-existing anticyclone and cyclonic eddy. On 11 October, the sustained wind-induced energy flux triggered deepening MLD on the typhoon's center and right-hand side (occurring at more than 60 m depth; red line in Figure 4.6a1). On 12 October, the MLD in the cyclonic eddy area became shallow along the typhoon track center, with a value of 25.0 m depth in Figure 4.6a2. This lifted-up MLD generated by the combined Ekman pumping and eddy upwelling could cause a decrease in SST, as shown in Figure 4.6a2. In contrast, wind stress power deepens the MLD on the right and left semicircles of the typhoon path in the red contour area over 60 m to a maximum value of 83.6 m depth (Figure 4.6a2). The overall MLD remained in a similar condition or deepened on the northern side. In contrast, the MLD was deeper and the thermocline was thicker within anticyclonic eddies (red area in Figures 4.6a1-a3). In terms of phytoplankton bloom in the sea surface, the depth of mixing layer controls phytoplankton growth with eddies (Maúre et al. 2017). In cyclonic eddy, the shallowing of the MLD increases in initial and consequent phytoplankton bloom, while anticyclonic eddy is mostly associated with the convective mixing that interrupts bloom. That is, strong vertical mixing where the typhoon's right and left bias triggered bloom suppression in Figure 4.5c, d. In addition, a deep mixed layer in the anticyclonic eddy was presumed to prevent deep, cold water from being entrained into the upper layer.

Figure 4.6b1-3 indicate the daily precipitation distribution observed by TRMM radar. Before the arrival of HAGIBIS in Japan, daily rainfall was approximately 100 mm (Figure 4.6 b1). The typhoon on the left-bias sides was accompanied by heavy rainfall of over 200 mm. Due to the impact of rainfall, some oceanic variables changed. Particularly, the SSS decreased within the rainfall range during and after the typhoon's passage. Ekman pumping casued by HAGIBIS contributed substantially to the increase in the SSS; however, heavy rainfall effectively reduced SSS. The degree of change and compensation still needs further research.

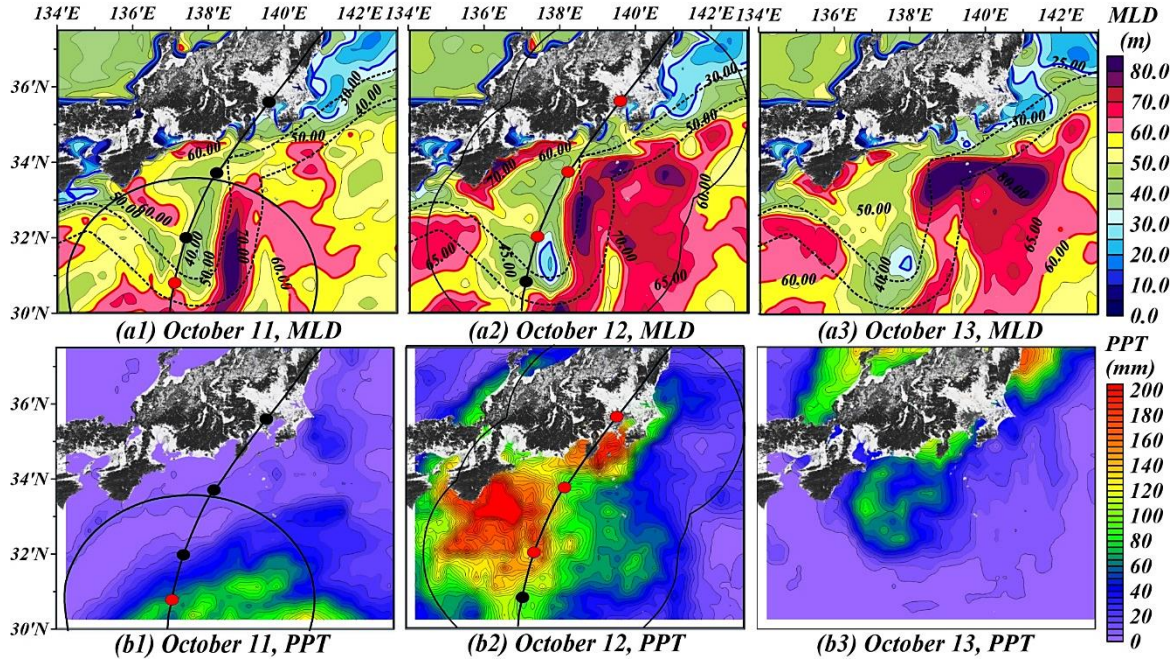

Figure 4.6 Daily mixed layer depth (MLD) and daily cumulative precipitation (PPT; mm); (a1, b1) October 11, (a2, b2) October 12, and (a3, b3) October 13. Black dotted line, black line, and red dotted denote the Kuroshio meander, the storm wind zone, and the location of the center typhoon corresponding date. The blue and red contour lines indicate 30 m and 60 m thickness in terms of MLD, respectively.

4.5. Response of Subsurface Ocean Variables

4.5.1. Favorable environmental conditions in phytoplankton bloom

To investigate the biological process, we analyzed vertical changes in temperature, salinity, dissolved oxygen (DO), nitrate, and Chl-a as measured by a BGC Argo float at point C1; before (No.98 on 9 October), C2; one day after (No.99 on 14 October), and C3; a week after (No.100 on 19 October) the typhoon, as shown in Figure 4.7, 4.8 and 4.9. The location of point C1, C2, and C3 existed at the offshore sea of the Tokai region, where the eddy's strength was weak (−0.084 m) and the KCM's influence on the BGC Argo float was small. On the contrary, HAGIBIS affected the area with strong Ekman pumping and heavy rainfall on 12 October. Therefore, we examined the direct impact on the center and left semicircle of the typhoon rather than the combined effect, such as eddies, the Kuroshio, and the typhoon.

Temperature (℃, solid line), below the *x*-axis, and salinity (psu, dotted line), above the *x*-axis, are shown in Figure 4.7. The temperature progressively decreased to 26 ℃ compared to before HAGIBIS (26.6 ℃), and the thermocline depth was transformed by replying to the typhoon from 60 m to 40 m. The greater the water depth, the higher the temperature difference

between before and one day after. Then, the ocean temperature showed a small variation of approximately 1 ℃ at around 100 m depth. This result is due to the Ekman upwelling of HAGIBIS bringing the deep cold temperature layer to the upper ocean. One week later, the sea temperature decreased to 25 ℃ near the surface, and the thermocline depth deepened to 50 m. The temperature at the bottom of the thermocline depth recovered to the levels before the typhoon. Meanwhile, based on the halocline on October 9 compared with October 14, the salinity layer rose from 60 m to 40 m, similar to the thermocline in Figure 4.7. A tendency for high SSS (34 to 34.2 psu) existed due to the prior influence of Ekman upwelling, and the heavy rainfall accompanied by HAGIBIS on October 12 stopped the supply of fresh water to the ocean. However, another heavy rainfall occurred on October 19, and the total precipitation exceeded 200 mm in the NPO. As a result, SSS swiftly dropped to a relatively lower salinity of 33.6 psu after one week. The salinity change is due to the influence of the typhoon; however, the effect of rainfall was dominant in the vicinity of the surface layer until approximately 40 m deep.

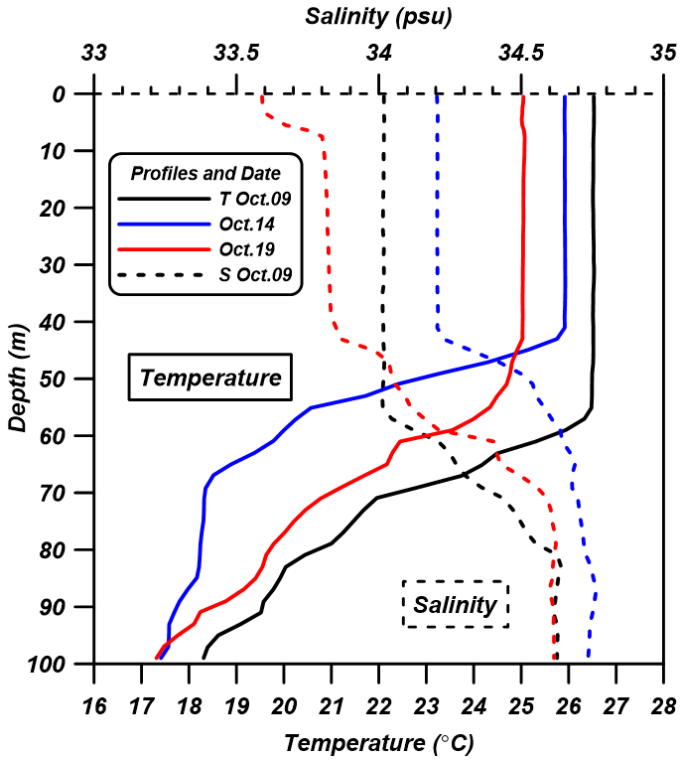

Figure 4.7 Depth-integrated temperature (℃, solid) and salinity (psu, dotted) until 100 m depth; Before (C1; October 9 in black), a day after (C2; October 14 in blue), and a week after (C3; October 19 in red) the passage of HAGIBIS observed by Code 2,902,754 BCG Argo float, respectively.

Biogeochemical components such as DO and nitrate in Figure 4.8 show exchanges at each depth following the passage of HAGIBIS. The DO concentration from the surface to 30

m depth was comparable for each variable when compared with before and one day after the typhoon. However, at depths greater than 30 m, the mass changed considerably. It was reduced by 140 μmol/kg (before, 163 μmol/kg) at a 53 m depth due to typhoon-induced upwelling that could bring the deep low-oxygen water to the upper layer. It also showed relatively high oxygen at approximately 80 m depth compared with before and one day after HAGIBIS. Physical processes established the decrease in DO at 53 m depth. From another aspect, the DO result was inversely correlated with nitrate and Chl-a at a specific depth. The decreased (increased) DO on the specific layer is related to the consumption (release) of oxygen by organisms (primary production). Although there are differences in typhoons' intensity and ocean environmental conditions, the correlation is consistent with a previous result from T. Wang et al. 2022. A week later, the DO mass amount increased with oxycline depth, possibly due to the effect of the other heavy rainfall. The DO concentration returns to the initial condition below approximately 40 m depth.

The nitrate concentration, the ocean nutrient index in the ocean, is monotonous despite the influence of HAGIBIS. The nitrate concentration largely increases due to strong Ekman upwellings bringing up a high amount of nitrate from deep water to the upper ocean one day after. One week after, the nitrate was restored to its original amount and depth compared with before HAGIBIS, as shown in Figure 4.8.

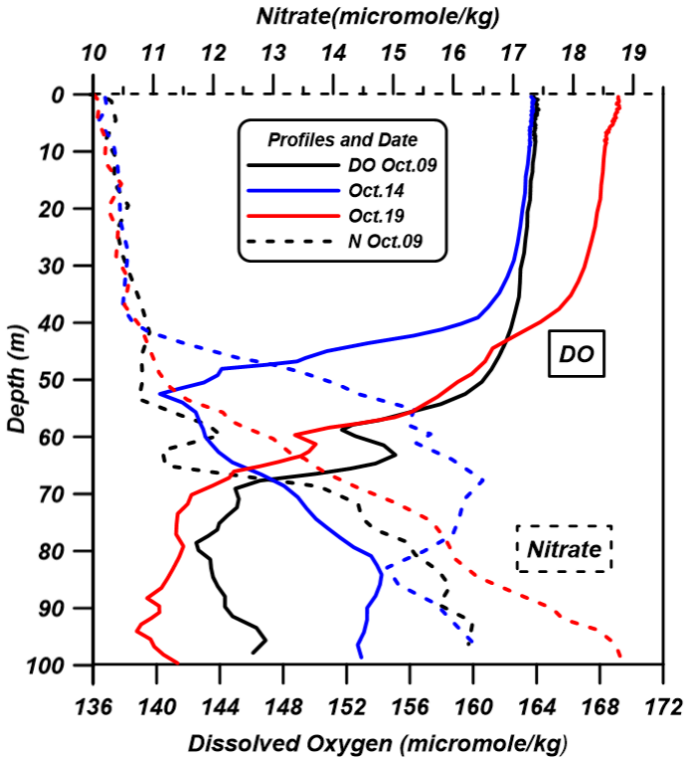

Figure 4.8 Depth-integrated dissolved oxygen (μmol/kg, solid) and nitrate (μmol/kg, dotted) until 100 m depth; Before (C1; October 9 in black), a day after (C2; October 14 in blue), and a week after (C3; October 19 in red) the passage of HAGIBIS observed by Code 2,902,754 BCG Argo float, respectively.

Finally, the concentration of Chl-a in Figure 4.9 shows the nutrient-rich layer as 1 mg/m^3 (SCML; over 0.7 mg/m^3) remaining at a 60 m depth before the typhoon. One day after HAGIBIS, the SCML (0.75 mg/m^3) was pumped up to a 40 m depth, and then the SCML reached the sea surface, maintaining the high Chl-a concentration. One week after HAGIBIS, Chl-a on the surface was sharply decreased up to 0.3 mg/m^3 whereas the redistribution of a nutrient-rich layer was 30 m. Considering the layer shift, the nutrient's favorable depth moved from 60 m to the upper ocean (less than 40 m deep), at which some ocean factors affect the PB's growth, considering the colder temperature, the lower salinity, the higher oxygen, and higher nitrate concentration than before the typhoon.

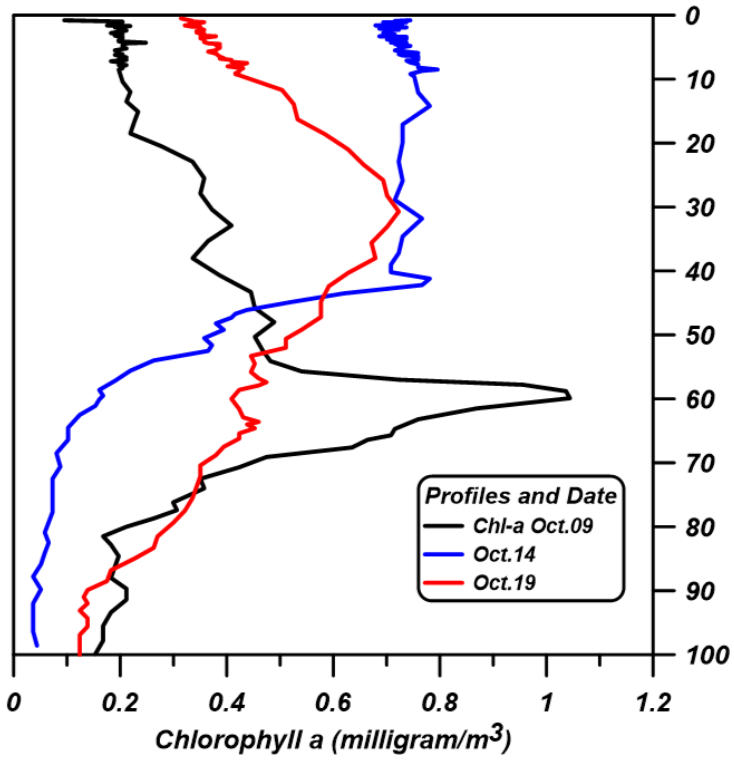

Figure 4.9 Depth-integrated Chl-a (mg/m^3, solid) until 100 m depth; Before (C1; October 9 in black), a day after (C2; October 14 in blue), and a week after (C3; October 19 in red) the passage of HAGIBIS observed by Code 2,902,754 BCG Argo float, respectively.

4.5.2. Relationship analysis based on linear regression

Simple linear regression analysis was conducted to assess the favorable environment to sustain the high concentration of Chl-a related to (a) temperature, (b) salinity, (c) DO, and (d)

nitrate before, one day after, and one week after HAGIBIS (Figure 4.10). The overall ocean variables before HAGIBIS were negligibly correlated with Chl-a ((a) R^2: 0.086, p > 0.05, (b) R^2: 0.0496, p > 0.05, (c) R^2: 0.0774, p < 0.05, and (d) R^2: 0.0559, p > 0.05), while the oceanic factors one day after HAGIBIS were strongly interrelated with Chl-a ((a) R^2: 0.9781, p < 0.05, (b) R^2: 0.9903, p < 0.05, (c) R^2: 0.647, p < 0.05, and (d) R^2: 0.9682, p < 0.05). One week after, the entire relationship decreased owing to another heavy rainfall on October 19. Chl-a was further shown to engage in the upper ocean favorable condition ((a) R^2: 0.6679, p < 0.05, (b) R^2: 0.4284, p < 0.05, (c) R^2: 0.2516, p < 0.05, and (d) R^2: 0.7157, p < 0.05). Note that, the salinity, which was rapidly altered by external factors mainly owing to the second rainfall, also showed a significant difference regarding Chl-a than sea temperature and nitrate. Chapter 4 provides evidence for the physical and biogeochemical ocean factors influencing Chl-a caused by the strong external impact of the typhoon and rainfall.

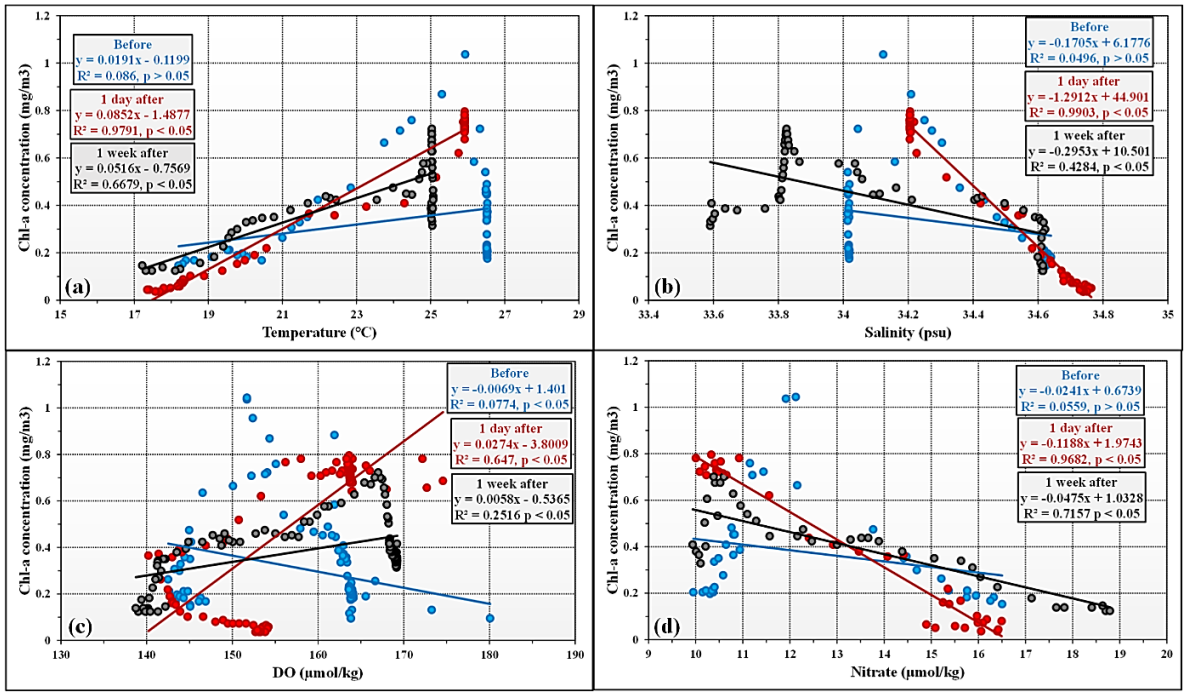

Figure 4.10 Scatterplots of oceanic variables to examine the relationship of (a) temperature, (b) salinity, (c) dissolved oxygen, and (d) nitrate compared to the Chl-a concentration; Before (C1; October 09 in blue), a day after (C2; October 14 in red), and a week after (C3; October 19 in black) the passage of HAGIBIS, respectively.

4.5.3. Comprehensive Quantitative Analysis

Until the preceding Chapter 3 and 4, individually estimated ocean responses to the typhoon's effects were analyzed and interpreted. For instance, on the sea surface, the typhoon mainly induced changes in the SST, SSS, and MLD due to the typhoon's physical impact. In

contrast, the Chl-a occurred in the upper ocean layer one day after HAGIBIS. Therefore, further analysis is needed to reveal the causes using a comprehensive approach such as internal ocean profile and external forcing.

Before HAGIBIS, the dominant vertical profile mainly had a massive cyclonic eddy (the strongest area had over −1.0 m SLA) and Kuroshio's path moving southeastward and northward with the current velocity over 1.0 m/s, propagating until 100 m depth (Figure 4.11a). The pre-existing cyclonic eddy induced eddy upwelling. In that process, some ocean responses existed; firstly, the SST was decreased by 26 ℃ in the strong cyclonic eddy zone (Figure 4.11b), and the MLD was also shallower than in other areas (approximately 20 m depth at 138.3°E in Figure 4.11a). Interestingly, the Chl-a concentration on the surface was affected by the cyclonic eddy and (approximately 0.2 mg/m^3 at 138°E in Figure 4.11c). Secondly, the strong Kuroshio current affected two areas at 136.3°–137°E and 138.5°-138.8 °E. In that area, the surface SST was decrease by 26 ℃ in the most strongest vertical Kuroshio current velocity area around 136.7 °E. At the same area, the surface Chl-a was increased 0.3 mg/m^3. The high subsurface chlorophyll (HSC) layer existed around the strong Kuroshio area (136.5°–137°E) and 100 m to 80 m depth with 0.5 mg/m^3. In summary, before HAGIBIS, the surface temperature, MLD, and Chl-a were affected by strong cyclonic eddy and intensive Kuroshio current area. Although different study areas, this result appears to agree with H. Zhang *et al.*, 2018 that mentioned the surface phytoplankton bloom extent is influenced by the water column stabilization, SST, and the Kuroshio flow.

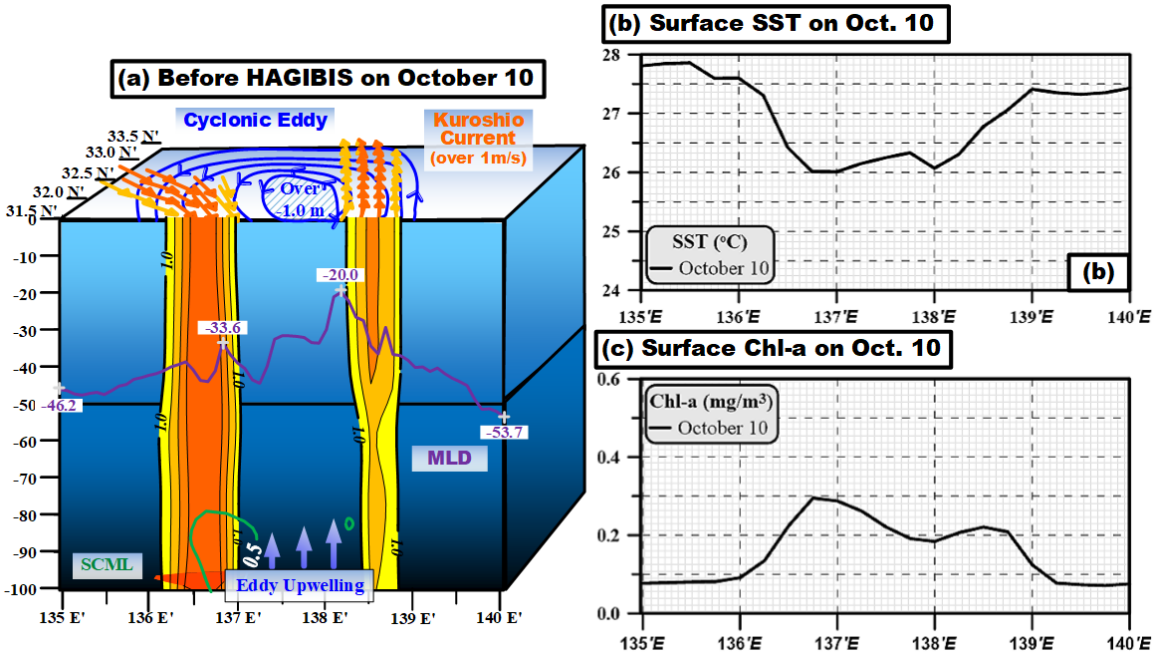

Figure 4.11 Quantitative schematic diagram of ocean variability from 100 m depth to the sea surface before HAGIBIS. Zonal transect in the Northwest Pacific Ocean (latitude 31.5°N; longitude 135°–140°E) including cyclonic eddy area [blue isolines; (a–c) in the sea surface], the Kuroshio current depicted by integrated horizontal velocities on different depths with orange; 1.0 < V < 1.5 m/s, and yellow; above 1.0 m/s. The subsurface layers comprise the MLD (Violet), HSC (light green; 0.5 mg/m^3). The two graphs indicate (b) surface sea temperature (℃) and (c) surface Chl-a (mg/m^3) before HAGIBIS.

During HAGIBIS, the typhoon effects were distinct in each region. Firstly, HAGIBIS provided intensive wind stress power on the left (average over 30 W/m^2; 135°–136.2°E) and right (over 35 W/m^2; 138°–140°E) semicircles, while had relatively weak stirring power in the center of the typhoon (25 W/m^2) in Figure 4.12a and d. In contrast, the high EPV (136.2°–138°E) largely influenced from a minimum of 0.5 to a maximum of $50 \times 10^{-6} m/s$ (Figure 4.12a and d) in the typhoon center. Strong Ekman pumping and wind stress power led to a faster Kuroshio current velocity and a larger Kuroshio extent than before the typhoon. Interestingly, the area around the strong cyclonic eddy activity was also affected by the intense Ekman upwelling (137.5°–138°E). Thus, the combined effect induced changes in the MLD, SST, and Chl-a in the upper ocean layer. For example, the SST was decreased by 24.6 ℃ at approximately 137.7°E (Figure 4.12b). The MLD became shallower at both high EPV (22.3 m depth in Figure 4.12a) and the surface Chl-a was increased by 0.5 mg/m^3 in Figure 4.12c. It is due to the HSC (0.5 mg/m^3) was redistributed at a depth of 100 m to 45 m driven by the combined effect (Eddy + Ekman upwelling). That is, the HSC provided massive nutrients to an upper ocean layer to induce bloom. On the other hand, the intensified Kuroshio current area (136.3°–137°E) induced by the typhoon also triggered the SST dropped down (mean 25.5 ℃), the MLD shallowed (34.0 m depth at 136.5°E), while the other MLD in the vicinity of 135°E and 140°E became deeper than before the typhoon (54.2 and 63.2 m depth at anticyclonic eddy area in Figure 4.12a). As same area, the Chl-a increased 0.45 mg/m^3. During HAGIBIS, the SST, MLD, Chl-a, and subsurface Chl-a layer largely affected by the combined effect on strong cyclonic eddy and intensive Ekman pumping as well as stronger Kuroshio current velocity.

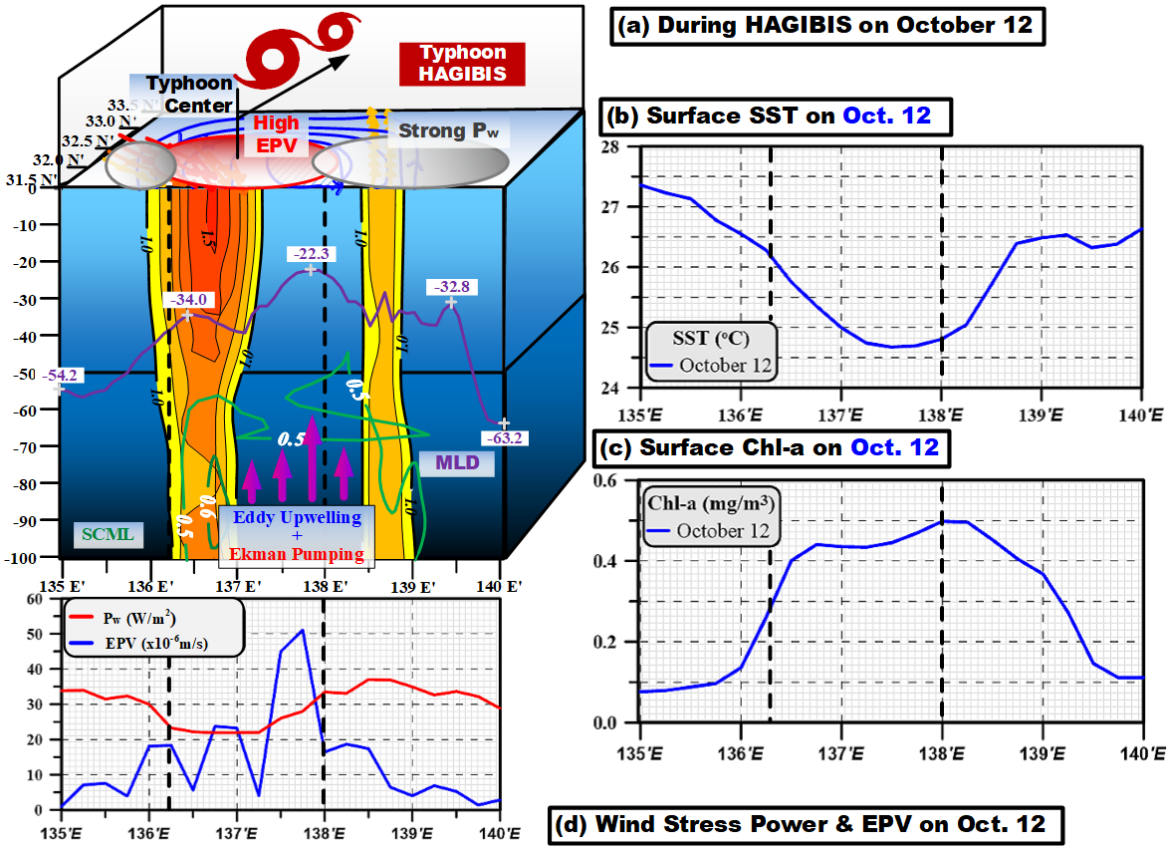

Figure 4.12 Quantitative schematic diagram of ocean variability from 100 m depth to the sea surface during HAGIBIS. Zonal transect in the Northwest Pacific Ocean (latitude 31.5°N; longitude 135°–140°E) including cyclonic eddy area [blue isolines; (a–c) in the sea surface], the Kuroshio current depicted by integrated horizontal velocities on different depths with red; over 1.5 m/s, orange; 1.0 < V < 1.5 m/s, and yellow; above 1.0 m/s, and typhoon HAGIBIS represented by the affected area where strong P_w (gray circles) and high EPV (red circle) in the sea surface. The subsurface layers comprise the MLD (Violet), HSC (light green; 0.5 mg/m^3). The three graphs indicate (b) surface sea temperature (℃) and (c) surface Chl-a (mg/m^3), and (d) P_w (W/m^2) and EPV ($\times 10^{-6}$ m/s) during HAGIBIS. Two vertical dashed lines marked on both the main plot and the subplot indicate the region with the strongest typhoon effect along the typhoon's center (longitude 136.5°–138°E).

One day after HAGIBIS, in the combined effect area, the SST slightly decreased around the combined effect area (137.7°–138.2°E in Figure 4.13b), the MLD deepened in the same area (25.5 m depth), and the Kuroshio current velocity was weakened (136.5°–137°E in Figure 4.13b). In other words, the fluctuation tendency of the SST and the MLD had approximately similar values during the typhoon, indicating the influence of the typhoon remained in the ocean, while the speed and range of the Kuroshio current returned to the pre-storm condition (Figure 4.13a). The previous section showed the favorable environmental conditions in the PB's growth through the BGC Argo float at the specific locations C1, C2, and C3. It concluded that a modulated environment (decrease in temperature, low salinity, and

high oxygen) caused by the typhoon effects could induce better conditions for PB growth. From this section, the synthesis vertical profiles could be explained largely by the SCML (over 0.7 mg/m^3) existing at 80 m to 60 m depth (138.0°–138.8°E), and the overall HSC (0.5 mg/m^3) supplying the whole upper ocean layer from 100 m depth to the sea surface (137.5°–139°E in Figure 4.13a). The nutrient-rich layers induced the massive PB at the sea surface a day after the typhoon (surface Chl-a; 0.56 mg/m^3). This explains why biological redistribution (HSC and SCML) is an important mechanism responsible for daily surface PB. In addition, the anticyclonic eddy areas (both 135.0°–136°E and 139.0°–140°E) was shown that low surface Chl-a (0.1 mg/m^3) due to not only the strong wind-induced vertical turbulence (deepening MLD), but also anticyclonic eddy downwelling. According to T. Wang et al. 2022, they found different mechanisms causing surface phytoplankton blooms in the environment of the Arabian sea in response to successive tropical cyclones. However, T. Wang et al. 2022, did not address the daily quantitative analysis between physical and phytoplankton dynamics. Our study demonstrated a significant difference in daily ocean variability for the typhoon period by employing a comprehensive approach to explain the daily variations in individually estimated physical and biological mechanisms.

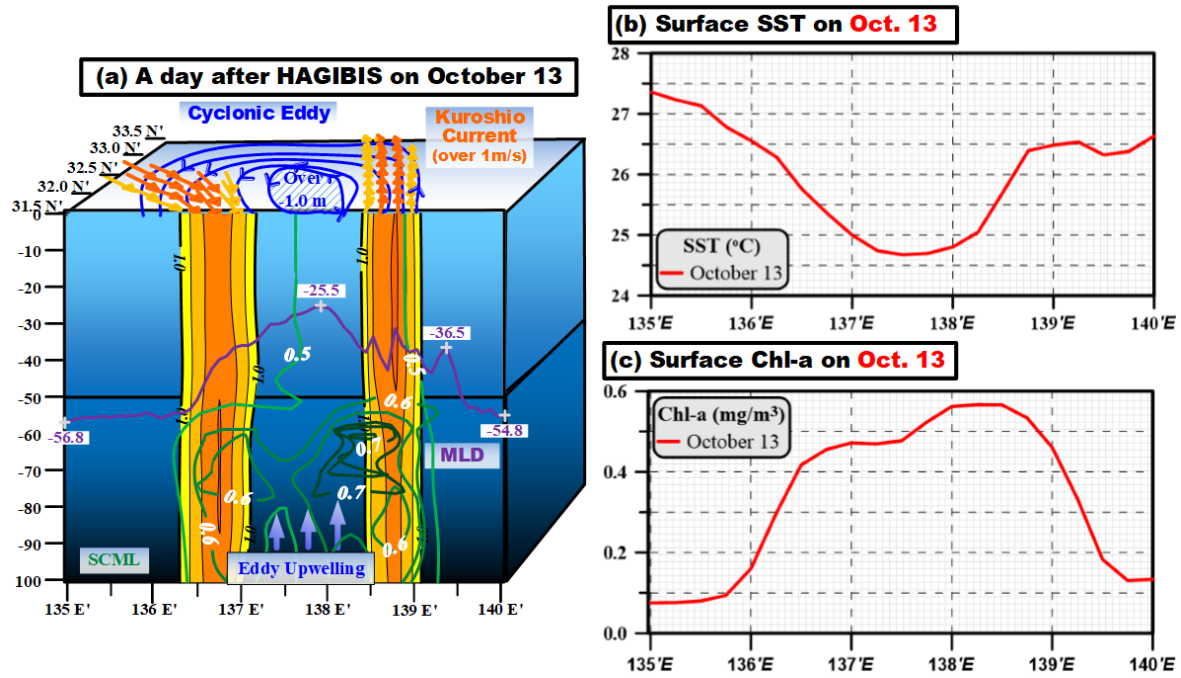

Figure 4.13 Quantitative schematic diagram of ocean variability from 100 m depth to the sea surface a day after HAGIBIS. Zonal transect in the Northwest Pacific Ocean (latitude 31.5°N; longitude 135°–140°E) including cyclonic eddy area [blue isolines; (a–c) in the sea surface], the Kuroshio current depicted by integrated horizontal velocities on different depths with orange; 1.0 < V < 1.5 m/s, and yellow; above 1.0 m/s. The subsurface layers comprise the MLD (Violet), HSC (light green; 0.5 mg/m^3), and SCML (deep green; above 0.7 mg/m^3). The two graphs indicate (b)

surface sea temperature (℃) and (c) surface Chl-a (mg/m^3) a day after.

4.6. Summary

In Chapter 4, the effects of the super typhoon HAGIBIS under the Kuroshio meander in the Northwest Pacific Ocean were investigated mainly using BGC Argo floats and CMEMS's model data for the undersea as follows;

- Although the sea level anomaly (indicating eddies) was little changed, however the Kuroshio current velocity (m/s) was changed according to wind stress power intensity and forcing direction. Especially, at 0 and 60 m depth, the high Kuroshio current velocity had a larger area (above 1.0 m/s), and then recovered at 100 m depth to before the typhoon condition.
- From analysis of favorable environmental condition in PB using in situ data of Argo float, the high nutrient layer moved from 60m to 40m depth until sea surface after the typhoon. Some underwater factors affected the PB's growth, such as the colder temperature, the lower salinity, and the higher oxygen, the higher nitrate compared with before the typhoon.
- According to comprehensive impact analysis, the nutrient-rich layers induced the massive PB at the sea surface one day after the typhoon. This explained why biological redistribution (HSC; 0.5 mg/m^3 and SCML; above 0.7 mg/m^3) is an important mechanism responsible for daily surface PB.
- The nutrient-rich layer redistribution also depended on the high Kuroshio current velocity area and the strong cyclonic eddy area.

CHAPTER 5. CONCLUSIONS

5.1. Main Findings

This study introduces a synthetic quantitative analysis of the cumulative impacts of the typhoon HAGIBIS and the large Kuroshio current meander on the ocean response of physical characteristics (sea temperature, salinity, and Chl-a) in the Northwest Pacific. Data comes from a variety of sources: from measurements (Satellites, Argo floats, and radar) and hybrid data (sparse observation complemented by model data such as CMEMS platform). The combining of satellite image, analytical model for subsurface variability outputs and in situ data provides a one-of-a-kind opportunity to study the daily influence of typhoon on the upper ocean. The study area, close to south of Japan during abnormal oceanic background, were chosen for application and verification from global dataset. Outcomes not only revealed the distinct spatial anomalies in sea surface, but also demonstrated the need and efficiency of integrating impact assessment with short-term period diversity between physical and biological mechanism so as to estimate the overall upper ocean response to the typhoon and the Kuroshio current. The most obvious findings to emerge from the main research question as "How clearly is it revealed that typhoons cause changes in upper ocean physical and biological variables, particularly, in interaction with Kuroshio current, which specifies the NPO using daily multi-source data? If so, could we categorize spatially distinct effects and responses? Could a comprehensive quantitative analysis replace the role of a theoretical synthesis explanation?" as answered below;

Firstly, from the distinct spatial assessment of the sea surface variation, this study identified critical local oceanic characters to classify cyclonic and anticyclonic eddy generated by Kuroshio mainstream before, during, and after HAGIBIS.

- **In the cyclonic eddy area (upwelling and counterclockwise)** during HAGIBIS
  I. Decrease in sea surface temperature (dropping down 0.5 to 1.5 ℃) in combination of the strong Ekman pumping.
  II. Shallowing mixed layer depth (negative anomaly; 5 m to 10 m) according to linear correlation with strong Ekman pumping velocity.
  III. High concentration of Chl-a reaching 0.40 and 0.45 $\mathrm{mg/m^3}$, however a day after HAGIBIS, the surface bloom reoccurred a high quantity of chlorophyll a (0.64 $\mathrm{mg/m^3}$) across a wide area (56,615 km^2; more than 0.5 $\mathrm{mg/m^3}$).
  IV. Occurrence in a little anomaly of sea surface salinity because the fast-moving

speed of HAGIBIS did not compensate for the degradation of SSS induced by heavy rainfall, mainly triggering a negative anomaly to drop down 0.2 psu on the left semicircle of the typhoon trajectory.

- **In the anticyclonic eddy area (downwelling and clockwise)** during HAGIBIS
  I. Deepening mixed layer depth (positive anomaly; 10 m to 15 m) according to negative linear correlation due to both strong wind stress power on the left and right side.
- **In the high Kuroshio current velocity area** during HAGIBIS
  I. Deepening mixed layer depth (positive anomaly; 5 m) due to the feature of Kuroshio current.

Secondly, from the vertically integrated assessment of the undersea variation, this study estimated the possible impact of not only the variability of Kuroshio current velocity but also a favorable biological environment condition for nutrient growth using model data and Argo float.

- **Variability of Kuroshio current velocity (0 m, 60 m, and 100 m)**
  I. **On October 11**, the high Kuroshio current velocity (maximum above 1.5 m/s) occurred by wind stress intensity and that of the same forcing direction on the dangerous semicircle at 0 and 60 m depth. Then the velocity was recovered at 100 m depth to before the typhoon condition.
  II. **On October 12**, the high velocity (mean above 1.0 m/s) was appeared around the navigable semicircle due to the coincidence of the return direction of wind stress power and Kuroshio flow.
  III. At 100 m depth, the overall velocity was recovered before the typhoon condition. This implies the influenced depth of the typhoon by 100 m.
- **Favorable condition observed by Argo float data**
  I. **During HAGIBIS**, the high nutrient layer moved from 60 m (observed pre-existing depth) to 40m depth until sea surface. The internal factors, considering colder temperature, lower salinity, higher oxygen, and high nitrate concentration, have a linear relationship to nutrient growth and relocation.

Thirdly, from the comprehensive quantitative assessment of the sea surface and subsurface variations, this study identified the spatially distinct external forcing (distinct spatial typhoon and Kuroshio impacts) and the internal dynamic (cyclonic and anticyclonic eddy area)

to evaluate the biological response and its anomaly before, during, and a day after HAGIBIS.

- **Before HAGIBIS**, the dominant vertical profiles mainly had a massive cyclonic eddy and Kuroshio's impact area, propagating until 100 m depth.
  I. In the pre-existing cyclonic eddy, the Chl-a concentration (0.2 mg/m^3) due to the eddy upwelling.
  II. In the high Kuroshio current velocity area around 136.7 °E, the surface Chl-a increase as 0.3 mg/m^3, and the high subsurface Chl-a layer (mean 0.5 mg/m^3) existed from 100 m to 80 m depth.
- **During HAGIBIS**, the primary distinct effect mainly was two wind stress power areas (135°–136.2°E and 138°–140°E) and the high Ekman pumping area (136.2°–138°E).
  I. In combined upwelling (eddy + Ekman) area (137.5°–138°E), the surface Chl-a increased by 0.5 mg/m^3 due to the redistribution of high subsurface Chl-a layer from 100 m to 45 m supplying massive nutrients to the sea surface.
  II. In intensified Kuroshio current area induced by the typhoon (136.3°–137°E), the Chl-a increase 0.45 mg/m^3. It is due to the typhoon effects made the HSC redistribute up to 55 m.
- **A day after HAGIBIS**, the internal oceanic factors response (SST and MLD) remained as same as during the typhoon, while the Kuroshio current returned to pre-storm condition.
  I. In the cyclonic eddy area (137.5-138.5°E), the nutrient-rich layers not only the redistribution of the subsurface Chl-a maximum layer (SCML; over 0.7 mg/m^3 at 80 – 60 m depth, 138.0°–138.8°E) but also high subsurface Chl-a layer occurred to the high surface Chl-a as 0.56 mg/m^3.
  II. In the anticyclonic eddy areas (both 135.0°–136°E and 139.0°–140°E) induced the low surface Chl-a (0.1 mg/m^3) due to the strong wind-induced turbulence and anticyclonic eddy downwelling.

5.2. Implications

The challenge of Remote Sensing studies considering hazardous climatic events, their changes, resource exploration, environmental monitoring, and forecasting will be achieved both the sustainable development of marine resources and the natural environment. This study is

particularly relevant to present scenarios. This study provides various data sources estimating ocean variability through their inhibition and growth both using individually estimated analysis and comprehensive quantitative impact analysis. As a comprehensive approach, this research contributes significantly to the following fields.;

- Contributions to the oceanography, the findings of this study provide the enhancement of new multifaceted phenomenon and maritime natural science, markedly from short-term variability associated with Kuroshio meandering, eddies, and strong typhoons. This would be to a better understanding of the actual ocean backdrop variability within impacted days of a typhoon passing through. Further the classification of fine spatial and temporal sampling (at least daily data) for each variability, is used to assess ocean internal profiles.
- Contributions to application of remote sensing, this study highlight the importance of short-term phenomenon and quantified evidence using for example multi-sensors from different missions (SST, SSS, currents, Chl-a, etc.) and verifying before, during, after typhoon conditions. This study enhanced vertical and temporal resolution of upper-ocean measurements in a basin-scale region and the addition of near-subsurface favorable condition estimation with biogeochemical observations.
- Contributions to climate change, this study could rise critical questions about the changes in typhoon-ocean interactions caused by rapid day-to-day ocean warming. If, in a warming climatic situation, considering the increased frequency of typhoons and their intensity gradually strengthens with abnormal ocean background, this study may help provide a pilot research to assess the sea surface and subsurface footprint in the NPO.
- Contributions to the conceptual and theoretical approach, the findings of this investigation complement those of earlier studies which are conceptual approaches by indicating integrated quantitative methodology, especially in near-surface ocean patterns (current, eddy, MLD, etc) and winds (wind stress power, Ekman). Taken together, this study can be drawn from the valued-hot spot area of the fine-scale vertical variability in each distinct area, further predicting the mapping area.
- Contributions to the open ocean close to the south of Japan, this study estimated

the multifaceted oceanic background and climatic factors (wind, precipitation, temperature, etc) enhancing shallow and deep ocean response. Moreover, this study may offer marine knowledge in the Northwest Pacific, which will be crucial for addressing challenges like the development of new ports and channels, the exploration of offshore oil, and the conservation of coastal ecosystems and biodiversity.

5.3. Limitations and Further Research

Despite the fact that this study did its best to consider all feasible interpretations of the relevant topic "Marine Environmental Responses to typhoon and Kuroshio current in the NPO", still there are limitations in this study. Further research will be introduced in this section in line with the study outcomes.

- **The shortage of resource data on fish and ecological organisms**

  Fishery is one of the major food chain sources and is essential for the health of marine environment and sustainable development. The Important factors should be considered when monitoring fish stocks: (i) studying fish distribution to identify possible sites where fish are available to assist the fishing industry in increasing capture rates, and (ii) evaluating habitat suitability for various species of fish to guarantee sustainable development. Identifying possible fishing zones is connected to fish distribution. However, the limited availability of local fish catch data, the relationship between the fish resource and the responses of ocean variables during typhoon season is difficult to estimate on a specific date. Therefore, further study is needed for the data-assimilating model to overcome the sampling limitations of in situ observational and statistical data. Further, using modern machine learning techniques, such as deep learning models, would enhance the categorization of aquaculture regions and the management of fisheries.

- **The uncertainty of wind data in the coastal area**

  The coastal wind extraction (wind speed and wind stress) is difficult because of the independent geographical barrier between the ocean and land. In this study, for example, the wind stress power was underestimated by the interpolation generated by the boundary between land and ocean. Updated information on air/ocean coupling in the potential database would have allowed for a more accurate depiction of regional typhoon characteristics

- **The effect of successive typhoons on the ocean**

  In 2019, ahead of typhoon HAGIBIS, another super typhoon FAXAI affected to the same area on September 07 to 13. That is, two strong intensities of the typhoons affected the same ocean background area with a short time gap. Moreover, in 2013, and 2016, with non-large Kuroshio current, the two successive typhoons affected the south of Japan with a short-term period (at most a month), respectively. Changes in the ocean variables due to successive typhoons have not yet been studied in detail. With further study instances, it would be feasible to analyze the oceanic reactions in non-large and large Kuroshio current meander cases according to successive typhoon effects.

- **The coupled remote sensing and modeling data**

  Although the different internal ocean processes between physical and biological in response to the typhoon and Kuroshio current were demonstrated well in this study, further studies are recommended to improve forecasting the mapping area via the numerical simulation with advanced statistical analysis methods to predict the ocean. This is helping to provide an early warning of changes in the marine environment and save lives, create new industries, and preserve ecosystems.

- **The machine learning approach**

  Big data and machine learning are examples of modern technologies that can be used to explore typhoon-ocean interactions (such as Jiang, Xu and Wei, 2018; Duo, Wang and Wang, 2019; Lou *et al.*, 2021). Besides, the feasibility of using big analytics and machine learning to examine the upper ocean reaction to a tropical storm requires additional investigation. Future scientific and technological advancements will reveal further processes and mechanisms of typhoon-ocean interactions, aiding in typhoon forecasting and improving our knowledge of local and international air-sea interactions.

REFERENCES

Amani, Meisam, Armin Moghimi, S. Mohammad Mirmazloumi, Babak Ranjgar, Arsalan Ghorbanian, Saeid Ojaghi, Hamid Ebrahimy, et al. 2022. “Ocean Remote Sensing Techniques and Applications: A Review (Part I).” *Water* 14 (21): 3400. https://doi.org/10.3390/w14213400.

Babin, S. M., J. A. Carton, T. D. Dickey, and J. D. Wiggert. 2004. “Satellite Evidence of Hurricane-Induced Phytoplankton Blooms in an Oceanic Desert.” *Journal of Geophysical Research: Oceans* 109 (C3). https://doi.org/10.1029/2003JC001938.

Banzon, Viva, Thomas M. Smith, Toshio Mike Chin, Chunying Liu, and William Hankins. 2016. “A Long-Term Record of Blended Satellite and in Situ Sea-Surface Temperature for Climate Monitoring, Modeling and Environmental Studies.” *Earth System Science Data* 8 (1): 165–76. https://doi.org/10.5194/essd-8-165-2016.

Bentamy, A., F. Girard-Ardhuin, D. Croizé-Fillon, and P. Queffeulou. 2006. “Validation and Analysis of Ocean Parameters Using ASCAT Data.” *European Space Agency, (Special Publication) ESA SP*, no. 618.

Bentamy, Abderrahim, Semyon A Grodsky, Gildas Cambon, Pierre Tandeo, Xavier Capet, Claude Roy, Steven Herbette, and Antoine Grouazel. 2021. “Twenty-Seven Years of Scatterometer Surface Wind Analysis over Eastern Boundary Upwelling Systems.” https://doi.org/https://doi.org/10.3390/rs13050940.

Bessho, Kotaro, Kenji Date, Masahiro Hayashi, Akio Ikeda, Takahito Imai, Hidekazu Inoue, Yukihiro Kumagai, et al. 2016. “An Introduction to Himawari-8/9 — Japan’s New-Generation Geostationary Meteorological Satellites.” *Journal of the Meteorological Society of Japan*. https://doi.org/10.2151/jmsj.2016-009.

Black, Peter G., Eric A. D’Asaro, William M. Drennan, Jeffrey R. French, Pearn P. Niiler, Thomas B. Sanford, Eric J. Terrill, Edward J. Walsh, and Jun A. Zhang. 2007. “Air-Sea Exchange in Hurricanes: Synthesis of Observations from the Coupled Boundary Layer Air-Sea Transfer Experiment.” *Bulletin of the American Meteorological Society*. https://doi.org/10.1175/BAMS-88-3-357.

Black, W. J., and Tommy D. Dickey. 2008. “Observations and Analyses of Upper Ocean Responses to Tropical Storms and Hurricanes in the Vicinity of Bermuda.” *Journal of Geophysical Research: Oceans* 113 (8): 1–25. https://doi.org/10.1029/2007JC004358.

Bôas, Ana B.Villas, Fabrice Ardhuin, Alex Ayet, Mark A. Bourassa, Peter Brandt, Betrand

Chapron, Bruce D. Cornuelle, et al. 2019. “Integrated Observations of Global Surface Winds, Currents, and Waves: Requirements and Challenges for the next Decade.” *Frontiers in Marine Science* 6 (JUL): 1–34. https://doi.org/10.3389/fmars.2019.00425.

Bourassa, Mark A., Thomas Meissner, Ivana Cerovecki, Paul Chang, Xiaolong Dong, Giovanna De Chiara, Craig Donlon, et al. 2019. “Remotely Sensed Winds and Wind Stresses for Marine Forecasting and Ocean Modeling.” *Frontiers in Marine Science* 6 (JUL). https://doi.org/10.3389/fmars.2019.00443.

Chai, Fei, Kenneth S. Johnson, Hervé Claustre, Xiaogang Xing, Yuntao Wang, Emmanuel Boss, Stephen Riser, Katja Fennel, Oscar Schofield, and Adrienne Sutton. 2020. “Monitoring Ocean Biogeochemistry with Autonomous Platforms.” *Nature Reviews Earth and Environment* 1 (6): 315–26. https://doi.org/10.1038/s43017-020-0053-y.

Chan, Johnny C.L. 2005. “Interannual and Interdecadal Variations of Tropical Cyclone Activity over the Western North Pacific.” *Meteorology and Atmospheric Physics* 89 (1–4): 143–52. https://doi.org/10.1007/s00703-005-0126-y.

Chaudhuri, Dipanjan, Debasis Sengupta, Eric D’Asaro, R. Venkatesan, and M. Ravichandran. 2019. “Response of the Salinity-Stratified Bay of Bengal to Cyclone Phailin.” *Journal of Physical Oceanography* 49 (5): 1121–40. https://doi.org/10.1175/JPO-D-18-0051.1.

Chelton, Dudley B, Michael G Schlax, Michael H Freilich, and Ralph F Milliff. 2004. “Satellite Measurements Reveal Persistent Small-Scale Features in Ocean Winds.” *Science* 303 (5660): 978–83. https://doi.org/10.1126/science.1091901.

Chen, Gengxin, Huijie Xue, Dongxiao Wang, and Qiang Xie. 2013. “Observed Near-Inertial Kinetic Energy in the Northwestern South China Sea.” *Journal of Geophysical Research: Oceans* 118 (10): 4965–77. https://doi.org/10.1002/jgrc.20371.

Chen, Jie, Changbo Jiang, Zhiyuan Wu, Yuannan Long, Bin Deng, and Xiaojian Liu. 2019. “Numerical Investigation of Fresh and Saltwater Distribution in the Pearl River Estuary during a Typhoon Using a Fully Coupled Atmosphere-Wave-Ocean Model.” *Water (Switzerland)* 11 (4). https://doi.org/10.3390/w11040646.

CHEN, Xiu hua, Liang sheng ZHU, and Hong sheng ZHANG. 2007. “Numerical Simulation of Summer Circulation in the East China Sea and Its Application in Estimating the Sources of Red Tides in the Yangtze River Estuary and Adjacent Sea Areas.” *Journal of Hydrodynamics* 19 (3): 272–81. https://doi.org/10.1016/S1001-6058(07)60059-6.

Chen, Yongqiang, and Danling Tang. 2012. “Eddy-Feature Phytoplankton Bloom Induced by

a Tropical Cyclone in the South China Sea." *International Journal of Remote Sensing* 33 (23): 7444–57. https://doi.org/10.1080/01431161.2012.685976.

Chereskin, Teresa K., and James F. Price. 2019. *Upper Ocean Structure: Ekman Transport and Pumping*. *Encyclopedia of Ocean Sciences*. Elsevier Inc. https://doi.org/10.1016/B978-0-12-409548-9.11161-3.

Chiang, Tzu Ling, Chau Ron Wu, and Lie Yauw Oey. 2011. "Typhoon Kai-Tak: An Ocean's Perfect Storm." *Journal of Physical Oceanography* 41 (1): 221–33. https://doi.org/10.1175/2010JPO4518.1.

Constantin, Adrian. 2021. "Frictional Effects in Wind-Driven Ocean Currents." *Geophysical and Astrophysical Fluid Dynamics* 115 (1): 1–14. https://doi.org/10.1080/03091929.2020.1748614.

Cullen, John J. 2015. "Subsurface Chlorophyll Maximum Layers: Enduring Enigma or Mystery Solved?" *Annual Review of Marine Science* 7: 207–39. https://doi.org/10.1146/annurev-marine-010213-135111.

D'Asaro, Eric A., Thomas B. Sanford, Peter P. Niiler, and Eric J. Terrill. 2007. "Cold Wake of Hurricane Frances." *Geophysical Research Letters* 34 (15): 2–7. https://doi.org/10.1029/2007GL030160.

D'Asaro, Eric, Peter Black, Luca Centurioni, Patrick Harr, Steven Jayne, I. I. Lin, Craig Lee, et al. 2011. "Typhoon-Ocean Interaction in the Western North Pacific: Part 1." *Oceanography* 24 (4): 24–31. https://doi.org/10.5670/oceanog.2011.91.

Dagestad, Knut Frode, and Johannes Röhrs. 2019. "Prediction of Ocean Surface Trajectories Using Satellite Derived vs. Modeled Ocean Currents." *Remote Sensing of Environment* 223 (January): 130–42. https://doi.org/10.1016/j.rse.2019.01.001.

Dare, Richard A., and John L. Mcbride. 2011. "Sea Surface Temperature Response to Tropical Cyclones." *Monthly Weather Review* 139 (12): 3798–3808. https://doi.org/10.1175/MWR-D-10-05019.1.

Desbiolles, Fabien, Abderrahim Bentamy, Bruno Blanke, Claude Roy, Alberto M. Mestas-Nuñez, Semyon A. Grodsky, Steven Herbette, Gildas Cambon, and Christophe Maes. 2017. "Two Decades [1992–2012] of Surface Wind Analyses Based on Satellite Scatterometer Observations." *Journal of Marine Systems* 168: 38–56. https://doi.org/10.1016/j.jmarsys.2017.01.003.

Dohan, Kathleen, and Nikolai Maximenko. 2010. "Monitoring Ocean Currents with Satellite

Sensors." *Oceanography* 23 (4): 94–103. https://doi.org/10.5670/oceanog.2010.08.

Domingues, Ricardo, Gustavo Goni, Francis Bringas, Sang-Ki Lee, Hyun-Sook Kim, George Halliwell, Jili Dong, Julio Morell, and Luis Pomales. 2015. "Upper Ocean Response to Hurricane Gonzalo (2014): Salinity Effects Revealed by Targeted and Sustained Underwater Glider Observations." *Geophysical Research Letters* 42 (17): 7131–38. https://doi.org/10.1002/2015GL065378.

Du, Jinyang, John S. Kimball, John Galantowicz, Seung Bum Kim, Steven K. Chan, Rolf Reichle, Lucas A. Jones, and Jennifer D. Watts. 2018. "Assessing Global Surface Water Inundation Dynamics Using Combined Satellite Information from SMAP, AMSR2 and Landsat." *Remote Sensing of Environment* 213 (April): 1–17. https://doi.org/10.1016/j.rse.2018.04.054.

Duo, Zijun, Wenke Wang, and Huizan Wang. 2019. "Oceanic Mesoscale Eddy Detection Method Based on Deep Learning." *Remote Sensing* 11 (16). https://doi.org/10.3390/rs11161921.

Ebuchi, Naoto, and Kimio Hanawa. 2003. "Influence of Mesoscale Eddies on Variations of the Kuroshio Path South of Japan." *Journal of Oceanography* 59 (1): 25–36. https://doi.org/10.1023/A:1022856122033.

Emanuel, Kerry. 2001. "Contribution of Tropical Cyclones to Meridional Heat Transport by the Oceans" 106 (1).

———. 2003. "Tropical Cyclones." *Annual Review of Earth and Planetary Sciences* 31: 75–104. https://doi.org/10.1146/annurev.earth.31.100901.141259.

Emanuel, Kerry, Christopher DesAutels, Christopher Holloway, and Robert Korty. 2004. "Environmental Control of Tropical Cyclone Intensity." *Journal of the Atmospheric Sciences* 61 (7): 843–58. https://doi.org/10.1175/1520-0469(2004)061<0843:ECOTCI>2.0.CO;2.

Fang, He, Tao Xie, William Perrie, Li Zhao, Jingsong Yang, and Yijun He. 2017. "Oceanwind and Current Retrievals Based on Satellite SAR Measurements in Conjunction with Buoy and HF Radar Data." *Remote Sensing* 9 (12). https://doi.org/10.3390/rs9121321.

Fedorov, Alexey V., Christopher M. Brierley, and Kerry Emanuel. 2010. "Tropical Cyclones and Permanent El Niño in the Early Pliocene Epoch." *Nature* 463 (7284): 1066–70. https://doi.org/10.1038/nature08831.

Feng, M., H. Mitsudera, and Y. Yoshikawa. 2000. “Structure and Variability of the Kuroshio Current in Tokara Strait.” *Journal of Physical Oceanography* 30 (9): 2257–76. https://doi.org/10.1175/1520-0485(2000)030<2257:SAVOTK>2.0.CO;2.

Foltz, Gregory R., Karthik Balaguru, and L. Ruby Leung. 2015. “A Reassessment of the Integrated Impact of Tropical Cyclones on Surface Chlorophyll in the Western Subtropical North Atlantic.” *Geophysical Research Letters* 42 (4): 1158–64. https://doi.org/10.1002/2015GL063222.

Fu, Lee-Lueng, Tong Lee, W. Timothy Liu, and Ronald Kwok. 2019. “50 Years of Satellite Remote Sensing of the Ocean.” *Meteorological Monographs* 59 (June): 5.1-5.46. https://doi.org/10.1175/amsmonographs-d-18-0010.1.

Gaube, Peter, Dennis J. McGillicuddy, and Aurélie J. Moulin. 2019. “Mesoscale Eddies Modulate Mixed Layer Depth Globally.” *Geophysical Research Letters* 46 (3): 1505–12. https://doi.org/10.1029/2018GL080006.

Girishkumar, M. S., K. Suprit, Jayaram Chiranjivi, T. V.S. Udaya Bhaskar, M. Ravichandran, R. Venkat Shesu, and E. Pattabhi Rama Rao. 2014. “Observed Oceanic Response to Tropical Cyclone Jal from a Moored Buoy in the South-Western Bay of Bengal.” *Ocean Dynamics* 64 (3): 325–35. https://doi.org/10.1007/s10236-014-0689-6.

Glenn, S. M., T. N. Miles, G. N. Seroka, Y. Xu, R. K. Forney, F. Yu, H. Roarty, O. Schofield, and J. Kohut. 2016. “Stratified Coastal Ocean Interactions with Tropical Cyclones.” *Nature Communications* 7 (May 2015). https://doi.org/10.1038/ncomms10887.

Groom, Steve B., Shubha Sathyendranath, Yai Ban, Stewart Bernard, Bob Brewin, Vanda Brotas, Carsten Brockmann, et al. 2019. “Satellite Ocean Colour: Current Status and Future Perspective.” *Frontiers in Marine Science* 6 (JUL). https://doi.org/10.3389/fmars.2019.00485.

Guinehut, S., A. L. Dhomps, G. Larnicol, and P. Y. Le Traon. 2012. “High Resolution 3-D Temperature and Salinity Fields Derived from in Situ and Satellite Observations.” *Ocean Science* 8 (5): 845–57. https://doi.org/10.5194/os-8-845-2012.

Hart, Robert E., Ryan N. Maue, and Michael C. Watson. 2007. “Estimating Local Memory of Tropical Cyclones through MPI Anomaly Evolution.” *Monthly Weather Review* 135 (12): 3990–4005. https://doi.org/10.1175/2007MWR2038.1.

Hernandez, Fabrice, Edward Blockley, Gary B. Brassington, Fraser Davidson, Prasanth Divakaran, Marie Drévillon, Shiro Ishizaki, et al. 2015. “Recent Progress in Performance

Evaluations and near Real-Time Assessment of Operational Ocean Products." *Journal of Operational Oceanography* 8: s221–38. https://doi.org/10.1080/1755876X.2015.1050282.

Ho, Ching Hsien, Long Jing Wu, Zhen Lu, Bo Yi Lu, and Yang Chi Lan. 2021. "Potential Effect of the Intrusion of the Kuroshio Current into the South China Sea on Catches of Japanese Eel (Anguilla Japonica) in the South China Sea and Taiwan Strait." *Journal of Marine Science and Engineering* 9 (12). https://doi.org/10.3390/jmse9121465.

Hsu, Po Chun, and Chung Ru Ho. 2019. "Typhoon-Induced Ocean Subsurface Variations from Glider Data in the Kuroshio Region Adjacent to Taiwan." *Journal of Oceanography* 75 (1): 1–21. https://doi.org/10.1007/s10872-018-0480-2.

Hu, Aixue, and Gerald A. Meehl. 2009. "Effect of the Atlantic Hurricanes on the Oceanic Meridional Overturning Circulation and Heat Transport." *Geophysical Research Letters* 36 (3): 1–6. https://doi.org/10.1029/2008GL036680.

Huisman, Jef, Nga N. Pham Thi, David M. Karl, and Ben Sommeijer. 2006. "Reduced Mixing Generates Oscillations and Chaos in the Oceanic Deep Chlorophyll Maximum." *Nature* 439 (7074): 322–25. https://doi.org/10.1038/nature04245.

Hung, Chin Chang, Chih Ching Chung, Gwo Ching Gong, Sen Jan, Yaling Tsai, Kuo Shu Chen, Wen Chen Chou, et al. 2013. "Nutrient Supply in the Southern East China Sea after Typhoon Morakot." *Journal of Marine Research* 71 (1–2): 133–50. https://doi.org/10.1357/002224013807343425.

Isern-Fontanet, Jordi, Joaquim Ballabrera-Poy, Antonio Turiel, and Emilio García-Ladona. 2017. "Remote Sensing of Ocean Surface Currents: A Review of What Is Being Observed and What Is Being Assimilated." *Nonlinear Processes in Geophysics* 24 (4): 613–43. https://doi.org/10.5194/npg-24-613-2017.

Jacob, S. D., L. K. Shay, A. J. Mariano, and P. G. Black. 2000. "The 3D Oceanic Mixed Layer Response to Hurricane Gilbert." *Journal of Physical Oceanography* 30 (6): 1407–29. https://doi.org/10.1175/1520-0485(2000)030<1407:TOMLRT>2.0.CO;2.

Jaimes, Benjamin, and Lynn K. Shay. 2009. "Mixed Layer Cooling in Mesoscale Oceanic Eddies during Hurricanes Katrina and Rita." *Monthly Weather Review* 137 (12): 4188–4207. https://doi.org/10.1175/2009MWR2849.1.

Jansen, Malte F., Raffaele Ferrari, and Todd A. Mooring. 2010. "Seasonal versus Permanent Thermocline Warming by Tropical Cyclones." *Geophysical Research Letters* 37 (3): n/a-

n/a. https://doi.org/10.1029/2009gl041808.

Jiang, Chen, Ruixue Cao, Qibin Lao, Fajin Chen, Shuwen Zhang, and Peiwang Bian. 2020. "Typhoon Merbok Induced Upwelling Impact on Material Transport in the Coastal Northern South China Sea." *PLoS ONE* 15 (2): 1–15. https://doi.org/10.1371/journal.pone.0228220.

Jiang, Guo Qing, Jing Xu, and Jun Wei. 2018. "A Deep Learning Algorithm of Neural Network for the Parameterization of Typhoon-Ocean Feedback in Typhoon Forecast Models." *Geophysical Research Letters* 45 (8): 3706–16. https://doi.org/10.1002/2018GL077004.

Jullien, S., C. E. Menkes, P. Marchesiello, N. C. Jourdain, M. Lengaigne, A. Koch-larrouy, J. Lefé vre, E. M. Vincent, and V. Faure. 2012. "Impact of Tropical Cyclones on the Heat Budget of the South Pacific Ocean." *Journal of Physical Oceanography* 42 (11): 1882–1906. https://doi.org/10.1175/JPO-D-11-0133.1.

Kara, A. Birol, Peter A. Rochford, and Harley E. Hurlburt. 2000. "An Optimal Definition for Ocean Mixed Layer Depth." *Journal of Geophysical Research: Oceans* 105 (C7): 16803–21. https://doi.org/10.1029/2000jc900072.

Kawabe, Masaki. 1985. "Sea Level Variations at the Izu Islands and Typical Stable Paths of the Kuroshio." *Journal of the Oceanographical Society of Japan* 41 (5): 307–26. https://doi.org/10.1007/BF02109238.

———. 1995. "Variations of Current Path, Velocity, and Volume Transport of the Kuroshio in Relation with the Large Meander." *Journal of Physical Oceanography* 25 (12): 3103–17. https://doi.org/10.1175/1520-0485(1995)025<3103:VOCPVA>2.0.CO;2.

Li, Min, Yunbin Yuan, Ningbo Wang, Zishen Li, Ying Li, and Xingliang Huo. 2017. "Estimation and Analysis of Galileo Differential Code Biases." *Journal of Geodesy* 91 (3): 279–93. https://doi.org/10.1007/s00190-016-0962-1.

Li, Xiaohui, Guoqi Han, Jingsong Yang, Dake Chen, Gang Zheng, and Nan Chen. 2018. "Using Satellite Altimetry to Calibrate the Simulation of Typhoon Seth Storm Surge OffSoutheast China." *Remote Sensing* 10 (4): 1–15. https://doi.org/10.3390/rs10040657.

Liao, Xiaomei, Yan Du, Haigang Zhan, Tianyu Wang, and Ming Feng. 2017. "Wintertime Phytoplankton Blooms in the Western Equatorial Indian Ocean Associated With the Madden-Julian Oscillation." *Journal of Geophysical Research: Oceans* 122 (12): 9855–69. https://doi.org/10.1002/2017JC013203.

Lin, I. I. 2012. “Typhoon-Induced Phytoplankton Blooms and Primary Productivity Increase in the Western North Pacific Subtropical Ocean.” *Journal of Geophysical Research: Oceans* 117 (3). https://doi.org/10.1029/2011JC007626.

Lin, I. I., W. Timothy Liu, Chun Chieh Wu, J. C.H. Chiang, and Chung Hsiung Sui. 2003. “Satellite Observations of Modulation of Surface Winds by Typhoon-Induced Upper Ocean Cooling.” *Geophysical Research Letters* 30 (3): 6–9. https://doi.org/10.1029/2002GL015674.

Lin, I. I., Iam Fei Pun, and Chun Chieh Wu. 2009. “Upper-Ocean Thermal Structure and the Western North Pacific Category 5 Typhoons. Part II: Dependence on Translation Speed.” *Monthly Weather Review* 137 (11): 3744–57. https://doi.org/10.1175/2009MWR2713.1.

Lin, Sheng, Wen Zhou Zhang, Shao Ping Shang, and Hua Sheng Hong. 2017a. “Ocean Response to Typhoons in the Western North Pacific: Composite Results from Argo Data.” *Deep-Sea Research Part I: Oceanographic Research Papers* 123 (December 2016): 62–74. https://doi.org/10.1016/j.dsr.2017.03.007.

———. 2017b. “Ocean Response to Typhoons in the Western North Pacific: Composite Results from Argo Data.” *Deep-Sea Research Part I: Oceanographic Research Papers* 123 (December 2016): 62–74. https://doi.org/10.1016/j.dsr.2017.03.007.

Liu, Fenfen, and Shilin Tang. 2018. “Influence of the Interaction Between Typhoons and Oceanic Mesoscale Eddies on Phytoplankton Blooms.” *Journal of Geophysical Research: Oceans* 123 (4): 2785–94. https://doi.org/10.1029/2017JC013225.

Liu, Fu, Han Zhang, Jie Ming, Jiayu Zheng, Di Tian, and Dake Chen. 2020. “Importance of Precipitation on the Upper Ocean Salinity Response to Typhoon Kalmaegi (2014).” *Water (Switzerland)* 12 (2): 1–21. https://doi.org/10.3390/w12020614.

Liu, Ling Ling, Wei Wang, and Rui Xin Huang. 2008. “The Mechanical Energy Input to the Ocean Induced by Tropical Cyclones.” *Journal of Physical Oceanography* 38 (6): 1253–66. https://doi.org/10.1175/2007JPO3786.1.

Liu, Shuhong, Jiagen Li, Liang Sun, Guihua Wang, Danling Tang, Ping Huang, Hong Yan, et al. 2020. “Basin-Wide Responses of the South China Sea Environment to Super Typhoon Mangkhut (2018).” *Science of the Total Environment* 731 (April): 1–24. https://doi.org/10.1016/j.scitotenv.2020.139093.

Liu, Xin, and Jun Wei. 2015. “Understanding Surface and Subsurface Temperature Changes

Induced by Tropical Cyclones in the Kuroshio." *Ocean Dynamics* 65 (7): 1017–27. https://doi.org/10.1007/s10236-015-0851-9.

Liu, Yupeng, Danling Tang, and Morozov Evgeny. 2019. "Chlorophyll Concentration Response to the Typhoon Wind-Pump Induced Upper Ocean Processes Considering Air-Sea Heat Exchange." *Remote Sensing* 11 (15): 1–22. https://doi.org/10.3390/rs11151825.

Liu, Yupeng, Danling Tang, Shilin Tang, Evgeny Morozov, Wenzhao Liang, and Yi Sui. 2020. "A Case Study of Chlorophyll a Response to Tropical Cyclone Wind Pump Considering Kuroshio Invasion and Air-Sea Heat Exchange." *Science of the Total Environment* 741: 140290. https://doi.org/10.1016/j.scitotenv.2020.140290.

Liu, Zenghong, Jianping Xu, Chaohui Sun, and Xiaofen Wu. 2014. "An Upper Ocean Response to Typhoon Bolaven Analyzed with Argo Profiling Floats." *Acta Oceanologica Sinica* 33 (11): 90–101. https://doi.org/10.1007/s13131-014-0558-7.

Lloyd, Ian D., and Gabriel A. Vecchi. 2011. "Observational Evidence for Oceanic Controls on Hurricane Intensity." *Journal of Climate* 24 (4): 1138–53. https://doi.org/10.1175/2010JCLI3763.1.

Lou, Ranran, Zhihan Lv, Shuping Dang, Tianyun Su, and Xinfang Li. 2021. "Application of Machine Learning in Ocean Data." *Multimedia Systems*, no. 0123456789. https://doi.org/10.1007/s00530-020-00733-x.

Maúre, E. R., J. Ishizaka, C. Sukigara, Y. Mino, H. Aiki, T. Matsuno, H. Tomita, J. I. Goes, and H. R. Gomes. 2017. "Mesoscale Eddies Control the Timing of Spring Phytoplankton Blooms: A Case Study in the Japan Sea." *Geophysical Research Letters* 44 (21): 11,115-11,124. https://doi.org/10.1002/2017GL074359.

Mei, Wei, Shang Ping Xie, François Primeau, James C. McWilliams, and Claudia Pasquero. 2015. "Northwestern Pacific Typhoon Intensity Controlled by Changes in Ocean Temperatures." *Science Advances* 1 (4). https://doi.org/10.1126/sciadv.1500014.

Morimoto, Akihiko, Shoichiro Kojima, Sen Jan, and Daisuke Takahashi. 2009. "Movement of the Kuroshio Axis to the Northeast Shelf of Taiwan during Typhoon Events." *Estuarine, Coastal and Shelf Science* 82 (3): 547–52. https://doi.org/10.1016/j.ecss.2009.02.022.

Morioka, Yushi, Sergey Varlamov, and Yasumasa Miyazawa. 2019. "Role of Kuroshio Current in Fish Resource Variability off Southwest Japan." *Scientific Reports* 9 (1). https://doi.org/10.1038/s41598-019-54432-3.

Nakamura, Hirohiko, Ayako Nishina, and Shoshiro Minobe. 2012. "Response of Storm

Tracks to Bimodal Kuroshio Path States South of Japan." *Journal of Climate* 25 (21): 7772–79. https://doi.org/10.1175/JCLI-D-12-00326.1.

Ning, Jue, and Qing Xu. 2021. "Biogeochemical Response of the Upper Ocean To Two Sequential Tropical Cyclones." *International Geoscience and Remote Sensing Symposium (IGARSS)* 2021-July (Mld): 7592–99. https://doi.org/10.1109/IGARSS47720.2021.9553474.

Ning, Jue, Qing Xu, Han Zhang, Tao Wang, and Kaiguo Fan. 2019. "Impact of Cyclonic Ocean Eddies on Upper Ocean Thermodynamic Response to Typhoon Soudelor." *Remote Sensing* 11 (8). https://doi.org/10.3390/rs11080945.

Pan, Jiayi, Lei Huang, Adam T. Devlin, and Hui Lin. 2018. "Quantification of Typhoon-Induced Phytoplankton Blooms Using Satellite Multi-Sensor Data." *Remote Sensing* 10 (2): 1–14. https://doi.org/10.3390/rs10020318.

Pan, Shanshan, Jie Shi, Huiwang Gao, Xinyu Guo, Xiaohong Yao, and Xiang Gong. 2017. "Contributions of Physical and Biogeochemical Processes to Phytoplankton Biomass Enhancement in the Surface and Subsurface Layers during the Passage of Typhoon Damrey." *Journal of Geophysical Research: Biogeosciences* 122 (1): 212–29. https://doi.org/10.1002/2016JG003331.

Park, Jong Jin, Young Oh Kwon, and James F. Price. 2011. "Argo Array Observation of Ocean Heat Content Changes Induced by Tropical Cyclones in the North Pacific." *Journal of Geophysical Research: Oceans* 116 (12): 1–12. https://doi.org/10.1029/2011JC007165.

Prakash, Kumar Ravi, and Vimlesh Pant. 2017. "Upper Oceanic Response to Tropical Cyclone Phailin in the Bay of Bengal Using a Coupled Atmosphere-Ocean Model." *Ocean Dynamics* 67 (1): 51–64. https://doi.org/10.1007/s10236-016-1020-5.

Price, J. F. 1981. "Upper Ocean Response to a Hurricane." *J. Phys. Oceanogr.* https://doi.org/10.1175/1520-0485(1981)011<0153:uortah>2.0.co;2.

Price, J. F., T. B. Sanford, and G. Z. Forristall. 1994. "Forced Stage Response to a Moving Hurricane." *Journal of Physical Oceanography* 24 (2): 233–60. https://doi.org/10.1175/1520-0485(1994)024<0233:FSRTAM>2.0.CO;2.

Price, J. F., R. A. Weller, and R. Pinkel. 1986. "Diurnal Cycling: Observations and Models of the Upper Ocean Response to Diurnal Heating, Cooling, and Wind Mixing." 91 (6): 8411–27. https://doi.org/10.1029/jc091ic07p08411.

Price, James F., Jan Morzel, and Pearn P. Niiler. 2008. “Warming of SST in the Cool Wake of a Moving Hurricane.” *Journal of Geophysical Research: Oceans* 113 (7): 1–19. https://doi.org/10.1029/2007JC004393.

Pun, Iamfei, Ya Ting Chang, I. I. Lin, Tswen Yung Tang, and Ren Chieh Lien. 2011. “Typhoon-Ocean Interaction in the Western North Pacific: Part 2.” *Oceanography* 24 (4): 32–41. https://doi.org/10.5670/oceanog.2011.92.

Qiu, Guoqiang, Xiaogang Xing, Fei Chai, Xiao Hai Yan, Zhiyu Liu, and Haili Wang. 2021. “Far-Field Impacts of a Super Typhoon on Upper Ocean Phytoplankton Dynamics.” *Frontiers in Marine Science* 8 (April): 1–10. https://doi.org/10.3389/fmars.2021.643608.

Rahmstorf, Stefan. 2003. “Thermohaline Circulation: The Current Climate.” *Nature* 421 (6924): 699–699. https://doi.org/10.1038/421699a.

Ribbe, Joachim, and Daniel Brieva. 2016. “A Western Boundary Current Eddy Characterisation Study.” *Estuarine, Coastal and Shelf Science* 183: 203–12. https://doi.org/10.1016/j.ecss.2016.10.036.

Rodríguez, Ernesto, Mark Bourassa, Dudley Chelton, J. Thomas Farrar, David Long, Dragana Perkovic-Martin, and Roger Samelson. 2019. “The Winds and Currents Mission Concept.” *Frontiers in Marine Science* 6 (JUL): 1–8. https://doi.org/10.3389/fmars.2019.00438.

Sakajo, Takashi, Shun Ohishi, and Tomoki Uda. 2022. “Identification of Kuroshio Meanderings South of Japan via a Topological Data Analysis for Sea Surface Height.” *Journal of Oceanography*, no. 0123456789. https://doi.org/10.1007/s10872-022-00656-3.

Samson, Guillaume, Hervé Giordani, Guy Caniaux, and Frank Roux. 2009. “Numerical Investigation of an Oceanic Resonant Regime Induced by Hurricane Winds.” *Ocean Dynamics* 59 (4): 565–86. https://doi.org/10.1007/s10236-009-0203-8.

Sanford, Thomas B., James F. Price, and James B. Girton. 2011. “Upper-Ocean Response to Hurricane Frances (2004) Observed by Profiling EM-APEX Floats.” *Journal of Physical Oceanography* 41 (6): 1041–56. https://doi.org/10.1175/2010JPO4313.1.

Sanford, Thomas B., James F. Price, James B. Girton, and Douglas C. Webb. 2007. “Highly Resolved Observations and Simulations of the Ocean Response to a Hurricane.” *Geophysical Research Letters* 34 (13): 1–5. https://doi.org/10.1029/2007GL029679.

Sekine, Yoshihiko. 1990. “Reference to the Formation of the Large Meander Path South of

Japan" 37 (3): 359–80.

Shang, Shaoling, Li Li, Fengqin Sun, Jingyu Wu, Chuanmin Hu, Dewen Chen, Xiuren Ning, Yun Qiu, Caiyun Zhang, and Shaoping Shang. 2008. "Changes of Temperature and Bio-Optical Properties in the South China Sea in Response to Typhoon Lingling, 2001." *Geophysical Research Letters* 35 (10): 2–7. https://doi.org/10.1029/2008GL033502.

Shay, Lynn K., Gustavo J. Goni, and Peter G. Black. 2000. "Effects of a Warm Oceanic Feature on Hurricane Opal." *Monthly Weather Review* 128 (5): 1366–83. https://doi.org/10.1175/1520-0493(2000)128<1366:EOAWOF>2.0.CO;2.

Shibano, Ryota, Yasuhiro Yamanaka, Naosuke Okada, Takashi Chuda, Shin Ichi Suzuki, Hiroshi Niino, and Mitsuhiro Toratani. 2011. "Responses of Marine Ecosystem to Typhoon Passages in the Western Subtropical North Pacific." *Geophysical Research Letters* 38 (18): 1–5. https://doi.org/10.1029/2011GL048717.

Sriver, Ryan L., and Matthew Huber. 2007. "Observational Evidence for an Ocean Heat Pump Induced by Tropical Cyclones." *Nature* 447 (7144): 577–80. https://doi.org/10.1038/nature05785.

Steinberg, Deborah K., Craig A. Carlson, Nicholas R. Bates, Rodney J. Johnson, Anthony F. Michaels, and Anthony H. Knap. 2001. "Overview of the US JGOFS Bermuda Atlantic Time-Series Study (BATS): A Decade-Scale Look at Ocean Biology and Biogeochemistry." *Deep-Sea Research Part II: Topical Studies in Oceanography* 48 (8–9): 1405–47. https://doi.org/10.1016/S0967-0645(00)00148-X.

Sugimoto, Shusaku, Bo Qiu, and Niklas Schneider. 2021. "Local Atmospheric Response to the Kuroshio Large Meander Path in Summer and Its Remote Influence on the Climate of Japan." *Journal of Climate* 34 (9): 3571–89. https://doi.org/10.1175/JCLI-D-20-0387.1.

Sun, Jingru, Lie Yauw Oey, Roger Chang, Fanghua Xu, and Shih Ming Huang. 2015. "Ocean Response to Typhoon Nuri (2008) in Western Pacific and South China Sea." *Ocean Dynamics* 65 (5): 735–49. https://doi.org/10.1007/s10236-015-0823-0.

Sun, Jingru, Gabriel Vecchi, and Brian Soden. 2021. "Sea Surface Salinity Response to Tropical Cyclones Based on Satellite Observations." *Remote Sensing* 13 (3). https://doi.org/10.3390/rs13030420.

Sun, Liang, Ying Xin Li, Yuan Jian Yang, Qiaoyan Wu, Xue Tao Chen, Qiu Yang Li, Yu Bin Li, and Tao Xian. 2014. "Effects of Super Typhoons on Cyclonic Ocean Eddies in the

Western North Pacific: A Satellite Data-Based Evaluation between 2000 and 2008." *Journal of Geophysical Research: Oceans* 119 (9): 5585–98. https://doi.org/10.1002/2013JC009575.

Traon, Pierre Yves Le, Antonio Reppucci, Enrique Alvarez Fanjul, Lotfi Aouf, Arno Behrens, Maria Belmonte, Abderrahim Bentamy, et al. 2019. "From Observation to Information and Users: The Copernicus Marine Service Perspective." *Frontiers in Marine Science* 6 (May). https://doi.org/10.3389/fmars.2019.00234.

Usui, Norihisa, Hiroyuki Tsujino, Hideyuki Nakano, and Yosuke Fujii. 2008. "Formation Process of the Kuroshio Large Meander in 2004." *Journal of Geophysical Research: Oceans* 113 (8): 1–20. https://doi.org/10.1029/2007JC004675.

Usui, Norihisa, Hiroyuki Tsujino, Hideyuki Nakano, and Satoshi Matsumoto. 2013. "Long-Term Variability of the Kuroshio Path South of Japan." *Journal of Oceanography* 69 (6): 647–70. https://doi.org/10.1007/s10872-013-0197-1.

Vincent, Emmanuel M., Matthieu Lengaigne, Jérôme Vialard, Gurvan Madec, Nicolas C. Jourdain, and Sébastien Masson. 2012. "Assessing the Oceanic Control on the Amplitude of Sea Surface Cooling Induced by Tropical Cyclones." *Journal of Geophysical Research: Oceans* 117 (5): 1–14. https://doi.org/10.1029/2011JC007705.

Vissa, Naresh Krishna, A. N.V. Satyanarayana, and B. Prasad Kumar. 2012. "Response of Upper Ocean during Passage of Mala Cyclone Utilizing Argo Data." *International Journal of Applied Earth Observation and Geoinformation* 14 (1): 149–59. https://doi.org/10.1016/j.jag.2011.08.015.

Walker, Nan D., Robert R. Leben, and Shreekanth Balasubramanian. 2005. "Hurricane-Forced Upwelling and Chlorophyll a Enhancement within Cold-Core Cyclones in the Gulf of Mexico." *Geophysical Research Letters* 32 (18): 1–5. https://doi.org/10.1029/2005GL023716.

Wang, Guihua, Lingwei Wu, Nathaniel C. Johnson, and Zheng Ling. 2016. "Observed Three-Dimensional Structure of Ocean Cooling Induced by Pacific Tropical Cyclones." *Geophysical Research Letters* 43 (14): 7632–38. https://doi.org/10.1002/2016GL069605.

Wang, Tongyu, Fajin Chen, Shuwen Zhang, Jiayi Pan, Adam T. Devlin, Hao Ning, and Weiqiang Zeng. 2022. "Physical and Biochemical Responses to Sequential Tropical Cyclones in the Arabian Sea." *Remote Sensing* 14 (3schematic sketch). https://doi.org/10.3390/rs14030529.

Wang, Wei, and Rui Xin Huang. 2004. “Wind Energy Input to the Ekman Layer.” *Journal of Physical Oceanography* 34 (5): 1267–75. https://doi.org/10.1175/1520-0485(2004)034<1267:WEITTE>2.0.CO;2.

Wang, Yueqi, and Zhiqiang Gao. 2020. “Contrasting Chlorophyll-a Seasonal Patterns between Nearshore and Offshore Waters in the Bohai and Yellow Seas, China: A New Analysis Using Improved Satellite Data.” *Continental Shelf Research* 203 (May): 104173. https://doi.org/10.1016/j.csr.2020.104173.

Wang, Zhankun, and Louis Goodman. 2010. “The Evolution of a Thin Phytoplankton Layer in Strong Turbulence.” *Continental Shelf Research* 30 (1): 104–18. https://doi.org/10.1016/j.csr.2009.08.006.

Webster, P. J., G. J. Holland, J. A. Curry, and H. R. Chang. 2005. “Atmospheric Science: Changes in Tropical Cyclone Number, Duration, and Intensity in a Warming Environment.” *Science* 309 (5742): 1844–46. https://doi.org/10.1126/science.1116448.

Wu, Chau Ron, Yu Lin Chang, Lie Yauw Oey, C. W.June Chang, and Yi Chia Hsin. 2008. “Air-Sea Interaction between Tropical Cyclone Nari and Kuroshio.” *Geophysical Research Letters* 35 (12): 1–7. https://doi.org/10.1029/2008GL033942.

Wu, Qiaoyan, and Dake Chen. 2012. “Typhoon-Induced Variability of the Oceanic Surface Mixed Layer Observed by Argo Floats in the Western North Pacific Ocean.” *Atmosphere - Ocean* 50 (SUPPL.1): 4–14. https://doi.org/10.1080/07055900.2012.712913.

Wu, Renhao, and Chunyan Li. 2018. “Upper Ocean Response to the Passage of Two Sequential Typhoons.” *Deep-Sea Research Part I: Oceanographic Research Papers* 132 (January): 68–79. https://doi.org/10.1016/j.dsr.2017.12.006.

Wu, Renhao, Han Zhang, and Dake Chen. 2020. “Effect of Typhoon Kalmaegi (2014) on Northern South China Sea Explored Using Muti-Platform Satellite and Buoy Observations Data.” *Progress in Oceanography* 180 (July 2019). https://doi.org/10.1016/j.pocean.2019.102218.

Wu, Renhao, Han Zhang, Dake Chen, Chunyan Li, and Jianmin Lin. 2018. “Impact of Typhoon Kalmaegi (2014) on the South China Sea: Simulations Using a Fully Coupled Atmosphere-Ocean-Wave Model.” *Ocean Modelling* 131 (February): 132–51. https://doi.org/10.1016/j.ocemod.2018.08.004.

Xing, Xiaogang, Mark L. Wells, Shuangling Chen, Sheng Lin, and Fei Chai. 2020. “Enhanced Winter Carbon Export Observed by BGC-Argo in the Northwest Pacific

Ocean." *Geophysical Research Letters* 47 (22). https://doi.org/10.1029/2020GL089847.

Xu, Yao, Hailun He, Jinbao Song, Yijun Hou, and Funing Li. 2017. "Observations and Modeling of Typhoon Waves in the South China Sea." *Journal of Physical Oceanography* 47 (6): 1307–24. https://doi.org/10.1175/JPO-D-16-0174.1.

Yang, Bing, and Yijun Hou. 2014. "Near-Inertial Waves in the Wake of 2011 Typhoon Nesat in the Northern South China Sea." *Acta Oceanologica Sinica* 33 (11): 102–11. https://doi.org/10.1007/s13131-014-0559-6.

Yang, Yiing Jang, Ming Huei Chang, Chia Ying Hsieh, Hung I. Chang, Sen Jan, and Ching Ling Wei. 2019. "The Role of Enhanced Velocity Shears in Rapid Ocean Cooling during Super Typhoon Nepartak 2016." *Nature Communications* 10 (1): 1–11. https://doi.org/10.1038/s41467-019-09574-3.

Yin, Xiaobin, Zhenzhan Wang, Yuguang Liu, and Yi Xu. 2007. "Ocean Response to Typhoon Ketsana Traveling over the Northwest Pacific and a Numerical Model Approach." *Geophysical Research Letters* 34 (21): 1–6. https://doi.org/10.1029/2007GL031477.

Yue, Xinxin, Biao Zhang, Guoqiang Liu, Xiaofeng Li, Han Zhang, and Yijun He. 2018. "Upper Ocean Response to Typhoon Kalmaegi and Sarika in the South China Sea from Multiple-Satellite Observations and Numerical Simulations." *Remote Sensing* 10 (3): 348. https://doi.org/10.3390/rs10020348.

Zhang, Hailong, Shengqiang Wang, Zhongfeng Qiu, Deyong Sun, Joji Ishizaka, Shaojie Sun, and Yijun He. 2018. "Phytoplankton Size Class in the East China Sea Derived from MODIS Satellite Data." *Biogeosciences* 15 (13): 4271–89. https://doi.org/10.5194/bg-15-4271-2018.

Zhang, Han, Dake Chen, Lei Zhou, Xiaohui Liu, Tao Ding, and Beifeng Zhou. 2016. "Upper Ocean Response to Typhoon Kalmaegi (2014)." *Journal of Geophysical Research: Oceans* 121 (8): 6520–35. https://doi.org/10.1002/2016JC012064.

Zhang, Han, Hailun He, Wen Zhou Zhang, and Di Tian. 2021. "Upper Ocean Response to Tropical Cyclones: A Review." *Geoscience Letters* 8 (1): 1–12. https://doi.org/10.1186/s40562-020-00170-8.

Zhang, Han, Xiaohui Liu, Renhao Wu, Dake Chen, Dongna Zhang, Xiaodong Shang, Yuan Wang, et al. 2020a. "Sea Surface Current Response Patterns to Tropical Cyclones." *Journal of Marine Systems* 208 (March): 103345. https://doi.org/10.1016/j.jmarsys.2020.103345.

———. 2020b. “Sea Surface Current Response Patterns to Tropical Cyclones.” *Journal of Marine Systems* 208 (March): 103345. https://doi.org/10.1016/j.jmarsys.2020.103345.

———. 2020c. “Sea Surface Current Response Patterns to Tropical Cyclones.” *Journal of Marine Systems* 208 (June 2019): 103345. https://doi.org/10.1016/j.jmarsys.2020.103345.

Zhang, Han, Xiaohui Liu, Renhao Wu, Fu Liu, Linghui Yu, Xiaodong Shang, Yongfeng Qi, et al. 2019. “Ocean Response to Successive Typhoons Sarika and Haima (2016) Based on Data Acquired via Multiple Satellites and Moored Array.” *Remote Sensing* 11 (20): 1–25. https://doi.org/10.3390/rs11202360.

Zhang, Jin Feng, Xiao Ning Zhang, and Cong Yu. 2016. “Wave-Induced Seabed Liquefaction around Composite Bucket Foundations of Offshore Wind Turbines during the Sinking Process.” *Journal of Renewable and Sustainable Energy* 8 (2): 225–30. https://doi.org/10.1063/1.4946874.

Zhang, Xuefeng, Peter C. Chu, Wei Li, Chang Liu, Lianxin Zhang, Caixia Shao, Xiaoshuang Zhang, Guofang Chao, and Yuxin Zhao. 2018. “Impact of Langmuir Turbulence on the Thermal Response of the Ocean Surface Mixed Layer to Supertyphoon Haitang (2005).” *Journal of Physical Oceanography* 48 (8): 1651–74. https://doi.org/10.1175/JPO-D-17-0132.1.

Zhang, Yufei, Bing Deng, and Ming Zhang. 2019. “Analysis of the Relation between Ocean Internal Wave Parameters and Ocean Surface Fl Uctuation” 13 (2): 336–50.

Zhao, Hui, Dan Ling Tang, and Yuqing Wang. 2008. “Comparison of Phytoplankton Blooms Triggered by Two Typhoons with Different Intensities and Translation Speeds in the South China Sea.” *Marine Ecology Progress Series* 365 (August): 57–65. https://doi.org/10.3354/meps07488.

Zheng, Zhe Wen, Chung Ru Ho, Quanan Zheng, Nan Jung Kuo, and Yao Tsai Lo. 2010. “Satellite Observation and Model Simulation of Upper Ocean Biophysical Response to Super Typhoon Nakri.” *Continental Shelf Research* 30 (13): 1450–57. https://doi.org/10.1016/j.csr.2010.05.005.

LIST OF PUBLICATIONS

[**For Chapter 3**] JEON Jonghyeok, and TOMITA Takashi. Marine environment analysis under super typhoon HAGIBIS using CMEMS data, Journal of Japan Society of Civil Engineers Ser. B3 (Ocean Engineering), 78(2), pp. 499-504, 2022. https://doi.org/10.2208/jscejoe.78.2_I_499

[**For Chapter 4**] JEON Jonghyeok, and TOMITA Takashi. Investigating the effects of super typhoon HAGIBIS in the Northwest Pacific Ocean using multiple observational data, Remote Sens, 14(22), 5667, 2022. https://doi.org/10.3390/rs14225667

[**For 2.2.3 Effect of Climate Change Aspect in Chapter 2**] JEON Jonghyeok, TOMITA Takashi, NAKAMURA Tomoaki, HORIIKE Masataka, and ICHINO Tomokazu. Field survey of damage due to storm surge and waves in Shimizu and Yaizu ports during typhoon HAGIBIS, Journal of Japan Society of Civil Engineers, Ser. B3 (Ocean Engineering), 76(2), pp. 983-988, **2020**. https://doi.org/10.2208/jscejoe.76.2_I_983

LEE Kwangho, JEON Jonghyeok, KIM Dosam, and LEE Yundu. Numerical Simulation on Control of Tsunami by Resonator (II) (for Samcheok port), Journal of Korean Society of Coastal and Ocean Engineers, 32(6), pp. 496-505, **2020**. https://doi.org/10.9765/KSCOE.2020.32.6.496

LEE Kwangho, JEON Jonghyeok, KIM Dosam, and LEE Yundu. Numerical Simulation on Control of Tsunami by Resonator (I) (for Imwon and Mukho ports), Journal of Korean Society of Coastal and Ocean Engineers, 32(6), pp. 481-495, **2020**. https://doi.org/10.9765/KSCOE.2020.32.6.481

JEON Jonghyeok, TOMITA Takashi. A Study on the Analysis of Specific Physical Characteristics of Typhoon Jebi at Osaka Bay, the 29th International Ocean and Polar Engineering Conference, ISOPE-I-19-729, **2019**.

ACKNOWLEDGEMENT

This is a long journey from the start to the finish of a Ph.D. programme. Fortunately, I wasn't walking alone. My supervisor, laboratory member, family, and all of my friends have been really supportive in coping with my struggles and loneliness on the path to this academic success. Such a valuable experience at Nagoya University will be with me for the rest of my life.

I enrolled in Nagoya University in October 2017 for a PhD programme in environmental studies. It was pretty difficult because I graduated from Korean Maritime & Ocean University with a master's degree in Civil engineering with a major in coastal engineering. The multidisciplinary scope made it difficult to continue my research for three years, but I trusted my characteristics and my supervisor's advice.

I would like to firstly express my highest appreciation to my supervisor, Professor TOMITA Takashi, who is the head of land and infrastructure Design lab in Nagoya University. He is one of the great leader in the disaster risk reduction and preventive strategy for tsunami and typhoons as well as sustainable Co-development research on Social Infrastructure. Under his guiding hand, I mastered a remote sensing technology and analytical tool for exploring worldwide marine areas, particularly those closely associated to typhoon and Kuroshio current activity in the Northwest Pacific Ocean. This research strategy subsequently evolved into one of the fundamental methodologies of my doctorate study.

I would like to express my honest appreciation to Professor KATO Hirokazu, who is the director of education and research in transportation and environmental planning and assessment, particularly strategy analysis from an interdisciplinary perspective. Thanks to his kind acceptance of my study and for giving a lot of valuable and priceless comments and suggestions that helped to make my thesis fluent.

I would like to convey my truthful appreciation to Professor TANIKAWA Hiroki, who is the leader of environmental system analysis and planning research Lab in Nagoya University. From the admission exam for a PhD course until the review of my thesis over three years, he provided valuable suggestions and comments that aided in the development and motivation of my research approach and design.

I would like to convey my sincere appreciation to Professor NAKAMURA Shinichiro, who is an associate Professor dealing with hydrology, water resources management, and land

& Infrastructure planning with a focus on climate change implications. I couldn't have handled my thesis advancement and development without his countless advice and feedback in laboratory meetings and one-on-one consulting. I am grateful for his precious help and encouragement during my Ph.D. course.

For our laboratory members, CHAMAL Perera, MASUDA Yuma MASUDA, OE Takashi OE, TAKANO Tsuyoshi, KITAZAWA Akemi, are grateful for their ongoing support, encouragement, and collaboration in my study.

In my life, I would like to express my deepest gratitude to my parents. Without their warmhearted encouragement and continuous support in my studies and life, I would not have been able to earn a Ph.D.

Finally, I would like to express my gratitude to Nagoya University and the Graduate School of Environmental Studies.